



**Melittin Interaction with Sulfated Sugars
and Cell Membranes**

INAUGURALDISSERTATION

zur

Erlangung der Würde eines Doktors der Philosophie

vorgelegt der

Philosophisch-Naturwissenschaftlichen Fakultät

der Universität Basel

von

Gabriela Klocek

aus

Cieszyn, Polen

Basel, 2008

Genehmigt von der Philosophisch-Naturwissenschaftlichen Fakultät auf Antrag von

Prof. Dr. Joachim Seelig

Prof. Dr. Dagmar Klostermeier

Basel, den 19.02.08

Prof. Dr. Hans-Peter Hauri

(Dekan)

TABLE OF CONTENTS

| | |
|--|-----|
| 1. Introduction | 3 |
| 1.1 Melittin – Structure and Conformation | 4 |
| 1.2 Melittin – Lipid Membranes Interaction | 6 |
| 1.3 Activity of Melittin on Cells..... | 9 |
| 1.4 Magainin 2 and Nisin Z - Two other Representatives of Antimicrobial Peptides Family | 12 |
| 1.5 Glycosaminoglycans - Structure, Biosynthesis and Function | 14 |
| 1.6 Interaction of HS and Heparin with Proteins and Peptides | 19 |
| 1.7 Literature | 20 |
| 2. Aim of Research | 32 |
| 3. Melittin Interaction with Sulfated Cell Surface Sugars[†] - manuscript..... | 34 |
| Appendix – Light Scattering Measurements | 72 |
| 4. Cytotoxicity of Melittin on Cells | 78 |
| Introduction..... | 78 |
| Materials and Methods..... | 80 |
| Results | 83 |
| Discussion..... | 84 |
| References..... | 87 |
| 5. Binding of RiDOM to Sulfated Cell Surface Sugars | 90 |
| Introduction..... | 90 |
| Materials and Methods..... | 91 |
| Results | 94 |
| Discussion..... | 107 |
| References..... | 109 |
| 6. Interaction of Melittin with Lipids | 111 |
| Introduction..... | 111 |
| Materials and Methods..... | 112 |
| Results | 113 |
| Discussion..... | 119 |
| References..... | 121 |
| 7. Summary | 126 |

| | |
|----------------------------------|-----|
| 8. Acknowledgments | 128 |
| 9. Curriculum Vitae | 130 |
| 10. Declaration | 131 |

1. INTRODUCTION

Bee venom from *Apis mellifera* is toxic substance, composed of only a few pharmacologically and enzymatically active components, such as phospholipase A, hyaluronidase, histamine, melittin and apamin, a mast cell degranulating (MCD) peptide (1).

Knowledge of its composition and mechanism of action has been not been established until 1940-1950s due to lack of proper methods of analysis. Thus, all effects of the bee venom had been attributed to its phospholipase activity. Development of different techniques, such as electrophoresis, chromatography, gel-filtration, combined with pharmacological and biochemical analysis allowed to fully identify the active components of bee venom.

Melittin is the major toxic component of the venom and it constitutes 50% of dry venom. It was identified in 1952 during the electrophoretic experiment with phospholipase A. Melittin is released from its precursor, promelittin, during its synthesis in the bee, and will be formylated at a later stage. It is a 26 amino acid residue long cationic peptide with hemolytic activity and a broad antimicrobial spectrum due to its ability to disrupt cell membranes (1, 2).

Melittin not only interacts with lipid membranes (described in more details in Chapter 1.2), but also exhibits various other effects. It inhibits transport pumps, such as ($H^+ + K^+$) ATPase (3) and ($Na^+ + K^+$) ATPase (4) and increases the permeability of cell membranes to ions. It induces inhibition and aggregation of membrane proteins (5-8), it stimulates activity of phospholipase A₂ (9) (cf. Chapter 1.3).

Melittin-lipid membrane interactions were studied extensively in order to determine the nature of this interaction, but even up to now, the molecular mechanism of action of melittin is not completely established. Much of the evidence indicates that different mechanisms are responsible for the different effects of the peptide (10).

In the present work we focused on an alternative action mechanism of melittin. As melittin carries a net positive charge and as negatively charged sulfate carrying glycosaminoglycans (GAGs) are found on almost all cell surfaces, it can be expected that melittin binds to the anionic groups of GAGs. There exist many studies concerning interactions between melittin and lipid membranes, but to the best of our knowledge the potential involvement of GAGs in the binding of melittin to cell membranes has not been explored yet.

1.1 Melittin – Structure and Conformation

Melittin is composed of 26 amino acid residues with the sequence shown in Figure 1.



Figure 1. Amino acid sequence of melittin in one letter code. Hydrophobic residues are presented in white, polar residues in grey and positively charged residues in red circles.

It is a cationic peptide with an amino terminus composed predominantly of hydrophobic amino acids (residues 1-20), and a carboxyl-terminal end composed of mostly hydrophilic amino acids (residues 21-26). The peptide has a net positive charge of $z = 5$ due to presence of three lysines and two arginines. Four of them form a cluster, -KRKR-, at the carboxy terminus. The K-7 is embedded in the hydrophobic N-terminal region of the peptide. The asymmetric distribution of non-polar and polar amino acids leads to an amphiphatic structure of melittin when it adopts α helical conformation. A crystal structure

of melittin in aqueous solution was determined by X-ray analysis at high-resolution of 2 Å (11) (Figure 2A). Each melittin molecule is composed of two α -helical segments with a bent due to presence of proline at position 14, therefore the overall shape is called “a bent rod”.

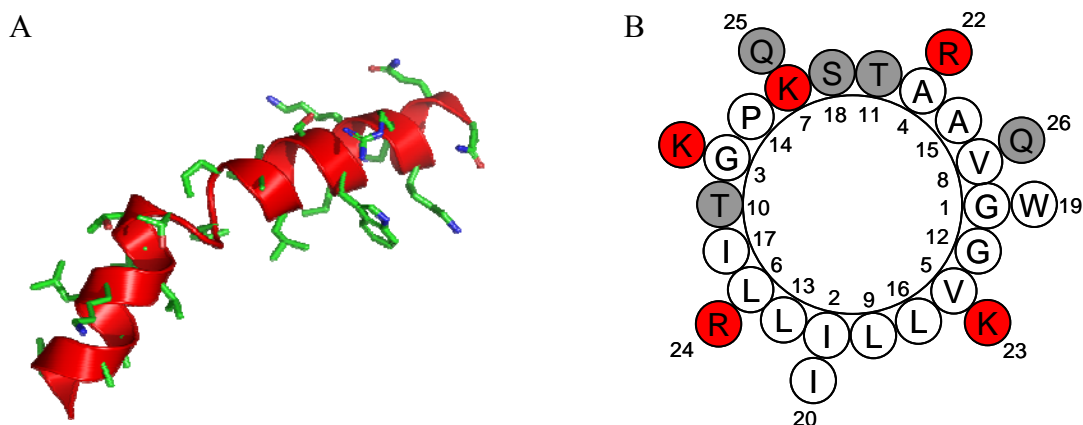


Figure 2. (A) Crystal structure of melittin α -helix determined by Terwilliger and Eisenberg (from PDB, entry 2MLT). (B) Helical wheel diagram of melittin; positively charged and polar amino acids are marked in red and grey, respectively.

Although melittin contains a high proportion of hydrophobic amino acids, it is highly soluble in water and moderately soluble in methanol. Melittin is very sensitive to the solution conditions and can adopt different conformations and aggregation states in aqueous solution. It is largely unstructured in water, but forms an α -helix upon binding to lipid membranes (12). At low peptide concentration and low ionic strength melittin occurs mostly as a monomer with essentially random coil conformation. When the peptide concentration and/or the salt concentration are increased, melittin aggregates into a tetramer with a high content of α -helix structure (13-15).

The pH of the aqueous solution also influences the conformational states of the peptide. A change of the conformation of melittin towards a tetramer at high pH was observed,

although the concentration of the peptide and the ionic strength of the solution were kept at low level (16).

All these studies show that the self association/aggregation of the peptide is a complex process and depends on the peptide concentration and the solution properties such as ionic strength and pH.

1.2 Melittin - Lipid Membranes Interaction

The interaction of melittin with lipid membranes has been investigated extensively, both experimentally and theoretically (17-23). The various studies show that the interaction depends on the properties of the peptide in aqueous solution, peptide concentration, lipid composition, hydration level, and the membrane potential (10). The affinity of melittin is larger for membranes composed of negatively charged lipids than for zwitterionic lipids. The partition constant of melittin into the membranes composed of POPC/POPG (80mol/20mol) is $K_p = 4.5 \times 10^4 \text{ M}^{-1}$ (18), whereas a 20-fold smaller partition constant of $K_p = 2.1 \times 10^3 \text{ M}^{-1}$ was found for pure POPC (21). This indicates that hydrophobic as well as electrostatic interactions are involved in the binding of melittin to membranes (18, 24).

Two different mechanisms have been proposed for the hemolytic activity of melittin. In one model melittin acts on the lipid membrane through pore formation. The peptides can insert into the hydrophobic core of the membrane, so the binding to the membrane is predominantly driven by hydrophobic interactions. Some studies envisage a barrel-stave mechanism (25-27); others suggest the formation of toroidal pores (23, 28). In barrel-stave model, shown schematically in Figure 3A transmembrane amphiphatic α -helices form bundles in which hydrophobic surfaces interact with the lipid core of the membrane, and the hydrophilic surfaces point inwards forming a pore. The peptide molecules with a length

of $\sim 37 \text{ \AA}$ span a nearly flat bilayer with thickness of $\sim 34 - 46 \text{ \AA}$, and aggregate to line an aqueous channel.

In the toroidal model, Figure 3B, the lipid layer continuously bends from the top leaflet to the bottom leaflet through the toroidal hole, so the pore is lined by both the lipid headgroups and peptide molecules.

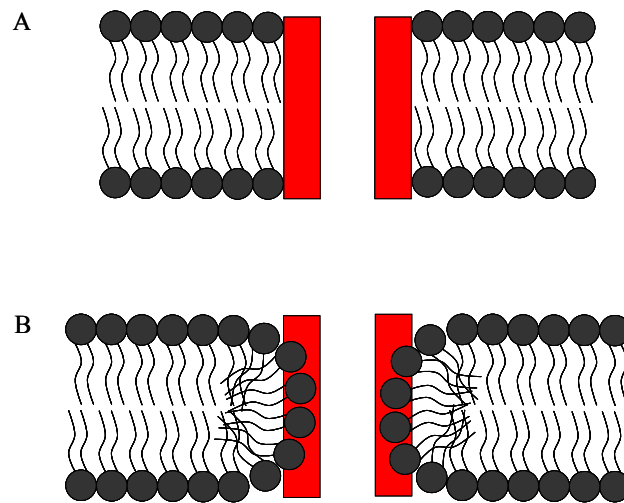


Figure 3. Schematic drawings of (A) 'barrel stave pore' and (B) 'toroidal pore' models. Peptide molecules are presented as red rectangles, and lipids are shown with dark grey circles as headgroups and wavy hydrocarbon chains.

An alternative 'detergent-like' model, schematically shown in Figure 4, assumes that melittin behaves much as a detergent. At low concentrations of the peptide, the molecules are oriented parallel to the surface of the bilayer (Figure 4A). The peptide does not insert into the hydrophobic core of the membrane, but rather binds to the lipid headgroups. The initial interaction with negatively charged phospholipids is electrostatically driven, since the peptide is positively charged. Increasing the peptide concentration causes aggregation and a reduction of the bilayer thickness (Figure 4B). When a critical concentration is

reached, the peptide changes its orientation and disrupts the bilayer, inducing disintegration of the membrane into micelles (29-32) (Figure 4C).

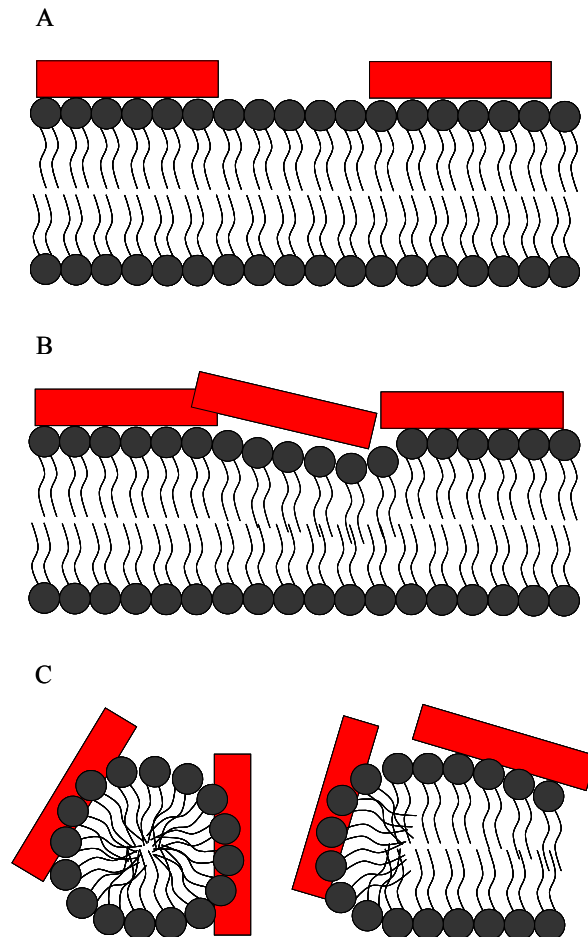


Figure 4. Detergent like model of melittin mode of action. (A) At low concentration the peptide molecules are oriented parallel to the surface of the lipid membrane; (B) increasing the peptide concentration causes aggregation of the peptide molecules and thinning of the membrane; (C) above the threshold concentration peptide molecules inserts into the membrane causing its disintegration into micelles. Peptide molecules are presented as red rectangles, and lipids are shown with dark grey circles as headgroups and wavy hydrocarbon chains.

A clear decision between the various models is not possible at present and the influence of various parameters such as the peptide-to-lipid ratio, membrane composition, temperature, hydration or buffer compositions needs to be considered (29).

Cholesterol, an essential component of eukaryotic membranes, also influences on the activity of melittin. Tryptophan which is present in melittin could potentially form a stable complex with cholesterol. On the other hand the tight lipid packing induced by cholesterol, could reduce the binding affinity of the peptide to membranes.

The erythrocyte membrane, which is the natural target for melittin, is rich in cholesterol. It was shown that cholesterol inhibits the lytic activity of melittin. The concentration of melittin required for 50% lysis was ~3 times lower in cholesterol-depleted erythrocytes, than in case of control erythrocytes. The LD₅₀ for melittin-induced lysis in control erythrocytes was found to be LD₅₀ ≈ 0.67 μM, whereas for cholesterol depleted erythrocytes LD₅₀ was only 0.21 μM (33). These results are in agreement with results obtained with model membranes, which showed that melittin binding and melittin-induced leakage decrease with increasing cholesterol concentration in lipid vesicles (28, 34).

1.3 Activity of Melittin on Cells

Melittin belongs to the larger group of antimicrobial peptides and has broad spectrum of antibacterial activity. It disrupts cell membranes and kills Gram-negative and Gram-positive bacteria in micromolar concentration range.

Melittin is also known for its high lytic activity on the human erythrocytes (2, 35) and other eukaryotic cells. It rapidly binds to human red blood cells already in sub-micromolar concentrations, induces release of hemoglobin, an increase of membrane permeability, and finally lysis of the cells. An apparent dissociation constant, K_d, of 30 nM and the maximum

binding capacity of 1.8×10^7 molecules/cell for melittin binding to the human red blood cells were found (2). Melittin produces lysis of human red blood cells by a colloid osmotic mechanism. In this mechanism damage to the erythrocyte membrane initiates leakage of cations, followed by swelling of the cells and hemolysis. This mechanism is supported by the observation that increased permeability of ions occurs during the first few minutes after the cells are treated with melittin and the release of hemoglobin is secondary to the formation of the lesions (2, 35).

Besides its powerful antimicrobial and lytic activity, melittin exhibits a variety of other biological effects. It is responsible for the non-specific inflammatory response, which is produced by bee venom (36). It was also reported that melittin is a weak allergen in humans (37-39). Melittin reduces the rotational mobility of band 3, which is a major protein component of the human erythrocyte (5, 6, 40). It also causes aggregation of membrane proteins including band 3 (5), bacteriorhodopsin (7) and the Ca^+ -ATPase (8, 41). It was shown that the immobilization and aggregation of these proteins depends on the melittin/protein ratio, not the melittin/lipid ratio, which suggests that melittin could cause these effects via direct interaction with the proteins. A crosslinking of the proteins into larger aggregates is induced by electrostatic interaction between positively charged residues from C-terminus of melittin and the negatively charged residues on membrane proteins.

Melittin is a potent inhibitor of the $(\text{H}^+ + \text{K}^+)$ ATPase (3, 42, 43), the $(\text{Na}^+ + \text{K}^+)$ ATPase (4) and Ca^+ -ATPase (8, 41). Inhibition of the functions of these proteins occurs through direct interaction with the protein. The $(\text{H}^+ + \text{K}^+)$ ATPase contains a binding site for polypeptides which exhibit an amphiphatic helical motif (43). When occupied by melittin this leads to the inhibition of the protein function. In case of the $(\text{Na}^+ + \text{K}^+)$ ATPase it was shown that conformational changes of the protein upon binding of melittin interfere with

the normal conformational changes induced by K^+ and Na^+ , which are required for the function of this pump (4).

Melittin also stimulates the activity of phospholipase A_2 up to about 5-fold, while similar effects could not be observed in the absence of the peptide (9). Melittin can also neutralize the activation of bovine brain phosphodiesterases by calmodulin via complex formation with calmodulin in the presence of Ca^{2+} (44).

The net positive charge and the ability to disrupt lipid membranes make melittin to an ideal candidate as a gene delivery vector. However, because melittin is showing high hemolytic activity, its therapeutic applications are mainly dependent on the development of non-hemolytic analogs. There are number of strategies to overcome the toxic effects of melittin and keep its therapeutic activity. Melittin and melittin analogs can be conjugated to polyethylenimine (PEI), a cationic polymer used in gene transfection. It was shown that melittin-PEI conjugates are non-hemolytic, form stable complexes with DNA and increase gene transfection up to 3 orders of magnitude when compared to unconjugated PEI (45, 46). Dioleoylmelittin is the conjugate formed by covalently coupling melittin to a derivative of dioleoylphosphatidylethanolamine (DOPE). This hybrid molecule binds DNA and form complexes that transfect with a high level of gene expression (47).

This enhanced gene transfer in case of melittin conjugates correlates with an improved endosomal release is connected with ability of melittin to disrupt membrane and thereby facilitate DNA release into the cytoplasm (45, 48).

1.4 Magainin 2 and Nisin Z - Two other Representatives of Antimicrobial Peptides Family

Antimicrobial peptides are large group of the peptides which share several properties. They consist of 12 to 50 amino acid residues, they have a net positive charge, a large proportion of hydrophobic residues and the ability to associate with and disrupt lipid membranes. Magainin 2 and nisin Z are two specific examples which belong to this group.

Magainin 2 is secreted from the skin of the african clawed frog, *Xenopus leavis*. It consists of 23 amino acid residues with a primary structure shown in Figure 5, and has a net positive charge of $z = 4$.



Figure 5. Amino acid sequence of magainin 2 in one letter code. Hydrophobic residues are presented in white, polar residues in grey, positively charged residues in red.

Similar to melittin, magainin 2 has a random coil conformation in aqueous solution, but assumes an α -helical conformation in the presence of lipid membranes. Magainin 2 helix is amphipathic, but, in contrast to melittin, hydrophobic and polar amino acid side chains are separated on opposite faces of the helix (49, 50).

Binding of magainin 2 to lipid membranes causes membrane destabilization and pore formation. The action mechanisms of magainin 2 on the lipid membranes include toroidal pore formation. Magainin 2 has a high affinity for negatively charged lipids and this affinity decreases with decreasing content of negatively charged lipids (51, 52).

Magainin 2 is known for its antimicrobial activity by permeabilizing the bacterial membrane. In contrast to melittin, magainin 2 does not cause lysis of the eukaryotic cells at

its effective antimicrobial concentrations. For example, the IC_{90} of melittin for its antimicrobial activity towards *E.Coli* is $\sim 5 \mu\text{M}$ which is comparable to the concentration required to induce hemolysis in the eukaryotic cells (2, 53). For magainin 2, the IC_{90} value against *E.Coli* bacteria is $\sim 19 \mu\text{M}$ (53), but the hemolysis is not detected up to $150 \mu\text{g/ml}$ (50). Recent studies show that magainin 2 is not toxic on red blood cells even up to $400 \mu\text{g/ml}$ (53).

Nisin Z is a 34 residue peptide produced by the lactic bacteria *Lactococcus lactis* with sequence shown in Figure 6. Because it is not toxic for humans and has high a activity against Gram-positive bacteria, it finds applications as a food preservative.

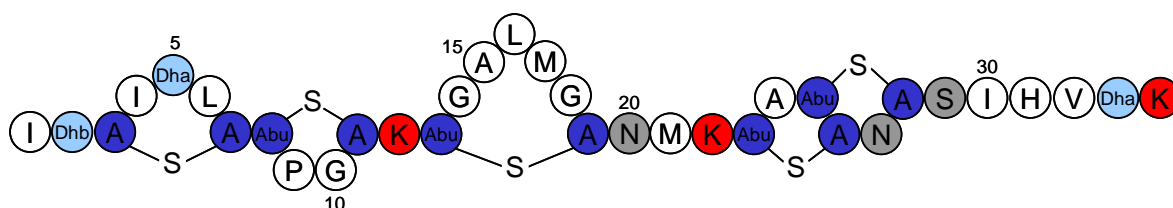


Figure 6. Amino acid sequence of nisin Z in one letter code. Hydrophobic residues are presented in white, polar residues in grey, positively charged residues in red, lanthionine residues in dark blue and dehydrated residues in light blue circles. Dha, dehydroalanine; Dhb, dehydrobutyrine; A-S-A, lanthionine; Abu-S-A, β -methylanthionine [from (54)].

Due to posttranslational modifications nisin Z contains several unusual dehydroresidues and five thioether-bridged lanthionines (54, 55). Nisin Z shares some characteristic with melittin and magainin 2. It has a net positive charge of $z = 4$ and its structure possesses amphiphatic properties.

Nisin Z kills cells by pore formation in the plasma membrane (54). The first step is binding to the target membrane, followed by insertion into the lipids phase leading to pore formation. Nisin Z binds preferably to anionic lipid membranes. It was shown that increase

of an anionic lipid content over 40% cause significant increase in the amount of bound nisin Z (56).

Compared to magainin 2 and melittin, nisin Z kills Gram-positive bacteria already in nanomolar range. This very high activity of nisin Z is due to high affinity of the peptide to Lipid II, a precursor in the bacterial cell wall synthesis. Before insertion of the peptide into the membrane and pore formation, nisin Z binds to Lipid II. The interaction with Lipid II, together with the membrane disturbing properties make nisin Z a powerful antimicrobial agent (54, 57).

1.5 Glycosaminoglycans - Structure, Biosynthesis and Function

Studies on the mechanism of action of melittin have focused almost exclusively on the membrane perturbing properties of this peptide, investigating in detail the melittin-lipid interaction. Melittin carries a net positive charge of $z = 5$ and it can be expected that it not only interacts with lipid membranes but can also bind to polyanions such as sulfate carrying glycosaminoglycans (GAGs) which are found on almost all cell surfaces.

Glycosaminoglycans are highly negatively charged polysaccharides composed almost entirely of repeating disaccharide units. The disaccharide units contain modified sugar moieties, either *N*-actetylgalactosamine or *N*-acetylglucosamine, and uronic acid, such as glucuronate or iduronate. Attached to the protein core (either glypicans or syndecans) they form proteoglycans, which are found on the cell surface of the eukaryotic cells and are involved in cell adhesion, migration, proliferation, differentiation (58, 59).

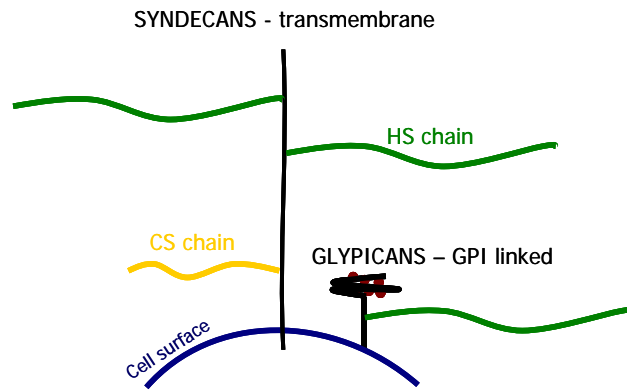


Figure 7. Schematic model of proteoglycans. HS – heparan sulfate, CS – chondroitin sulfate.

Heparan sulfate (HS) and heparin are members of GAG family. These linear polysaccharides vary in length from 30 to 200 disaccharides. The disaccharide unit is built of uronic acid-(1→4)-D-glucosamine repeating disaccharides. Heparin and HS are not molecules with a well-defined sequence of disaccharide units but rather a heterogeneous, polydisperse family of related molecules.

The uronic acid may be present as β -D-glucuronic acid (GlcA) or as the C-5 epimer α -L-iduronic acid (IdoA). Both of them may be 2-O-sulfated (GlcA(2S) and IdoA(2S)). The β -D-glucosamine (GlcN) may be either N-sulfated (GlcNS) or N-acetylated (GlcNAc), both of them may be 6-O-sulfated (GlcNS(6S) and GlcNAc(6S)). The N-sulfated glucosamine may be also 3-O-sulfated (GlcNS(3S) and GlcNS(3,6S)). The different patterns of the monosaccharide substitution give rise to a large number of complex primary sequences.

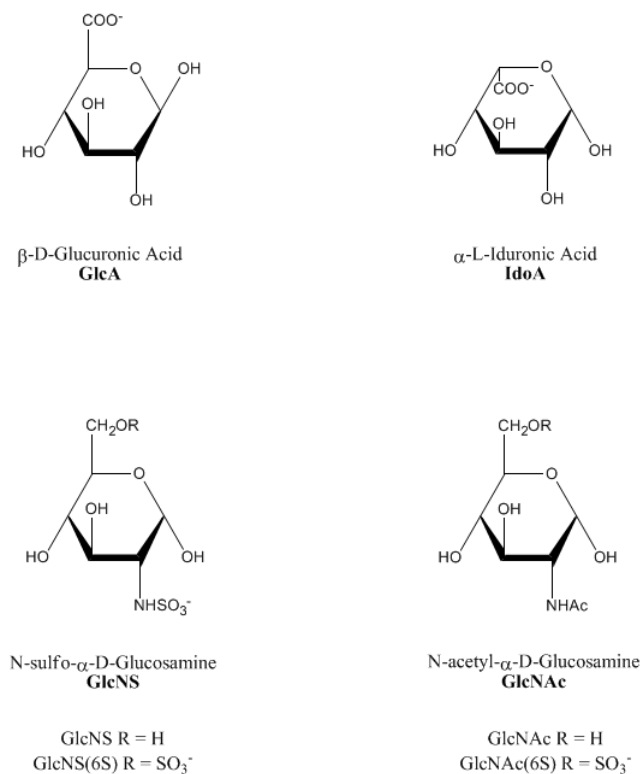


Figure 8. Monosaccharides building blocks for HS and heparin [from (59)].

HS and heparin contain the same repeating disaccharide units. The units are present in different proportions, so that their primary structure differs significantly from each other. IdoA(2S)-(1→4)-GlcNS(6S) is the most abundant disaccharide unit of heparin. The GlcA/IdoA and GlcNAc/GlcNS ratios are higher, but the sulfates content is lower in HS than in heparin. HS has a domain structure, with NA domains, heparin-like NS domains, and NA/NS transition segments. The NA domain is built from repeating GlcA-(1→4)-GlcNAc disaccharides and this domain is not sulfated. Highly sulfated NS domains are the IdoA-(1→4)-GlcNS disaccharides units. These two domains are separated by segments consist of GlcNAc- and GlcNS-containing disaccharides. Also common for HS is the observation that all chains contain approximately equal concentrations of acetylated and sulfated disaccharides (59-61).

NMR spectroscopy and molecular modeling methods (62-65) are often employed to determine the three-dimensional structure of heparin and HS. The overall conformation is mainly determined by torsion angles of the glycosidic bonds that link the monosaccharides and the conformation of the monosaccharides. It was shown that the pyranose rings of GlcA and GlcN are in the rigid 4C_1 chair conformation. The pyranose ring of IdoA is more flexible, having the ability to adopt multiply low-energy conformations such as 1C_4 , 4C_1 , 2S_0 , 0C_2 (66, 67). Heparin and HS do not fold into structures resembling the tertiary structure of proteins, but they adopt structures that have spatially defined patterns of anionic groups for the interaction with proteins (68, 69).

HS and heparin are synthesized as HS/heparin proteoglycans. The polysaccharide chain is synthesized as non-sulfated precursor by sequential addition of GlcNAc and GlcA to a core protein primed by a tetrasacchride acceptor attached through xylose to specific serine residues. Transformation of the synthesized polymer chains starts with replacement of the acetyl groups of GlcNAc monosaccharides with sulfate groups. This deacetylation and sulfation is initiated at random sites on the polymer chains, and then continues along the chain. The modification also involves conversion of GlcA into IdoA and sulfation at various sites. In heparin, modification of the polymer chains are far more extensive than in HS and heparin lacks both the distinctive domain structure of HS (NA/NS transition segment) and the core acetylated sequence (NA domain). The number of O-sulfated groups is more variable in HS than in heparin, in the range of 0.2-0.7 O-sulfates per disaccharide, whereas for heparin an average is 2.4 O-sulfates per disaccharide.

The synthesis of HS and heparin is regulated by set of enzymes, including transferases, sulfotransferases and epimerases, which are arrayed in the Golgi apparatus (58). Upon conclusion of the synthesis and the modifications membrane associated HS/heparin proteoglycans are rapidly transferred to the cell surface or extracellular matrix (70). The scheme of HS biosynthesis is shown in Figure 9.

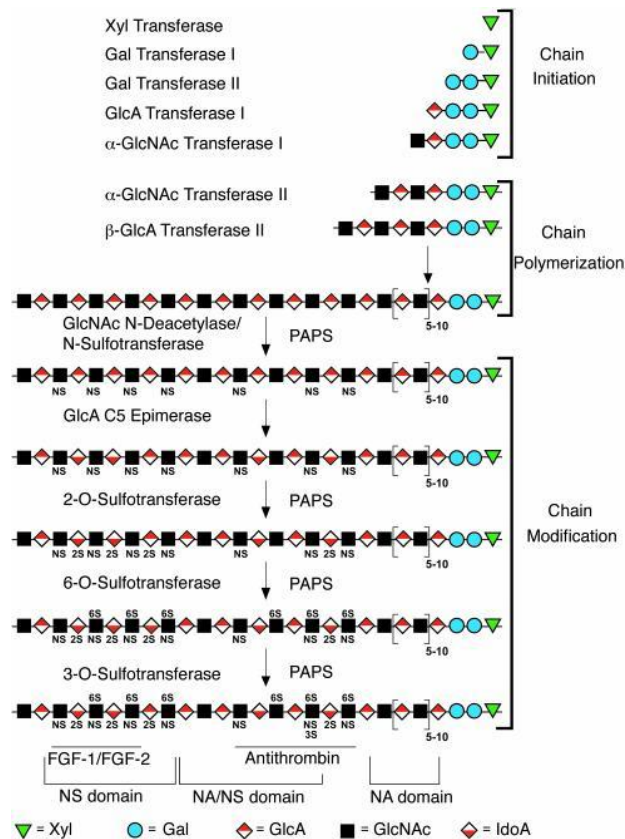


Figure 9. Scheme of HS chain biosynthesis. Xyl-xylose; Gal-galactose; GlcA-glucuronic acid; GlcNAc-N-acetylated glucosamine; IdoA-iduronic acid. Regions that have been implicated in binding of specific ligands, such as FGF-1/FGF-2 and antithrombin are show. Taken from (58).

HS is expressed and secreted by most of the mammalian cells. HS is located on the cell surface and in the extracellular matrix. It has a wide range of activities and functions, including cell adhesion (71), regulation of cellular growth and proliferation, developmental processes (72), and blood coagulation (73). HS interacts with basic fibroblast growth factor (bFGF), other proteins from this family and their receptor tyrosine kinase (74), transforming growth factors (TGFs), bone morphogenetic proteins (BMPs) (75), chemokines, interleukins, enzymes and enzymes inhibitors, lipases and apolipoproteins (76, 77), plasma proteins and others (78, 79). It is involved in the internalization of viruses (80, 81), basic peptides and polycation-nucleic acid complexes (82), as well as in

angiogenesis (83) and tumor metastasis (84). All of these processes involve interaction between HS and proteins.

Heparin is found only in the secretory granules of mast cells and is released during the inflammatory degranulation reactions (85, 86). Heparin is mainly used clinically as an anticoagulant. It was shown that it binds hundreds of proteins. Since it is found only in secretory granules of mast cells, its physiological significance has been questioned. However, there is increasing interest in the characterization of the interaction of heparin with proteins, because of its potential use in therapy, e.g. as modulation of angiogenesis (87), tumor metastasis(88) and viral invasion (89, 90). Also, binding of heparin to proteins can be used as a model for the interaction of highly sulfated domains of HS chains with different proteins and peptides.

1.6 Interaction of HS and Heparin with Proteins and Peptides

HS and heparin interact with a large variety of different proteins. These interactions are primarily driven by electrostatic interactions and they involve interactions between anionic groups of the polysaccharides with positively charged residues of the proteins and peptides. HS and heparin have highly negative charge densities and they behave as polyelectrolytes in solution. According to polyelectrolyte theory, considerable fraction of these highly charged poly-anions is neutralized by Na^+ due to counterion condensation (91). Upon binding of the peptides and proteins with HS, there is a release of Na^+ counterions from the polysaccharides. The binding reactions between HS and proteins are ion exchange processes with the cationic residues of the bound peptides and proteins serving as counterions.

It was shown that HS/heparin interact electrostatically with short charged peptides, BNP (92), HIP peptide (93), bFGF (94), LPL (95). The dissociation constants, K_d , range from 0.3 nM (LPL) over 0.5 μ M (bFGF) to 43 μ M (HIP). Salt dependence studies confirm that electrostatic interactions are involved in the binding process. The binding affinity decreases with increasing salt concentration as predicted by polyelectrolyte theory. The ionic contribution to the binding process can be calculated (91, 96). In all cases it was however shown that the binding interactions are not purely electrostatic, but they comprised also a nonionic component.

The spatial arrangement of the positive charged residues also plays a role in binding of the peptides and proteins to HS/heparin. In the case of HIP peptide, the all D-peptide with the same sequence binds equally well and is equally effective, while the peptide with scrambled HIP peptide sequence had no effect.

It was also shown in model experiments that that lysine binds distinctly less to heparin than does arginine (97). Similar results were obtained for the interaction with HS (98). Likewise, histidine does not contribute significantly to the binding of the peptides to HS. This suggests that arginines could promote a tighter interaction with glycosaminoglycans than lysine and histidine (97, 98).

1.7 Literature

1. Habermann, E. (1972) Bee and wasp venoms. *Science* 177, 314-22.
2. Tosteson, M. T., Holmes, S. J., Razin, M., and Tosteson, D. C. (1985) Melittin lysis of red cells. *J Membr Biol* 87, 35-44.

3. Cuppoletti, J., Blumenthal, K. M., and Malinowska, D. H. (1989) Melittin inhibition of the gastric (H⁺ + K⁺) ATPase and photoaffinity labeling with [125I]azidosalicylyl melittin. *Arch Biochem Biophys* 275, 263-70.
4. Cuppoletti, J., and Abbott, A. J. (1990) Interaction of melittin with the (Na⁺ + K⁺)ATPase: evidence for a melittin-induced conformational change. *Arch Biochem Biophys* 283, 249-57.
5. Clague, M. J., and Cherry, R. J. (1988) Comparison of p25 presequence peptide and melittin. Red blood cell haemolysis and band 3 aggregation. *Biochem J* 252, 791-4.
6. Dufton, M. J., Hider, R. C., and Cherry, R. J. (1984) The influence of melittin on the rotation of band 3 protein in the human erythrocyte membrane. *Eur Biophys J* 11, 17-24.
7. Hu, K. S., Dufton, M. J., Morrison, I. E., and Cherry, R. J. (1985) Protein rotational diffusion measurements on the interaction of bee venom melittin with bacteriorhodopsin in lipid vesicles. *Biochim Biophys Acta* 816, 358-64.
8. Mahaney, J. E., and Thomas, D. D. (1991) Effects of melittin on molecular dynamics and Ca-ATPase activity in sarcoplasmic reticulum membranes: electron paramagnetic resonance. *Biochemistry* 30, 7171-80.
9. Mollay, C., and Kreil, G. (1974) Enhancement of bee venom phospholipase A2 activity by melittin, direct lytic factor from cobra venom and polymyxin B. *FEBS Lett* 46, 141-4.
10. Dempsey, C. E. (1990) The actions of melittin on membranes. *Biochim Biophys Acta* 1031, 143-61.
11. Terwilliger, T. C., and Eisenberg, D. (1982) The structure of melittin. II. Interpretation of the structure. *J Biol Chem* 257, 6016-22.
12. Vogel, H. (1981) Incorporation of melittin into phosphatidylcholine bilayers. Study of binding and conformational changes. *FEBS Lett* 134, 37-42.

13. Bello, J., Bello, H. R., and Granados, E. (1982) Conformation and aggregation of melittin: dependence on pH and concentration. *Biochemistry* 21, 461-5.
14. Quay, S. C., and Condie, C. C. (1983) Conformational studies of aqueous melittin: thermodynamic parameters of the monomer-tetramer self-association reaction. *Biochemistry* 22, 695-700.
15. Wilcox, W., and Eisenberg, D. (1992) Thermodynamics of melittin tetramerization determined by circular dichroism and implications for protein folding. *Protein Sci* 1, 641-53.
16. Knoppel, E., Eisenberg, D., and Wickner, W. (1979) Interactions of melittin, a preprotein model, with detergents. *Biochemistry* 18, 4177-81.
17. Berneche, S., Nina, M., and Roux, B. (1998) Molecular dynamics simulation of melittin in a dimyristoylphosphatidylcholine bilayer membrane. *Biophys J* 75, 1603-18.
18. Beschiaschvili, G., and Seelig, J. (1990) Melittin binding to mixed phosphatidylglycerol/phosphatidylcholine membranes. *Biochemistry* 29, 52-8.
19. Dempsey, C., Bitbol, M., and Watts, A. (1989) Interaction of melittin with mixed phospholipid membranes composed of dimyristoylphosphatidylcholine and dimyristoylphosphatidylserine studied by deuterium NMR. *Biochemistry* 28, 6590 - 6596.
20. Glattli, A., Chandrasekhar, I., and Gunsteren, W. F. (2006) A molecular dynamics study of the bee venom melittin in aqueous solution, in methanol, and inserted in a phospholipid bilayer. *Eur Biophys J* 35, 255-67.
21. Kuchinka, E., and Seelig, J. (1989) Interaction of melittin with phosphatidylcholine membranes. Binding isotherm and lipid head-group conformation. *Biochemistry* 28, 4216-21.

22. Papo, N., and Shai, Y. (2003) Exploring peptide membrane interaction using surface plasmon resonance: differentiation between pore formation versus membrane disruption by lytic peptides. *Biochemistry* 42, 458-66.
23. Yang, L., Harroun, T. A., Weiss, T. M., Ding, L., and Huang, H. W. (2001) Barrel-stave model or toroidal model? A case study on melittin pores. *Biophys J* 81, 1475-85.
24. Batenburg, A. M., van Esch, J. H., and de Kruijff, B. (1988) Melittin-induced changes of the macroscopic structure of phosphatidylethanolamines. *Biochemistry* 27, 2324-31.
25. Katsu, T., Ninomiya, C., Kuroko, M., Kobayashi, H., Hirota, T., and Fujita, Y. (1988) Action mechanism of amphipathic peptides gramicidin S and melittin on erythrocyte membrane. *Biochim Biophys Acta* 939, 57-63.
26. Ladokhin, A. S., Selsted, M. E., and White, S. H. (1997) Sizing membrane pores in lipid vesicles by leakage of co-encapsulated markers: pore formation by melittin. *Biophys J* 72, 1762-6.
27. Rex, S., and Schwarz, G. (1998) Quantitative studies on the melittin-induced leakage mechanism of lipid vesicles. *Biochemistry* 37, 2336-45.
28. Allende, D., Simon, S. A., and McIntosh, T. J. (2005) Melittin-induced bilayer leakage depends on lipid material properties: evidence for toroidal pores. *Biophys J* 88, 1828-37.
29. Bechinger, B., and Lohner, K. (2006) Detergent-like actions of linear amphipathic cationic antimicrobial peptides. *Biochim Biophys Acta* 1758, 1529-39.
30. Ladokhin, A. S., and White, S. H. (2001) 'Detergent-like' permeabilization of anionic lipid vesicles by melittin. *Biochim Biophys Acta*. 1514, 253-60.
31. Monette, M., and Lafleur, M. (1995) Modulation of melittin-induced lysis by surface charge density of membranes. *Biophys J* 68, 187-95.

32. Shai, Y. (2002) Mode of action of membrane active antimicrobial peptides. *Biopolymers* 66, 236-48.
33. Raghuraman, H., and Chattopadhyay, A. (2005) Cholesterol inhibits the lytic activity of melittin in erythrocytes. *Chem Phys Lipids* 134, 183-9.
34. Raghuraman, H., and Chattopadhyay, A. (2004) Interaction of melittin with membrane cholesterol: a fluorescence approach. *Biophys J* 87, 2419-32.
35. DeGrado, W. F., Musso, G. F., Lieber, M., Kaiser, E. T., and Kezdy, F. J. (1982) Kinetics and mechanism of hemolysis induced by melittin and by a synthetic melittin analogue. *Biophys J* 37, 329-38.
36. Mackler, B. F., and Kreil, G. (1977) Honey bee venom melittin: correlation of nonspecific inflammatory activities with amino acid sequences. *Inflammation* 2, 55-65.
37. Hoffman, D. R., and Shipman, W. H. (1976) Allergens in bee venom. I. Separation and identification of the major allergens. *J Allergy Clin Immunol* 58, 551-62.
38. Paull, B. R., Yunginger, J. W., and Gleich, G. J. (1977) Melittin: an allergen of honeybee venom. *J Allergy Clin Immunol* 59, 334-8.
39. Sobotka, A. K., Franklin, R. M., Adkinson, N. F., Jr., Valentine, M., Baer, H., and Lichtenstein, L. M. (1976) Allergy to insect stings. II. Phospholipase A: the major allergen in honeybee venom. *J Allergy Clin Immunol* 57, 29-40.
40. Clague, M. J., and Cherry, R. J. (1989) A comparative study of band 3 aggregation in erythrocyte membranes by melittin and other cationic agents. *Biochim Biophys Acta* 980, 93-9.
41. Voss, J., Birmachu, W., Hussey, D. M., and Thomas, D. D. (1991) Effects of melittin on molecular dynamics and Ca-ATPase activity in sarcoplasmic reticulum membranes: time-resolved optical anisotropy. *Biochemistry* 30, 7498-506.

42. Cuppoletti, J. (1990) [125I]azidosalicylyl melittin binding domains: evidence for a polypeptide receptor on the gastric (H⁺ + K⁺)ATPase. *Arch Biochem Biophys* 278, 409-15.
43. Cuppoletti, J., and Malinowska, D. H. (1992) Interaction of polypeptides with the gastric (H⁺ + K⁺)ATPase: melittin, synthetic analogs, and a potential intracellular regulatory protein. *Mol Cell Biochem* 114, 57-63.
44. Comte, M., Maulet, Y., and Cox, J. A. (1983) Ca²⁺-dependent high-affinity complex formation between calmodulin and melittin. *Biochem J* 209, 269-72.
45. Boeckle, S., Wagner, E., and Ogris, M. (2005) C- versus N-terminally linked melittin-polyethylenimine conjugates: the site of linkage strongly influences activity of DNA polyplexes. *J Gene Med* 7, 1335-47.
46. Boeckle, S., Fahrmeir, J., Roedl, W., Ogris, M., and Wagner, E. (2006) Melittin analogs with high lytic activity at endosomal pH enhance transfection with purified targeted PEI polyplexes. *J Control Release* 112, 240-8.
47. Legendre, J. Y., Trzeciak, A., Bohrmann, B., Deuschle, U., Kitas, E., and Supersaxo, A. (1997) Dioleoylmelittin as a novel serum-insensitive reagent for efficient transfection of mammalian cells. *Bioconjug Chem* 8, 57-63.
48. Ogris, M., Carlisle, R. C., Bettinger, T., and Seymour, L. W. (2001) Melittin enables efficient vesicular escape and enhanced nuclear access of nonviral gene delivery vectors. *J Biol Chem* 276, 47550-5.
49. Bechinger, B. (1997) Structure and functions of channel-forming peptides: magainins, cecropins, melittin and alamethicin. *J Membr Biol* 156, 197-211.
50. Zasloff, M. (1987) Magainins, a class of antimicrobial peptides from *Xenopus* skin: isolation, characterization of two active forms, and partial cDNA sequence of a precursor. *Proc Natl Acad Sci U S A* 84, 5449-53.

51. Wenk, M. R., and Seelig, J. (1998) Magainin 2 amide interaction with lipid membranes: calorimetric detection of peptide binding and pore formation. *Biochemistry* 37, 3909-16.
52. Wieprecht, T., Beyermann, M., and Seelig, J. (1999) Binding of antibacterial magainin peptides to electrically neutral membranes: thermodynamics and structure. *Biochemistry* 38, 10377-87.
53. Maher, S., and McClean, S. (2006) Investigation of the cytotoxicity of eukaryotic and prokaryotic antimicrobial peptides in intestinal epithelial cells in vitro. *Biochem Pharmacol* 71, 1289-98.
54. Breukink, E., and de Kruijff, B. (1999) The lantibiotic nisin, a special case or not? *Biochim Biophys Acta* 1462, 223-34.
55. Breukink, E., Ganz, P., de Kruijff, B., and Seelig, J. (2000) Binding of Nisin Z to bilayer vesicles as determined with isothermal titration calorimetry. *Biochemistry* 39, 10247-54.
56. Breukink, E., van Kraaij, C., Demel, R. A., Siezen, R. J., Kuipers, O. P., and de Kruijff, B. (1997) The C-terminal region of nisin is responsible for the initial interaction of nisin with the target membrane. *Biochemistry* 36, 6968-76.
57. Breukink, E., Wiedemann, I., van Kraaij, C., Kuipers, O. P., Sahl, H., and de Kruijff, B. (1999) Use of the cell wall precursor lipid II by a pore-forming peptide antibiotic. *Science* 286, 2361-4.
58. Esko, J. D., and Lindahl, U. (2001) Molecular diversity of heparan sulfate. *J Clin Invest* 108, 169-73.
59. Rabenstein, D. L. (2002) Heparin and heparan sulfate: structure and function. *Nat Prod Rep* 19, 312-31.

60. Gallagher, J. T., Turnbull, J. E., and Lyon, M. (1992) Patterns of sulphation in heparan sulphate: polymorphism based on a common structural theme. *Int J Biochem* 24, 553-60.
61. Gallagher, J. T., and Walker, A. (1985) Molecular distinctions between heparan sulphate and heparin. Analysis of sulphation patterns indicates that heparan sulphate and heparin are separate families of N-sulphated polysaccharides. *Biochem J* 230, 665-74.
62. Ferro, D. R., Gajdos, J., Ragazzi, M., Ungarelli, F., and Piani, S. (1995) Conformational analysis of heparin epoxide: molecular mechanics computations. *Carbohydr Res* 277, 25-8.
63. Ferro, D. R., Provasoli, A., Ragazzi, M., Casu, B., Torri, G., Bossennec, V., Perly, B., Sinay, P., Petitou, M., and Choay, J. (1990) Conformer populations of L-iduronic acid residues in glycosaminoglycan sequences. *Carbohydr Res* 195, 157-67.
64. Ferro, D. R., Pumilia, A., and Ragazzi, M. (1997) An improved force field for conformational analysis of sulfated polysaccharides. *J Comp Chem* 18, 351-367.
65. Mulloy, B., Forster, M. J., Jones, C., and Davies, D. B. (1993) N.m.r. and molecular-modelling studies of the solution conformation of heparin. *Biochem J* 293 (Pt 3), 849-58.
66. Ernst, S., Venkataraman, G., Sasisekharan, V., Langer, R., Cooney, C. L., and Sasisekharan, R. (1998) Pyranose ring flexibility. Mapping of physical data for iduronate in continuous conformational space. *J Am Chem Soc* 120, 2099-2107.
67. Mulloy, B., and Forster, M. J. (2000) Conformation and dynamics of heparin and heparan sulfate. *Glycobiology* 10, 1147-56.

68. Fromm, J. R., Hileman, R. E., Caldwell, E. E., Weiler, J. M., and Linhardt, R. J. (1997) Pattern and spacing of basic amino acids in heparin binding sites. *Arch Biochem Biophys* 343, 92-100.
69. Margalit, H., Fischer, N., and Ben-Sasson, S. A. (1993) Comparative analysis of structurally defined heparin binding sequences reveals a distinct spatial distribution of basic residues. *J Biol Chem* 268, 19228-31.
70. Yanagishita, M., and Hascall, V. C. (1992) Cell surface heparan sulfate proteoglycans. *J Biol Chem* 267, 9451-4.
71. Lindahl, U., Lidholt, K., Spillmann, D., and Kjellen, L. (1994) More to "heparin" than anticoagulation. *Thromb Res* 75, 1-32.
72. Perrimon, N., and Bernfield, M. (2000) Specificities of heparan sulphate proteoglycans in developmental processes. *Nature* 404, 725-8.
73. Marcum, J. A., McKenney, J. B., Galli, S. J., Jackman, R. W., and Rosenberg, R. D. (1986) Anticoagulant active heparin-like molecules from mast cell-deficient mice. *Am J Physiol* 250, H879-88.
74. Mohammadi, M., Olsen, S. K., and Ibrahimi, O. A. (2005) Structural basis for fibroblast growth factor receptor activation. *Cytokine Growth Factor Rev* 16, 107-37.
75. Kram, V., Zcharia, E., Yacoby-Zeevi, O., Metzger, S., Chajek-Shaul, T., Gabet, Y., Muller, R., Vlodavsky, I., and Bab, I. (2006) Heparanase is expressed in osteoblastic cells and stimulates bone formation and bone mass. *J Cell Physiol* 207, 784-92.
76. Cheng, C. F., Oosta, G. M., Bensadoun, A., and Rosenberg, R. D. (1981) Binding of lipoprotein lipase to endothelial cells in culture. *J Biol Chem* 256, 12893-8.

77. Shimada, K., Gill, P. J., Silbert, J. E., Douglas, W. H., and Fanburg, B. L. (1981) Involvement of cell surface heparin sulfate in the binding of lipoprotein lipase to cultured bovine endothelial cells. *J Clin Invest* 68, 995-1002.
78. Taipale, J., and Keski-Oja, J. (1997) Growth factors in the extracellular matrix. *Faseb J* 11, 51-9.
79. Tumova, S., Woods, A., and Couchman, J. R. (2000) Heparan sulfate proteoglycans on the cell surface: versatile coordinators of cellular functions. *Int J Biochem Cell Biol* 32, 269-88.
80. Chen, Y., Maguire, T., Hileman, R. E., Fromm, J. R., Esko, J. D., Linhardt, R. J., and Marks, R. M. (1997) Dengue virus infectivity depends on envelope protein binding to target cell heparan sulfate. *Nat Med* 3, 866-71.
81. Shukla, D., Liu, J., Blaiklock, P., Shworak, N. W., Bai, X., Esko, J. D., Cohen, G. H., Eisenberg, R. J., Rosenberg, R. D., and Spear, P. G. (1999) A novel role for 3-O-sulfated heparan sulfate in herpes simplex virus 1 entry. *Cell* 99, 13-22.
82. Derossi, D., Chassaing, G., and Prochiantz, A. (1998) Trojan peptides: the penetratin system for intracellular delivery. *Trends Cell Biol* 8, 84-7.
83. Sasisekharan, R., Ernst, S., and Venkataraman, G. (1997) On the regulation of fibroblast growth factor activity by heparin-like glycosaminoglycans. *Angiogenesis* 1, 45-54.
84. Hulett, M. D., Freeman, C., Hamdorf, B. J., Baker, R. T., Harris, M. J., and Parish, C. R. (1999) Cloning of mammalian heparanase, an important enzyme in tumor invasion and metastasis. *Nat Med* 5, 803-9.
85. Humphries, D. E., Wong, G. W., Friend, D. S., Gurish, M. F., Qiu, W. T., Huang, C., Sharpe, A. H., and Stevens, R. L. (1999) Heparin is essential for the storage of specific granule proteases in mast cells. *Nature* 400, 769-72.

86. Zehnder, J. L., and Galli, S. J. (1999) Mast-cell heparin demystified. *Nature* 400, 714-5.
87. Folkman, J., and Shing, Y. (1992) Control of angiogenesis by heparin and other sulfated polysaccharides. *Adv Exp Med Biol* 313, 355-64.
88. Parish, C. R., Freeman, C., Brown, K. J., Francis, D. J., and Cowden, W. B. (1999) Identification of sulfated oligosaccharide-based inhibitors of tumor growth and metastasis using novel in vitro assays for angiogenesis and heparanase activity. *Cancer Res* 59, 3433-41.
89. Herold, B. C., Gerber, S. I., Polonsky, T., Belval, B. J., Shaklee, P. N., and Holme, K. (1995) Identification of structural features of heparin required for inhibition of herpes simplex virus type 1 binding. *Virology* 206, 1108-16.
90. Rider, C. C., Coombe, D. R., Harrop, H. A., Hounsell, E. F., Bauer, C., Feeney, J., Mulloy, B., Mahmood, N., Hay, A., and Parish, C. R. (1994) Anti-HIV-1 activity of chemically modified heparins: correlation between binding to the V3 loop of gp120 and inhibition of cellular HIV-1 infection in vitro. *Biochemistry* 33, 6974-80.
91. Manning, G. S. (1978) The molecular theory of polyelectrolyte solutions with applications to the electrostatic properties of polynucleotides. *Q Rev Biophys* 11, 179-246.
92. Hileman, R. E., Jennings, R. N., and Linhardt, R. J. (1998) Thermodynamic analysis of the heparin interaction with a basic cyclic peptide using isothermal titration calorimetry. *Biochemistry* 37, 15231-7.
93. Liu, S., Zhou, F., Hook, M., and Carson, D. D. (1997) A heparin-binding synthetic peptide of heparin/heparan sulfate-interacting protein modulates blood coagulation activities. *Proc Natl Acad Sci U S A* 94, 1739-44.

-
94. Thompson, L. D., Pantoliano, M. W., and Springer, B. A. (1994) Energetic characterization of the basic fibroblast growth factor-heparin interaction: identification of the heparin binding domain. *Biochemistry* 33, 3831-40.
 95. Lookene, A., Chevreuil, O., Ostergaard, P., and Olivecrona, G. (1996) Interaction of lipoprotein lipase with heparin fragments and with heparan sulfate: stoichiometry, stabilization, and kinetics. *Biochemistry* 35, 12155-63.
 96. Record, M. T., Jr., Anderson, C. F., and Lohman, T. M. (1978) Thermodynamic analysis of ion effects on the binding and conformational equilibria of proteins and nucleic acids: the roles of ion association or release, screening, and ion effects on water activity. *Q Rev Biophys* 11, 103-78.
 97. Fromm, J. R., Hileman, R. E., Caldwell, E. E., Weiler, J. M., and Linhardt, R. J. (1995) Differences in the interaction of heparin with arginine and lysine and the importance of these basic amino acids in the binding of heparin to acidic fibroblast growth factor. *Arch Biochem Biophys* 323, 279-87.
 98. Caldwell, E. E., Nadkarni, V. D., Fromm, J. R., Linhardt, R. J., and Weiler, J. M. (1996) Importance of specific amino acids in protein binding sites for heparin and heparan sulfate. *Int J Biochem Cell Biol* 28, 203-16.

2. AIM OF RESEARCH

Melittin is a short cationic peptide with cytolytic and antimicrobial properties. Studies on the action mechanism of melittin have focused almost exclusively on the membrane perturbing properties of this peptide, investigating in detail the melittin-lipid interaction. Although extensive of studies the molecular mechanism of action of melittin is not completely established.

In the present work we focused on an alternative mechanism of action of melittin on the cell membranes. As melittin carries a net positive charge of $z = 5$ it can be expected that it not only interacts with lipid membranes but can also bind to polyanions such as sulphate carrying glycosaminoglycans (GAGs) which are found on almost all cell surfaces. The melittin-GAG interaction could initiate cell lysis enhancing the melittin-lipid interaction.

The first step of this work was to investigate if melittin exhibits any affinity to GAGs. We used high-sensitivity isothermal titration calorimetry (ITC) to obtain a complete thermodynamic characterization of melittin binding to three different GAGs, namely heparan sulfate, heparin and dermatan sulfate. The structural changes of melittin induced by binding to these polyanions were followed by circular dichroism (CD) spectroscopy. In addition, right-angle static light-scattering and dynamic light-scattering were employed, to gain information about size and the polydispersity of aggregates/complexes which are formed upon melittin-HS interaction. We wanted also to compare the specificity of melittin binding to GAGs to analogous measurements with magainin 2 and nisin Z, two amphiphatic and antimicrobial peptides with similar lipid binding properties as melittin. Magainin 2 is known of its antimicrobial properties, but in contrast to melittin does not cause lysis of eukaryotic cells. Nisin Z shows activity against various Gram-positive bacteria. With this study we wanted to answer the question if the interaction with GAGs is general property of antimicrobial peptides or is just unique for melittin.

Once the thermodynamic data of the melittin-GAG equilibrium were established, it was interesting to investigate the cytotoxic effect of melittin on cells, which lack GAGs on the surface. For this purpose a pgsA-745 cell line defective in the biosynthesis of GAGs was used. PgsA-745 cells are deficient in xylosyltransferase, the enzyme responsible for the initiation of chondroitin sulfate and heparan sulfate biosynthesis *in vivo*. This mutant cell line does not produce GAGs. As a control CHO K1 (Chinese hamster ovary cells), a corresponding wild-type cell line, was employed.

In the last part of this work, we describe the interaction of retro-inverso dioleoylmelittin (riDOM) with HS. RiDOM is a hybrid molecule, obtained by covalently coupling of retro-inverso analog of melittin to a lipid moiety, to form a stable and efficient gene transfer system, which shows no haemolytic activity. The net positive charge of this conjugate, suggest that similarly to other cationic lipids and cell-penetrating peptides, the cellular uptake is mediated by GAGs. Again we used ITC to characterize the thermodynamic equilibrium between riDOM and HS and CD spectroscopy to follow the conformational changes upon binding of riDOM to HS. Dynamic light-scattering measurement provided the information about size and polydispersity of the aggregates/complexes.

Furthermore, we use ITC to describe binding of melittin to large unilamellar lipid vesicles as there are yet only few thermodynamic parameters of the interaction between melittin and lipid vesicles.

Manuscript accepted for publication by *Biochemistry*.

3. Melittin Interaction with Sulfated Cell Surface Sugars[†]

Gabriela Klocek and Joachim Seelig*

Department of Biophysical Chemistry, Biozentrum, University of Basel,
Klingelbergstrasse 50/70, CH-4056 Basel, Switzerland

* To whom correspondence should be addressed:

Tel: +41-61-267 2190, Fax: +41-61-267 2189, e-mail: joachim.seelig@unibas.ch

[†] Supported by the Swiss National Science Foundation Grant# 3100-107793

Running title: Interaction of melittin with heparan sulfate

Keywords: Melittin, heparan sulfate, heparin, dermatan sulfate, isothermal titration calorimetry

ABBREVIATIONS

DS, dermatan sulfate

HS, heparan sulfate

GAG, glycosaminoglycan

ITC, isothermal titration calorimetry

CD, circular dichroism spectroscopy

CHO, Chinese hamster ovary

ABSTRACT

Melittin is a 26-residue cationic peptide with cytolytic and antimicrobial properties. Studies on the action mechanism of melittin have focused almost exclusively on the membrane perturbing properties of this peptide, investigating in detail the melittin-lipid interaction. Here we report physical-chemical studies on an alternative mechanism by which melittin could interact with the cell membrane. As the outer surface of many cells is decorated with anionic (sulfated) glycosaminoglycans (GAGs), a strong coulombic interaction between the two oppositely charged molecules can be envisaged. Indeed, the present study using isothermal titration calorimetry reveals a high affinity of melittin for several GAGs, i.e. heparan sulfate (HS), dermatan sulfate, and heparin. The microscopic binding constant of melittin for HS is $2.4 \times 10^5 \text{ M}^{-1}$, the reaction enthalpy is $\Delta H_{\text{melittin}}^0 = -1.50 \text{ kcal/mol}$ and the peptide-to-HS stoichiometry is ~ 11 at 10 mM Tris, 100 mM NaCl, pH 7.4 and 28 °C. $\Delta H_{\text{melittin}}^0$ is characterized by a molar heat capacity of $\Delta C_p^0 = -227 \text{ cal mol}^{-1} \text{ K}^{-1}$. The large negative heat capacity change indicates that hydrophobic interactions must also be involved in the binding of melittin to HS. Circular dichroism spectroscopy demonstrates that the binding of the peptide to HS induces a conformational change to a predominantly α -helical structure. A model for the melittin-HS complex is presented. Melittin binding was compared with that of magainin 2 and nisin Z to HS. Magainin 2 is known for its antimicrobial properties, but does not cause lysis of the eukaryotic cells. Nisin Z shows activity against various Gram-positive bacteria. Isothermal titration calorimetry demonstrates that magainin 2 and nisin Z do not bind to HS (5-50 °C, 10 mM Tris, 100 mM NaCl, pH 7.4).

Melittin is the major protein component of the bee venom of the honey bee *Apis Melifera* and has hemolytic activity and antimicrobial properties (1, 2). Melittin is composed of 26 amino acid residues with the sequence H₂N-GIGAVLKVLTTGLPALISWIKRKRQQ-CONH₂. It is a cationic peptide in which the amino-terminal end is composed predominantly of hydrophobic amino acids (residues 1-20), whereas the carboxyl-terminal end has a stretch of mostly hydrophilic amino acids (residues 21-26). This uneven distribution of hydrophobic and polar residues gives melittin its amphipathic properties. Melittin is water soluble and exhibits strong affinity to lipid membranes. It is largely unstructured in water, but forms an α -helix upon binding to lipid membranes (3). Melittin is very sensitive to the solution conditions and can adopt different conformations and aggregation states in aqueous solution. At low peptide concentration and low ionic strength melittin occurs as a monomer with a mostly random coil conformation. When the peptide concentration and/or the salt concentration are increased, melittin aggregates into a tetramer with a high content of α -helix structure (4-6).

The interaction of melittin with the lipid membrane has been investigated extensively, both experimentally and theoretically (7-13). The various of studies show that the interaction depends on the lipid composition, the peptide concentration, the hydration level, and the membrane potential (14). The affinity of melittin is larger for membranes composed of negatively charged lipids than for zwitterionic lipids, indicating that hydrophobic as well as electrostatic interactions are involved in the binding of melittin to membranes (8, 15).

Two different action mechanisms have been proposed for the hemolytic activity of melittin. In one model melittin acts on the lipid membrane through pore formation. Some studies envisage a barrel-stave mechanism (16-18), others suggest the formation of toroidal pores (13, 19). The alternative 'detergent-like' model assumes that melittin behaves much as a detergent. At low concentrations of peptide, the molecules are oriented parallel to the surface of the bilayer. Increase of the peptide concentration causes aggregation and

reduction of the bilayer thickness. When a critical concentration is reached, the peptide changes its orientation and disrupts the bilayer, inducing disintegration of the membrane into micelles (20-23). A decision between the various models is not possible at present and the influence of various parameters such as the peptide-to-lipid ratio, membrane composition, temperature, hydration or buffer compositions, needs to be considered (23).

As melittin carries a net positive charge of $z = 5$ it can be expected that it not only interacts with lipid membranes but can also bind to polyanions such as sulfate carrying glycosaminoglycans (GAGs) which are found on almost all cell surfaces. This interaction has not been investigated before, but related studies with two melittin analogs have recently been reported (24).

In the present study we have used high-sensitivity isothermal titration calorimetry (ITC) to obtain a complete thermodynamic characterization of melittin binding to three different glycosaminoglycans, namely heparan sulfate, heparin and dermatan sulfate. In addition, the structural changes of melittin induced by binding to these polyanions were followed by circular dichroism (CD) spectroscopy. Finally, we have compared the specificity of melittin binding to GAGs with analogous measurements with magainin 2 and nisin Z, two amphiphatic and antimicrobial peptides with similar lipid binding properties as melittin.

MATERIALS AND METHODS

Materials. Melittin from bee venom was purchased from SIGMA (St. Louis, MO). Synthetic melittin and magainin 2 were purchased from BACHEM AG (Bubendorf BL, Switzerland) (purity >97% by reverse phase HPLC). The peptides were used without further purification. The concentration of melittin in aqueous solution was determined by UV spectroscopy at 280nm using absorption coefficient of $5570 \text{ M}^{-1}\text{cm}^{-1}$ (5). Nisin Z was kindly provided by Dr. E. Breukink from Utrecht University. Heparan sulfate (HS), sodium salt (from porcine intestinal mucosa, average molecular weight, 13655 Da, sulfur content

5.51%) and dermatan sulfate (DS), sodium salt (from porcine intestinal mucosa, average molecular weight, 41 400 Da, sulfur content 6.85%) were from Celsus Laboratories (Cincinnati, OH). Low molecular weight heparin, sodium salt (from porcine intestinal mucosa, average molecular weight 3000) was from SIGMA (St. Louis, MO). All other chemicals were of analytical or reagent grade. Tris buffer (10mM tris(hydroxymethyl)aminoethane, pH 7.4) was prepared from 18MΩ water obtained from a NANOpure A filtration system. NaCl concentrations were variable (50 to 250 mM) and are specified in the legends of each figure. The samples were degassed immediately before use.

Isothermal Titration Calorimetry. All measurements were made with a Microcal VP-ITC calorimeter (Microcal, Northampton, MA). Titrations were performed by injecting 10 μL aliquots of the glycosaminoglycan solution into the calorimeter cell ($V_{\text{cell}} = 1.4037 \text{ mL}$) containing peptide at a concentration of typically 90-100 μM. The concentrations of the injected glycosaminoglycan solution were about 100 μM for HS, 35 μM for DS and 500 μM for heparin.

The heats of dilution were determined in control titrations by injecting glycosaminoglycan solution into pure buffer. The heats of dilution were small (~ -1 to 1 μcal), and were included in the final analysis. Raw data were processed using the Origin software provided with the instrument. The temperature was set as indicated in the legends of the figures. All measurements were performed in Tris buffer (10 mM, pH 7.4) with varying NaCl concentrations.

Circular Dichroism Spectroscopy. CD measurements of melittin in the absence and the presence of glycosaminoglycan (buffer 10 mM Tris, 100 mM NaF, pH 7.4) were made using a Chirascan CD spectrometer (Applied Photophysics Ltd., Leatherhead, UK). A quartz cuvette with a path length of 0.1 cm was used. All spectra were corrected by

subtracting the buffer baseline. Results are reported as mean residue ellipticity in units of $\text{deg cm}^2 \text{ dmol}^{-1}$. The percentage of peptide secondary structure was estimated from a computer simulation based on the reference spectra obtained by Reed and Reed (25).

RESULTS

Binding of melittin to HS. Figure 1A shows a representative calorimetric heat flow trace obtained by titration of synthetic melittin with HS (at 28 °C). A 91 μM solution of melittin was filled into the calorimeter cell ($V_{\text{cell}}=1.4037 \text{ mL}$) and 10 μL aliquots of a 100 μM HS solution were injected at 10 minutes intervals. The corresponding titration curve is shown in Figure 1B, where the reaction heats are plotted as a function of the HS / melittin molar ratio. The reaction heats were obtained by integration of the titrations peaks shown in Figure 1A and were corrected for the heats of dilution obtained in a separate HS-into-buffer titration.

Figure 1 demonstrates an *exothermic* reaction at 28 °C. The heats measured after few first injections are rather constant with $h_i \cong -15.5 \mu\text{cal}$ per injection. As melittin is much in excess over HS it is reasonable to assume that all injected HS (10 nmol per injection) is completely bound to melittin. The molar heat of reaction of HS can thus be evaluated as $\Delta H_{\text{HS}}^0 = -15.5 \mu\text{cal}/10 \text{ nmol} = -15.5 \text{ kcal/mol HS}$. As more HS is injected the concentration of free melittin decreases and the heats of reaction become progressively smaller. When all peptide is bound to HS, the residual heats of the last few injections are due to the dilution of HS into buffer. The molar binding enthalpy of melittin is then determined from the total heat released in the titration ($\sim 170.8 \mu\text{cal}$) and the amount of peptide in the calorimeter cell (127.7 nmol). For the experiment shown in Figure 1 the heat of reaction is $\Delta H_{\text{melittin}}^0 \approx -1.34 \text{ kcal/mol}$. The ratio $\Delta H_{\text{HS}}^0 / \Delta H_{\text{melittin}}^0 = 11.5$ provides the number of melittin molecules

bound per HS. This result can also be derived from the midpoint of the transition (Figure 1B) at HS/mel = 0.086, the reciprocal value of which is $n = 11.6$.

Figure 1

For a complete thermodynamic characterization of the binding process including the free energy, ΔG^0 , and the entropy, ΔS^0 , the calorimetric data were analyzed with a multisite binding model, which was also used to describe the binding equilibrium of other peptides to HS (26, 27). In this model a long polymer such as HS is visualized as a macromolecule with n independent and equivalent binding sites for a ligand like melittin. The binding model is represented by the following equation:

$$\frac{[P]_b}{[HS]_t} = \frac{nK[P]}{1 + K[P]} \quad (1)$$

$[P]$ and $[P]_b$ are the concentrations of free and bound melittin, respectively, $[HS]_t$ is the total concentration of heparan sulfate, K is the intrinsic binding constant, and n is the number of melittin molecules bound per heparan sulfate polysaccharide chain.

Because of mass conservation, the concentration of bound peptide can be described by:

$$[P]_b = \frac{1}{2} \left(\frac{1}{K} + [P]_t + n[HS]_t \right) - \frac{1}{2} \sqrt{\left(\frac{1}{K} + [P]_t + n[HS]_t \right)^2 - 4n[HS]_t[P]_t} \quad (2)$$

The index t denotes the total concentration of peptide and heparan sulfate in the calorimeter cell after each injection step. The peptide concentration changes during the titration with HS because of dilution effects.

The concentration of bound peptide is linked to the calorimetric data by the following equation:

$$\delta Q_i = \Delta H_{\text{melittin}}^0 \delta [P]_{\text{b},i} V \quad (3)$$

where δQ_i is the heat absorbed or released at the i^{th} injection. $\Delta H_{\text{melittin}}^0$ is the peptide binding enthalpy, $\delta [P]_{\text{b},i}$ is the change (increase) in *bound* peptide concentration upon injection i , and V is the volume of the calorimeter cell. The solid line in Figure 1B is the best least-square fit to the data using eq. 1 – 3 with the following set of parameters: $n = 11$, $K = 2.4 \times 10^5 \text{ M}^{-1}$, and $\Delta H_{\text{melittin}}^0 = -1.50 \text{ kcal/mol}$ (cf. Table 1). n and $\Delta H_{\text{melittin}}^0$ are consistent with simple calculations given above. In addition, the multisite binding model provides the binding constant, K , and, in turn, the free energy of binding, $\Delta G_{\text{melittin}}^0$. Calorimetric titrations were performed at various temperatures in the range of 5-50 °C. Table 1 summarizes the thermodynamic parameters derived by using the binding model described above.

Table 1

The binding stoichiometry melittin/HS varies between 9.5 to 13.5 and becomes smaller at higher temperatures. The reaction enthalpy shows an even stronger temperature dependence and changes from *endothermic* below 15 °C ($\Delta H_{\text{melittin}}^0 > 0$) to *exothermic* above this temperature. $\Delta H_{\text{melittin}}^0$ decreases linearly with increasing temperature as demonstrated in Figure 2A. The slope of the straight line yields a molar heat capacity change of $\Delta C_{\text{p,melittin}}^0 = -227 \text{ cal mol}^{-1} \text{ K}^{-1}$. This result is quite different from previous HS

binding studies obtained with cell penetrating peptides such as TAT and R₉, which reveal positive heat capacity values of $\Delta C_{p,TAT}^0 = 135 \text{ cal mol}^{-1} \text{ K}^{-1}$ (27) and $\Delta C_{p,R_9}^0 = 155 \text{ cal mol}^{-1} \text{ K}^{-1}$ (26) respectively. The negative ΔC_p^0 is indicative of a hydrophobic contribution to the binding process, whereas the positive ΔC_p^0 values are the signature for the electrostatic interactions (28). The solid line in Figure 2B describes the predicted temperature dependence of the binding constant K based on van't Hoff's law $\text{dln}K/\text{d}T = \Delta H_{\text{melittin}}^0 / RT^2$ taking into account the temperature dependence of the reaction enthalpy as $\Delta H(T) = \Delta H^0 + \Delta C_p^0(T - T_0)$.

Table 1 demonstrates that the reaction is completely entropy-driven below 15 °C as $\Delta H^0 > 0$ but becomes mainly enthalpy-driven at 50 °C. On the other hand, the free energy of binding is fairly constant which is also reflected in the weak temperature dependence of the binding constant K (Figure 2B). A plot of ΔH^0 vs. $T\Delta S^0$ yields a straight line in the temperature interval measured (not shown). The large heat capacity change then provides an explanation for this enthalpy-entropy compensation phenomenon, that is, the linear correlation between ΔH^0 and $T\Delta S^0$. The temperature coefficient of ΔH^0 is ΔC_p^0 , that of $T\Delta S^0$ is close to $\Delta C_p^0 + \Delta S^0$. As $\Delta C_p^0 \gg \Delta S^0$ (cf. Table 1) the two thermodynamic parameters ΔH^0 and $T\Delta S^0$ vary in parallel.

The binding constant at 28 °C is $K = 2.4 \times 10^5 \text{ M}^{-1}$ and is of the same order of magnitude as observed for other peptide-HS equilibria measured previously (TAT, R₉, mel-SH, ri-mel-SH). This is rather unexpected since the electrostatic and hydrophobic contributions appear to vary quite considerably between the different peptides.

Figure 2

We have studied the specificity of melittin binding with two further GAGs, i.e. heparin and dermatan sulfate (DS). Heparin is composed of the same monosaccharide building blocks as HS, but has higher degree of sulfation. In DS glucosamine is replaced by the galactosamine residue. ITC titration curves exhibit the same pattern as those observed for HS at identical temperatures and the binding isotherms can again be described by the multisite binding model of eqs 1-3. The results are shown in Table 2.

Table 2

For both GAGs the binding constants, K and the reaction enthalpies $\Delta H_{\text{melittin}}^0$ are larger than those obtained for HS. For heparin and DS the binding constants are of order of 10^6 M^{-1} . The peptide molar binding enthalpies, $\Delta H_{\text{melittin}}^0$ at $37 \text{ }^\circ\text{C}$ are -3.90 kcal/mol for heparin and -2.50 kcal/mol for DS. Likewise, the molar heat capacity changes are more negative with $\Delta C_p^0 = -285.1 \text{ cal mol}^{-1} \text{ K}^{-1}$ for heparin and $-241.3 \text{ cal mol}^{-1} \text{ K}^{-1}$ for DS. The main difference found between these glycosaminoglycans is, however, the binding stoichiometry. The number of binding sites for melittin at $37 \text{ }^\circ\text{C}$ is 2.7 for heparin, 10.4 for HS, and 38 for DS. However, this result is not surprising as the three polyanions have quite different chain lengths. A better comparison is the number of binding sites per 1kDa. With this normalization one finds ~ 0.76 binding sites for HS, ~ 0.90 for heparin and ~ 0.92 for DS per 1 kDa molecular weight.

ITC studies with magainin 2 and nisin Z. Melittin belongs to a large group of amphipathic peptides which either disrupt the lipid bilayer in a detergent-like manner or form pores or related structures. The question then arises if the interaction with sulfated glycosaminoglycans is a general property of these microbial antibiotics. As additional

example we have therefore studied the binding of magainin 2 and nisin Z to HS. Magainin 2 is secreted from the skin of the african clawed frog, *Xenopus leavis*. It consists of 23 amino acid residues and has a net positive charge of $z = 4$. Magainin 2 is known for its antimicrobial properties, but in contrast to melittin does not cause lysis of the eukaryotic cells (29). Nisin Z, secreted by lactic bacteria *Lactococcus lactis*, is a 34 amino acid residue peptide with also a net positive charge $z = 4$, with several unusual dehydro residues and five thioether-bridged lanthionines (30). It finds application as a food preservative and exerts its activity against Gram-positive bacteria. The interactions of magainin 2 and nisin Z with HS were studied here with isothermal titration calorimetry. We performed titrations of HS into magainin 2 (110-120 μM) and nisin Z (50 μM) solutions at three different temperatures in 10 mM Tris 100 mM NaCl, pH 7.4. The data did not reveal any binding of magainin 2 or nisin Z to heparan sulfate in the temperature of 5-50 $^{\circ}\text{C}$. At least in this series of experiments binding to GAGs appears to be a unique property of melittin.

The effect of NaCl on the interaction between HS and melittin. As ionic interactions play an important role in the binding of melittin to HS, we performed HS-into-melittin titrations at various NaCl concentrations. The thermodynamic parameters obtained at 28 $^{\circ}\text{C}$ and evaluated with the binding model described above are summarized in Table 3.

Table 3

As expected for electrostatic interactions the binding affinity of HS to melittin decreases with increasing salt content of the buffer. We have analyzed the salt dependence of the binding constant with a popular model for protein-polyelectrolyte interactions (31). HS is a highly charged poly-anion but a considerable fraction of its sulfate groups is probably neutralized by Na^+ due to counterion condensation (32). Upon binding of melittin the

counterions are released into the bulk solution as described by the following reaction scheme:



with the corresponding equilibrium

$$K_T = \frac{[\text{HS} \cdot \text{Mel}_n][\text{Na}^+]^z}{[\text{HS}(\text{Na})_z][\text{Mel}]^n} = K[\text{Na}^+]^z \quad (5)$$

K_T is the binding constant at 1 M Na^+ concentration and is usually described as K_{nonionic} , as ionic interactions are much reduced at this concentration. On the other hand, K is the actual binding constant derived directly from the ITC experiment which varies with the Na^+ concentration (table 3). Taking the logarithm on both sides of equation (5) and rearranging gives

$$\log K = \log K_T - z \log [\text{Na}^+] \quad (6)$$

A plot of the experimental $\log K$ as a function of $\log [\text{Na}^+]$ should be linear with slope z and y-intercept $\log K_T$. Figure 3 shows this linear relation for the melittin/HS system. Linear regression analysis yields $z_{\text{Na}^+} = -2.26$ (about two Na^+ ions are released when melittin binds to HS) and the nonionic binding constant $K_T = 1.4 \times 10^3 \text{ M}^{-1}$.

Figure 3

The variation of the thermodynamic parameters with salt concentration is displayed in Figure 4. The reaction enthalpy $\Delta H_{\text{melittin}}^0$ is independent of NaCl concentration, but $\Delta S_{\text{melittin}}^0$ decreases with increasing ionic strength. This indicates that the salt dependence of $\Delta G_{\text{melittin}}^0$ is entropic in origin. This was also observed for the binding of oligolysines to duplex DNA (33) and singles-stranded polynucleotides (34, 35) and for the binding of tripeptide containing lysine to heparin (36).

Figure 4

Structural properties of melittin binding to HS. Structural changes of synthetic melittin induced by binding to HS were followed by circular dichroism (CD) spectroscopy. The

Figure 5

CD spectra of melittin in buffer (10 mM Tris, 100 mM NaF, pH 7.4, room temperature) were measured at a peptide concentration of 44 μM and were titrated with a 22 μM solution of HS.

The corresponding CD spectra are displayed in Figure 5. For better visualization they are separated into three regions of low (A), middle (B), and high (C) HS content. Figure 5 demonstrates that melittin adopts an essentially random coil (rc) conformation in the absence of HS. The random coil content is 60% but α -helix and β -structure contribute 22% and 19%, respectively. Upon addition of HS the α -helix content increases steeply to about 56% at a HS-to-melittin ratio of ~ 0.12 , whereas further addition of HS induces a slow increase to 63% α -helix at a HS-to-melittin ratio of 0.5. The conformational change involves several structural transitions and cannot be described by a 2-state equilibrium over the full range. However, at low HS-to-melittin ratios (0-0.02) a 2-state equilibrium is observed with isosbestic points at $\lambda \sim 195$ and 228 nm (5A). For high HS-to-melittin ratios ($0.06 \leq r \leq 0.1$) a second 2-state transition region appears with an isosbestic point at $\lambda \sim 208$ nm (5C). The conformational changes in the intermediate region $0.04 > r > 0.1$ are characterized by a steep increase and decrease of β -turn structure (cf. 5B). Analogous CD titrations of melittin were performed with dermatan sulfate and heparin. The corresponding CD spectra are qualitatively and quantitatively very similar to those obtained for HS.

Helix formation in aqueous solution is an exothermic process with a reaction enthalpy of $\Delta H_{\text{helix}}^0 \sim -0.9$ to -1.1 kcal/mol (37, 38). The increase in α -helix content of melittin by 41%, corresponding to 10.7 amino acid residues, should thus entail a reaction enthalpy of about -10 kcal/mol. In addition, the electrostatic interaction of the 3 Lys and 2 Arg side chains with the HS sulfate groups could also make an exothermic contribution. However, the experimental result $\Delta H_{\text{mel}}^0 \sim -1.5$ kcal/mol is far different from this theoretical expectation. As an explanation it may be speculated that the helix-coil transition in the melittin-HS system has an enthalpy close to zero or that the enthalpy is even slightly positive. The classical example for a positive ΔH_{helix} is the coil-to-helix transition of poly(γ -benzy-L-glutamate) (PBGL) with $\Delta H_{\text{helix}}^0 = +890$ cal/mol per residue (39), taking place in ethylene dichloride/dichloroacetic acid (DCA). The random coil conformation is stabilized by specific PBGL-DCA interactions which are broken up at higher temperatures. In analogy, it can be argued that binding of melittin to HS requires removal of water molecules from melittin and/or HS, which is an endothermic process. The release of water would make a positive contribution to the entropy. We have measured CD spectra of melittin bound to HS as a function of temperature in the range 5-40°C. We observe a 15% reduction in the mean residual ellipticity while the shape of the spectra remains unchanged. As the CD-spectrum of a perfect helix is itself sensitive to temperature (37), the observed change is consistent with the literature data and excludes a melting of the helix. This measurement also supports the conclusion the enthalpy of the coil \rightleftharpoons helix transition of the melittin-HS system is close to zero. It may further be noted that $\Delta H_{\text{helix}}^0$ was found to decrease in mixed H₂O/trifluoroethanol (TFE) solvents (37) assuming a value $\Delta H_{\text{helix}}^0 = -0.1$ kcal/mol residue in pure TFE.

DISCUSSION

We observe a strong binding of melittin to three different GAGs, but no binding of nisin Z or magainin 2. Nisin Z has lysine residues at positions 12, 22 and 34. The cationic charges are spaced far apart and they cannot act in concert. For magainin 2 with lysines at positions 4, 10, 11 and 14 the electric charge density is higher but the spatial distances appear not to agree with the stereochemistry of the sulfated sugars. Melittin on the other hand, has a cluster of 4 cationic charges at amino acids. 21-24 followed by 2 glutamines at 25-26 which could make additional H-bridges. The significance of the spatial arrangement of the lysine and arginine residues is supported by a related study of synthetic peptides interacting with the heparin binding domain of the heparin/heparan sulfate interacting protein. The all-L-amino acid peptide and the all-D-amino acid version of the same peptide had the same efficacy as agents for neutralization of the anticoagulant activity of heparin. In contrast, a peptide with a scrambled peptide sequence had no effect. The spatial pattern of the charged amino acids was found to be of critical significance (40).

Structural Model. The HS employed in the present binding studies is composed of about 29 disaccharide units, based on an average molecular weight of 13'655 Da for HS and 464 Da for a sulfated disaccharide unit. On the other hand, a sulfur content of 5.51% leads to 23.5 SO_4^- groups. As each disaccharide unit also carries a $-\text{COO}^-$ group the total anionic charge of HS is about $z_{\text{HS}} = -53 \pm 5$. Charge neutralization is achieved if 10-11 melittin molecules are bound, provided each melittin contributes 5 positive charges. This is only possible if melittin with its helical axis is extended parallel to the HS chain as 4 cationic amino acids are clustered at the C-terminus whereas the 5th (Lys-7) is located at the other end of the molecule. Figure 6 shows a schematic representation to approximate scale of a complex consisting of

Figure 6

HS (29 disaccharide units) and 11 melittin molecules in helical conformation. In a 3-dimensional picture the melittin molecules should be wrapped around the disaccharide string producing hydrophobic interactions between neighboring melittins. The HS itself may also adopt a curled conformation. Inspection of the crystal structure of melittin (41) reveals a distance of 9.22 Å (10.05 Å) between the $^+\text{NH}_3$ groups of Lys 21 - Arg 24 (Arg 22 - Lys 23). The distance between 2 sulfate groups on heparin has been estimated as 8 - 8.6 Å ((42); fig. 1D). As there is no perfect match of distances, both melittin and HS must rearrange their structure to produce optimum ion pair formation.

The binding stoichiometry of melittin ($n = 11$) is distinctly smaller than those of the analogs [Cys¹] melittin ($n = 15.5 \pm 0.7$) and retro-inverso [Cys¹] melittin (14 ± 1.5) investigated previously (24). The replacement of the N-terminal glycine of melittin by cysteine in the analogs appears to modify the binding properties such that only the cationic -KRKR- carboxy terminus but not K-7 in the hydrophobic N-terminal region bind to HS. A larger number of ligands compared to natural melittin is hence required to guarantee electroneutrality of the HS-melittin-analog complexes. The increased ligand density requires a different packing model for the two melittin analogs. While the charged N-terminus is associated with the HS chain, part of the C-terminus must extend away from the chain axis into the aqueous phase.

Thermodynamic and structural aspects of melittin binding to HS. Melittin has a high affinity to HS as shown by the calorimetric data presented here. The binding constant at 28 °C is $K = 2.4 \times 10^5 \text{ M}^{-1}$, corresponding to a dissociation constant of 4.2 μM.

At low temperatures ($\leq 15^\circ\text{C}$) the melittin-HS interaction is endothermic and binding is exclusively driven by entropic forces. Above 15°C the reaction enthalpy changes to

exothermic but even at 50°C the entropy term accounts for 35% of the total free energy ΔG^0 . The large negative heat capacity change of $C_{p,\text{melittin}}^0 = -227 \text{ cal/mol}$ suggests hydrophobic interactions as the source of the entropy gain. The binding affinity of natural melittin is somewhat smaller than those of its analogs [Cys¹]melittin ($6.5 \times 10^5 \text{ M}^{-1}$) and retro-inverso [Cys¹]melittin ($4.0 \times 10^5 \text{ M}^{-1}$) (24).

Coulombic interactions between the cationic peptide and the anionic HS make an essential contribution to the free energy of binding. The Mel-HS binding constant decreases with increasing salt concentration to $K = 1.3 \times 10^3 \text{ M}^{-1}$ (extrapolated) at 1 M NaCl. Compared to $K = 3 \times 10^5 \text{ M}^{-1}$ at 100 mM NaCl this corresponds to a reduction of 43% in the free energy ΔG . The change in ΔG^0 is essentially entropic in nature as the reaction enthalpy ΔH^0 is virtually independent of the salt concentration.

Melittin binding to HS may be compared with the interaction of a basic cyclic peptide to heparin for which an extensive ITC study was performed (43). The brain natriuretic peptide (BNP) has a cyclic structure which is related to an acidic fibroblast growth factor. BNP contains 32 amino acids with 3 Lys and 4 Arg and is comparable in size and charge to melittin. The binding constant to heparin is $K = 2 \times 10^5 \text{ M}^{-1}$ (100 mM NaCl, 50 mM PO_4^- , 25°C, pH 7.4) which is very similar to melittin binding to HS ($3 \times 10^5 \text{ M}^{-1}$). On the other hand, heparin carries more sulfate groups than HS and the BNP-heparin interaction normalized to the charge density is thus weaker than the melittin-HS interaction. The reaction enthalpy is in the range of $-3.2 \text{ kcal/mol} \leq \Delta H_{\text{BNP}} \leq -0.4 \text{ kcal/mol}$ depending on the salt concentration. The molar heat capacity is $\Delta C_p = 1 \text{ kcal mol}^{-1} \text{ K}^{-1}$ (referred to heparin) and thus opposite in sign to that of the melittin-HS reaction ($\Delta C_{p,\text{melittin}} = -227 \text{ cal mol}^{-1} \text{ K}^{-1}$). The positive heat capacity suggest strong polar interactions. This is, however, contradicted by the rather small salt dependence of the BNP-heparin binding constant. The ionic contribution was estimated as only 6% which is much lower than that found for

melittin-HS or other heparin-binding proteins (44-48). Only 0.5 Na⁺ ions are replaced upon BNP binding.

BNP binding to heparin is accompanied by a distinct protonation reaction. 5 H⁺ are bound upon complex formation (43). We have therefore investigated the buffer dependence of the melittin-HS reaction. The reaction enthalpy varies only slightly between -1.5 kcal/mol (TRIS) over -1.8 kcal/mol (phosphate) to -2.6 kcal/mol (MOPS, HEPES), but is not correlated with the buffer dissociation enthalpies. A proton uptake or release can thus be excluded. The binding constant in phosphate buffer is only $1.1 \times 10^5 \text{ M}^{-1}$ (50 mM PO₄⁻, 100 mM NaCl) which can be explained by a specific interaction between melittin and PO₄⁻ (49).

In elucidating the cytolytic action mechanism of melittin most researchers have focused on the interaction of melittin with the lipid part of the cell membrane and only a few reports have discussed the role of glycosaminoglycans. It was suggested, for example, that melittin forms a complex with heparin secreted from mast cells neutralizing, in turn, the cytotoxic effect of melittin (50). Complexes between melittin and heparin result in an enhanced immune response to the peptide present in the complex (51). Melittin-induced cell lysis has been described in some detail for red blood cells (2), human lymphoblastoid cells (52, 53) or Caco-2 cells (54). However, the molecular mechanism of cell lysis was not addressed in these studies.

The present data suggest that the melittin-GAG interaction should be investigated as a potential target initiating cell lysis enhancing, perhaps, the melittin-lipid interaction. As a first step in this direction we have investigated the effect of melittin on two related Chinese hamster ovary (CHO) cell lines, one of which has a reduced content of sulfated GAGs. We have used the pgsA-745 mutant cell line (ATCC, Manassas, VA) which is deficient in xylosyltransferase, the enzyme responsible for the initiation of chondroitin sulfate and

heparan sulfate biosynthesis *in vivo* (55). As a control we used CHO K1 cells (ATCC, Manassas, VA). After incubation with melittin the cell viability was determined with CytoTox-One™ Homogeneous Membrane Integrity Assay (Promega Corporation, Madison, WI) according to the manufacturer's instruction. Differences in the cytotoxic effect of melittin for these two cell lines were observed in the range of peptide concentrations 3 to 5 μM . At 3 μM melittin the percent cytotoxicity is 44.8 ± 4.3 % for CHO K1 cells but only 31.6 ± 2 % for pgsA-745 cells with reduced GAG content. Even though the main mechanism is probably the permeabilization of the lipid membrane these data suggest that the role of GAGs cannot be ignored. A more detailed report including results from different cell lines and confocal microscopy is in preparation.

ACKNOWLEDGEMENTS

We thank Dr. K. Ballmer-Hofer (Paul-Scherrer-Institut, Villigen, Switzerland) for kindly providing the CHO cell lines. We are indebted to Dr. E. Breukink (University of Utrecht) for a gift of purified nisin Z.

REFERENCES

1. Habermann, E. (1972) Bee and wasp venoms, *Science* 177, 314-322.
2. Tosteson, M. T., Holmes, S. J., Razin, M., and Tosteson, D. C. (1985) Melittin lysis of red cells, *J Membr Biol* 87, 35-44.
3. Vogel, H. (1981) Incorporation of melittin into phosphatidylcholine bilayers. Study of binding and conformational changes, *FEBS Lett* 134, 37-42.
4. Bello, J., Bello, H. R., and Granados, E. (1982) Conformation and aggregation of melittin: dependence on pH and concentration, *Biochemistry* 21, 461-465.

5. Quay, S. C., and Condie, C. C. (1983) Conformational studies of aqueous melittin: thermodynamic parameters of the monomer-tetramer self-association reaction, *Biochemistry* 22, 695-700.
6. Wilcox, W., and Eisenberg, D. (1992) Thermodynamics of melittin tetramerization determined by circular dichroism and implications for protein folding, *Protein Sci* 1, 641-653.
7. Berneche, S., Nina, M., and Roux, B. (1998) Molecular dynamics simulation of melittin in a dimyristoylphosphatidylcholine bilayer membrane, *Biophys J* 75, 1603-1618.
8. Beschiaschvili, G., and Seelig, J. (1990) Melittin binding to mixed phosphatidylglycerol/phosphatidylcholine membranes, *Biochemistry* 29, 52-58.
9. Dempsey, C., Bitbol, M., and Watts, A. (1989) Interaction of melittin with mixed phospholipid membranes composed of dimyristoylphosphatidylcholine and dimyristoylphosphatidylserine studied by deuterium NMR, *Biochemistry* 28, 6590 - 6596.
10. Glattli, A., Chandrasekhar, I., and Gunsteren, W. F. (2006) A molecular dynamics study of the bee venom melittin in aqueous solution, in methanol, and inserted in a phospholipid bilayer, *Eur Biophys J* 35, 255-267.
11. Kuchinka, E., and Seelig, J. (1989) Interaction of melittin with phosphatidylcholine membranes. Binding isotherm and lipid head-group conformation, *Biochemistry* 28, 4216-4221.
12. Papo, N., and Shai, Y. (2003) Exploring peptide membrane interaction using surface plasmon resonance: differentiation between pore formation versus membrane disruption by lytic peptides, *Biochemistry* 42, 458-466.

13. Yang, L., Harroun, T. A., Weiss, T. M., Ding, L., and Huang, H. W. (2001) Barrel-stave model or toroidal model? A case study on melittin pores, *Biophys J* 81, 1475-1485.
14. Dempsey, C. E. (1990) The actions of melittin on membranes, *Biochim Biophys Acta* 1031, 143-161.
15. Batenburg, A. M., van Esch, J. H., and de Kruijff, B. (1988) Melittin-induced changes of the macroscopic structure of phosphatidylethanolamines, *Biochemistry* 27, 2324-2331.
16. Katsu, T., Ninomiya, C., Kuroko, M., Kobayashi, H., Hirota, T., and Fujita, Y. (1988) Action mechanism of amphipathic peptides gramicidin S and melittin on erythrocyte membrane, *Biochim Biophys Acta* 939, 57-63.
17. Ladokhin, A. S., Selsted, M. E., and White, S. H. (1997) Sizing membrane pores in lipid vesicles by leakage of co-encapsulated markers: pore formation by melittin, *Biophys J* 72, 1762-1766.
18. Rex, S., and Schwarz, G. (1998) Quantitative studies on the melittin-induced leakage mechanism of lipid vesicles, *Biochemistry* 37, 2336-2345.
19. Allende, D., Simon, S. A., and McIntosh, T. J. (2005) Melittin-induced bilayer leakage depends on lipid material properties: evidence for toroidal pores, *Biophys J* 88, 1828-1837.
20. Ladokhin, A. S., and White, S. H. (2001) Protein chemistry at membrane interfaces: non-additivity of electrostatic and hydrophobic interactions, *J Mol Biol* 309, 543-552.
21. Monette, M., and Lafleur, M. (1995) Modulation of melittin-induced lysis by surface charge density of membranes, *Biophys J* 68, 187-195.
22. Shai, Y. (2002) Mode of action of membrane active antimicrobial peptides, *Biopolymers* 66, 236-248.

23. Bechinger, B., and Lohner, K. (2006) Detergent-like actions of linear amphipathic cationic antimicrobial peptides, *Biochim Biophys Acta* 1758, 1529-1539.
24. Goncalves, E., Kitas, E., and Seelig, J. (2006) Structural and thermodynamic aspects of the interaction between heparan sulfate and analogues of melittin, *Biochemistry* 45, 3086-3094.
25. Reed, J., and Reed, T. A. (1997) A set of constructed type spectra for the practical estimation of peptide secondary structure from circular dichroism, *Anal Biochem* 254, 36-40.
26. Goncalves, E., Kitas, E., and Seelig, J. (2005) Binding of oligoarginine to membrane lipids and heparan sulfate: structural and thermodynamic characterization of a cell-penetrating peptide, *Biochemistry* 44, 2692-2702.
27. Ziegler, A., and Seelig, J. (2004) Interaction of the protein transduction domain of HIV-1 TAT with heparan sulfate: binding mechanism and thermodynamic parameters, *Biophys J* 86, 254-263.
28. Gomez, J., Hilser, V. J., Xie, D., and Freire, E. (1995) The heat capacity of proteins, *Proteins* 22, 404-412.
29. Zasloff, M. (1987) Magainins, a class of antimicrobial peptides from *Xenopus* skin: isolation, characterization of two active forms, and partial cDNA sequence of a precursor, *Proc Natl Acad Sci U S A* 84, 5449-5453.
30. Breukink, E., Ganz, P., de Kruijff, B., and Seelig, J. (2000) Binding of Nisin Z to bilayer vesicles as determined with isothermal titration calorimetry, *Biochemistry* 39, 10247-10254.
31. Record, M. T., Jr., Anderson, C. F., and Lohman, T. M. (1978) Thermodynamic analysis of ion effects on the binding and conformational equilibria of proteins and nucleic acids: the roles of ion association or release, screening, and ion effects on water activity, *Q Rev Biophys* 11, 103-178.

32. Manning, G. S. (1978) The molecular theory of polyelectrolyte solutions with applications to the electrostatic properties of polynucleotides, *Q Rev Biophys* 11, 179-246.
33. Lohman, T. M., deHaseth, P. L., and Record, M. T., Jr. (1980) Pentalysine-deoxyribonucleic acid interactions: a model for the general effects of ion concentrations on the interactions of proteins with nucleic acids, *Biochemistry* 19, 3522-3530.
34. Mascotti, D. P., and Lohman, T. M. (1992) Thermodynamics of single-stranded RNA binding to oligolysines containing tryptophan, *Biochemistry* 31, 8932-8946.
35. Mascotti, D. P., and Lohman, T. M. (1993) Thermodynamics of single-stranded RNA and DNA interactions with oligolysines containing tryptophan. Effects of base composition, *Biochemistry* 32, 10568-10579.
36. Mascotti, D. P., and Lohman, T. M. (1995) Thermodynamics of charged oligopeptide-heparin interactions, *Biochemistry* 34, 2908-2915.
37. Luo, P., and Baldwin, R. L. (1997) Mechanism of helix induction by trifluoroethanol: a framework for extrapolating the helix-forming properties of peptides from trifluoroethanol/water mixtures back to water, *Biochemistry* 36, 8413-8421.
38. Scholtz, J. M., Marqusee, S., Baldwin, R. L., York, E. J., Stewart, J. M., Santoro, M., and Bolen, D. W. (1991) Calorimetric determination of the enthalpy change for the alpha-helix to coil transition of an alanine peptide in water, *Proc Natl Acad Sci U S A* 88, 2854-2858.
39. Zimm, B. H., Doty, P., and Iso, K. (1959) Determination of the parameters for helix formation in poly-gamma-benzyl-L-glutamate, *Proc Natl Acad Sci U S A* 45, 1601-1607.

40. Wang, J., and Rabenstein, D. L. (2006) Interaction of Heparin with Two Synthetic Peptides that Neutralize the Anticoagulant Activity of Heparin, *Biochemistry* 45, 15740-15747.
41. Terwilliger, T. C., and Eisenberg, D. (1982) The structure of melittin. II. Interpretation of the structure, *J Biol Chem* 257, 6016-6022.
42. Silvian, L., Jin, P., Carmillo, P., Boriack-Sjodin, P. A., Pelletier, C., Rushe, M., Gong, B., Sah, D., Pepinsky, B., and Rossomando, A. (2006) Artemin crystal structure reveals insights into heparan sulfate binding, *Biochemistry* 45, 6801-6812.
43. Hileman, R. E., Jennings, R. N., and Linhardt, R. J. (1998) Thermodynamic analysis of the heparin interaction with a basic cyclic peptide using isothermal titration calorimetry, *Biochemistry* 37, 15231-15237.
44. Thompson, L. D., Pantoliano, M. W., and Springer, B. A. (1994) Energetic characterization of the basic fibroblast growth factor-heparin interaction: identification of the heparin binding domain, *Biochemistry* 33, 3831-3840.
45. Olson, S. T., Halvorson, H. R., and Bjork, I. (1991) Quantitative characterization of the thrombin-heparin interaction. Discrimination between specific and nonspecific binding models, *J Biol Chem* 266, 6342-6352.
46. Olson, S. T., and Bjork, I. (1991) Predominant contribution of surface approximation to the mechanism of heparin acceleration of the antithrombin-thrombin reaction. Elucidation from salt concentration effects, *J Biol Chem* 266, 6353-6364.
47. Faller, B., Mely, Y., Gerard, D., and Bieth, J. G. (1992) Heparin-induced conformational change and activation of mucus proteinase inhibitor, *Biochemistry* 31, 8285-8290.
48. Fath, M. A., Wu, X., Hileman, R. E., Linhardt, R. J., Kashem, M. A., Nelson, R. M., Wright, C. D., and Abraham, W. M. (1998) Interaction of secretory leukocyte

- protease inhibitor with heparin inhibits proteases involved in asthma, *J Biol Chem* 273, 13563-13569.
49. Podo, F., Strom, R., Crifo, C., and Zulauf, M. (1982) Dependence of melittin structure on its interaction with multivalent anions and with model membrane systems, *Int J Pept Protein Res* 19, 514-527.
 50. Higginbotham, R. D., and Karnella, S. (1971) The significance of the mast cell response to bee venom, *J Immunol* 106, 233-240.
 51. Kind, L. S., and Allaway, E. (1982) Enhanced IgE and IgG anti-melittin antibody formation induced by heparin-Melittin complexes in mice, *Allergy* 37, 225-229.
 52. Weston, K. M., Alsalami, M., and Raison, R. L. (1994) Cell membrane changes induced by the cytolytic peptide, melittin, are detectable by 90 degrees laser scatter, *Cytometry* 15, 141-147.
 53. Weston, K. M., and Raison, R. L. (1998) Interaction of melittin with a human lymphoblastoid cell line, HMy2, *J Cell Biochem* 68, 164-173.
 54. Maher, S., and McClean, S. (2006) Investigation of the cytotoxicity of eukaryotic and prokaryotic antimicrobial peptides in intestinal epithelial cells in vitro, *Biochem Pharmacol* 71, 1289-1298.
 55. Seelig, J. (1997) Titration calorimetry of lipid-peptide interactions, *Biochim Biophys Acta* 1331, 103-16.

TABLES

Table 1 – Titration of synthetic melittin with HS. Thermodynamic parameters as a function of temperature in buffer (10 mM Tris 100 mM NaCl at pH 7.4.)

| T (°C) | n | K (M ⁻¹) | $\Delta H_{\text{melittin}}^0$ (kcal/mol) | $\Delta G_{\text{melittin}}^0$ (kcal/mol) | $T\Delta S_{\text{melittin}}^0$ (kcal/mol) | ΔS_{mol}^0 (cal/molK) |
|-----------|------|-------------------------|--|--|---|---|
| 5 | 11.2 | 1.9 x 10 ⁵ | 4.60 | -6.71 | 11.31 | 40.7 |
| 10 | 13.5 | 2.0 x 10 ⁵ | 2.80 | -6.86 | 9.66 | 34.1 |
| 15 | 12.5 | 2.2 x 10 ⁵ | 2.30 | -7.04 | 9.34 | 32.4 |
| 28 | 11.0 | 2.4 x 10 ⁵ | -1.50 | -7.41 | 5.91 | 19.6 |
| 37 | 10.4 | 2.3 x 10 ⁵ | -2.20 | -7.60 | 5.40 | 17.4 |
| 50 | 9.5 | 2.0 x 10 ⁵ | -6.10 | -7.83 | 1.73 | 5.4 |

Table 2 – Thermodynamic parameters for synthetic melittin binding to heparin and DS.

Buffer: 10 mM Tris 100 mM NaCl, pH 7.4.

| T (°C) | n | K (M ⁻¹) | $\Delta H_{\text{melittin}}^0$ (kcal/mol) | $\Delta G_{\text{melittin}}^0$ (kcal/mol) | $T\Delta S_{\text{melittin}}^0$ (kcal/mol) |
|-------------------------|------|-------------------------|--|--|---|
| <u>Heparin</u> | | | | | |
| 5 | 2.6 | 0.9 x 10 ⁶ | 5.40 | -7.57 | 12.97 |
| 10 | 2.6 | 1.0 x 10 ⁶ | 3.50 | -7.77 | 11.27 |
| 37 | 2.7 | 0.9 x 10 ⁶ | -3.90 | -8.45 | 4.55 |
| <u>Dermatan Sulfate</u> | | | | | |
| 10 | 30.5 | 1.1 x 10 ⁶ | 3.90 | -7.82 | 11.72 |
| 28 | 40.0 | 1.2 x 10 ⁶ | -0.90 | -8.37 | 7.47 |
| 37 | 38.0 | 1.0 x 10 ⁶ | -2.50 | -8.51 | 6.01 |

Table 3 – The effect of NaCl on the thermodynamic parameters of HS binding to bee venom melittin at 28 °C. Buffer: 10 mM Tris and variable concentrations of NaCl at pH 7.4.

| NaCl (mM) | n | K (M ⁻¹) | $\Delta H_{\text{melittin}}^0$ (kcal/mol) | $\Delta G_{\text{melittin}}^0$ (kcal/mol) | $T\Delta S_{\text{melittin}}^0$ (kcal/mol) |
|-------------------|------|-----------------------|---|---|--|
| 50 | 9.8 | 1.0 x 10 ⁶ | -1.40 | -8.26 | 6.86 |
| | 9.5 | 1.0 x 10 ⁶ | -1.50 | -8.26 | 6.76 |
| 100 ^{a)} | 8.5 | 3.0 x 10 ⁵ | -1.70 | -7.54 | 5.84 |
| | 10.0 | 3.5 x 10 ⁵ | -1.20 | -7.64 | 6.44 |
| 150 | 10.0 | 1.0 x 10 ⁵ | -1.50 | -6.89 | 5.39 |
| | 10.0 | 1.0 x 10 ⁵ | -1.50 | -6.89 | 5.39 |
| 250 | 10.0 | 2.5 x 10 ⁴ | -1.40 | -6.06 | 4.66 |
| | 10.0 | 3.0 x 10 ⁴ | -1.30 | -6.17 | 4.87 |

^{a)} The small differences to the data in table 1 can be explained by the different source of melittin which is melittin from natural source in table 3 but synthetic melittin in table 1.

LEGENDS


FIGURE 1. Titration of HS into synthetic melittin. (A) Calorimetric trace obtained at 28 °C by titration of HS (100 μM) into a solution of melittin (91 μM). Each peak corresponds to the injection of 10 μL of HS into the calorimeter cell. (B) Heats of reaction (integrated from the calorimetric trace) plotted as a function of the HS/melittin ratio. The solid line is the best fit to the experimental data (■) using the binding model described by eqs 1-3 with the following parameters: $\Delta H_{\text{melittin}}^0 = -1.50 \text{ kcal/mol}$, $K = 2.4 \times 10^5 \text{ M}^{-1}$, $n = 11$. Buffer: 10 mM Tris, 100 mM NaCl, pH 7.4.

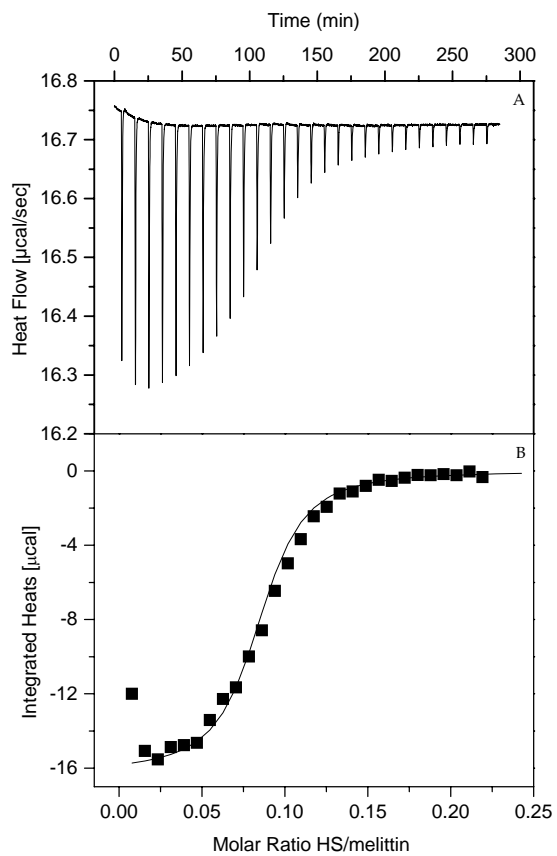
FIGURE 2. Temperature dependence of the thermodynamic parameters. (A) $\Delta H_{\text{melittin}}^0$ for synthetic melittin binding to HS. Linear regression analysis of the experimental data in yields $\Delta H_{\text{melittin}}^0 = 5.47 - 0.227T \text{ (}^\circ\text{C)}$ (solid line). (B) Binding constant K_0 . The solid line in (B) is the predicted temperature dependence of K_0 based on the van't Hoff equation and using the above regression formula for $\Delta H_{\text{melittin}}^0 (T)$. Buffer: 10 mM Tris, 100 mM NaCl, pH 7.4.

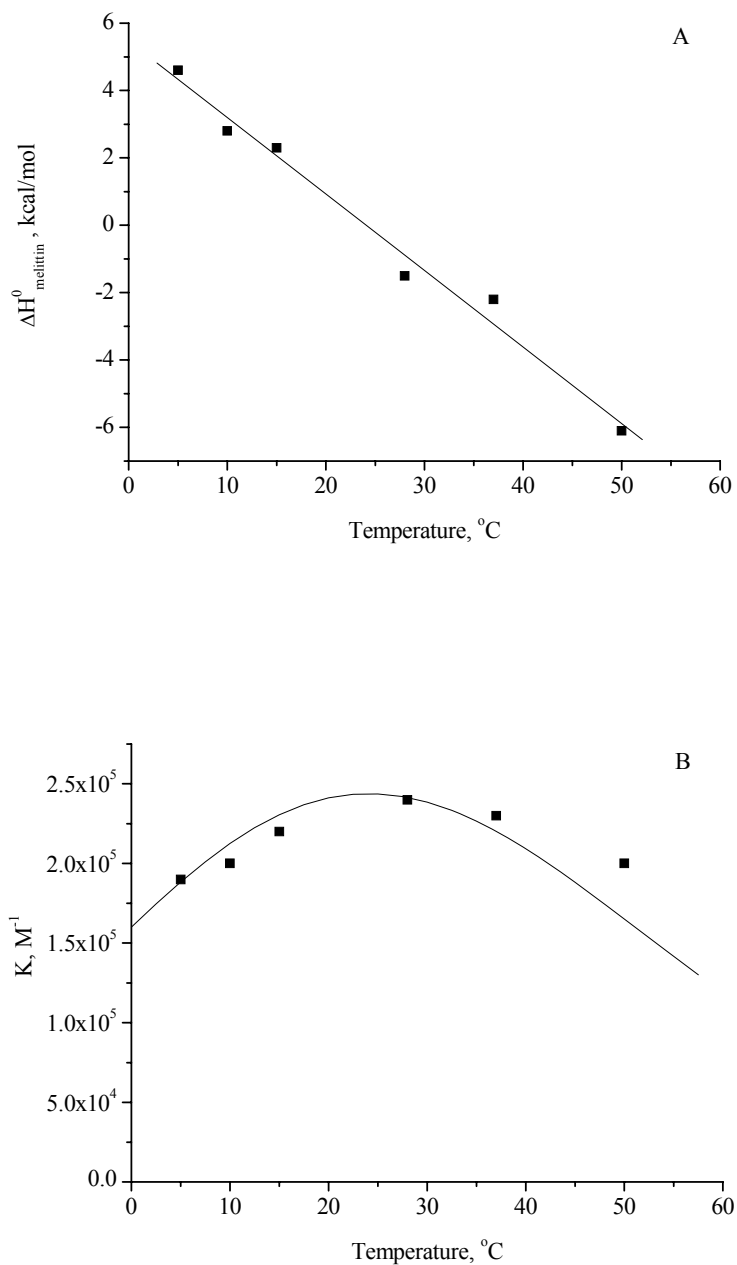
FIGURE 3. Salt dependence of the interaction between HS and bee venom melittin. Binding constant (K_0) for HS binding to melittin was determined as a function of NaCl concentration in Tris buffer (10 mM Tris, pH 7.4) from ITC measurements at 28 °C. K values are plotted as a function of the NaCl concentration on log/log scale. Linear regression analysis of the experimental data yields $\log K = 3.14 - 2.26 \log [\text{NaCl}]$ (solid line).

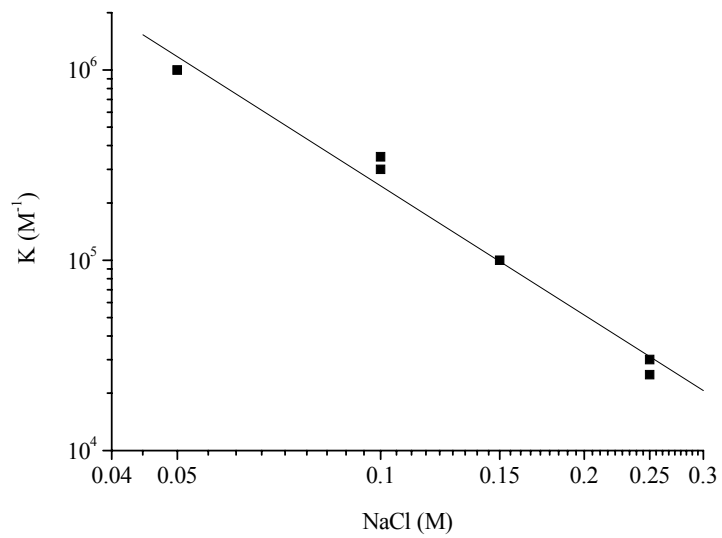
FIGURE 4. Dependence of $\Delta G_{\text{melittin}}^0$, $\Delta H_{\text{melittin}}^0$, and $T\Delta S_{\text{melittin}}^0$ on the NaCl concentration in Tris buffer (10 mM Tris, pH 7.4) at 28 °C for the interaction of bee venom melittin with HS.

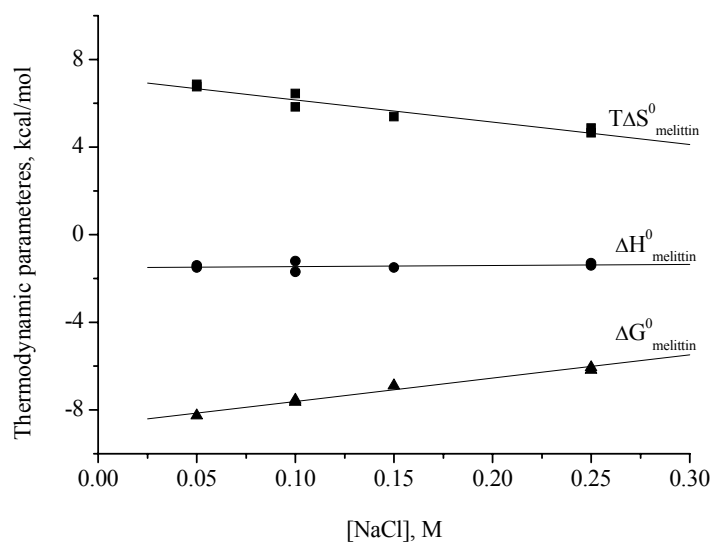
FIGURE 5. CD spectra monitoring conformational changes in bee venom melittin upon addition of heparan sulfate. Mean residue ellipticity values of melittin (44.3 μM) in the absence and upon titration with heparan sulfate (22 μM) are plotted as a function of the wavelength. (A) black – melittin; red – HS/melittin 0.01; green – HS/melittin 0.02; (B) blue – HS/melittin 0.04; cyan – HS/melittin 0.06; magenta – HS/melittin 0.08; orange – HS/melittin 0.10; (C) dark grey – HS/melittin 0.12; violet – HS/melittin 0.16; pink – HS/melittin 0.20; yellow – HS/melittin 0.30; dark yellow – HS/melittin 0.50. Buffer: 10 mM Tris, 100 mM NaF, pH 7.4.

FIGURE 6. Schematic representation of melittin-HS interactions. HS with 29 disaccharide units (\blacklozenge), total length ~ 290 Å. Melittin helix () length ~ 37 Å, diameter ~ 11 Å.

**FIGURE 1**

**FIGURE 2**

**FIGURE 3**

**FIGURE 4**

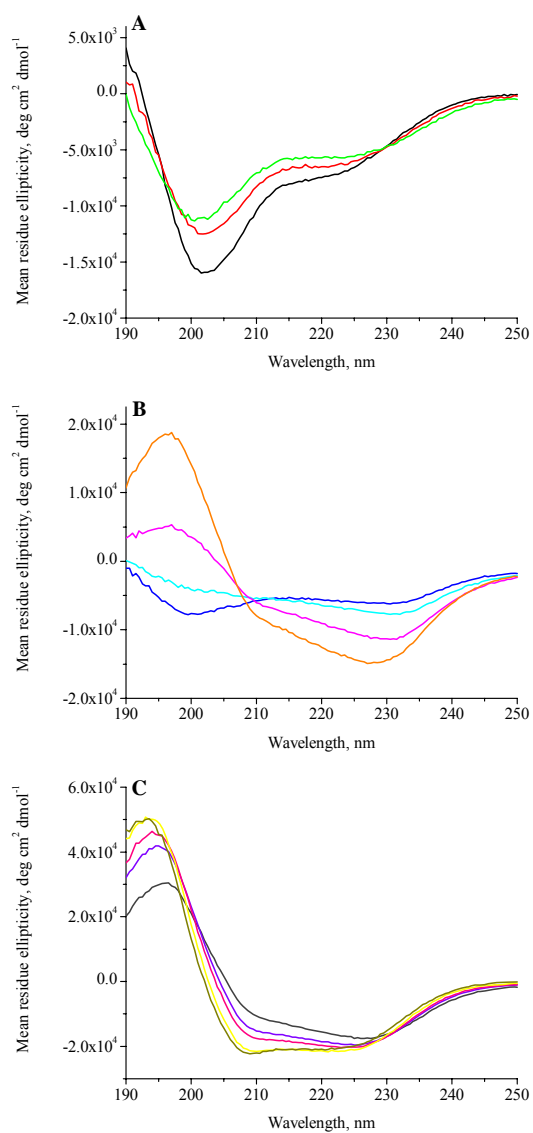


FIGURE 5

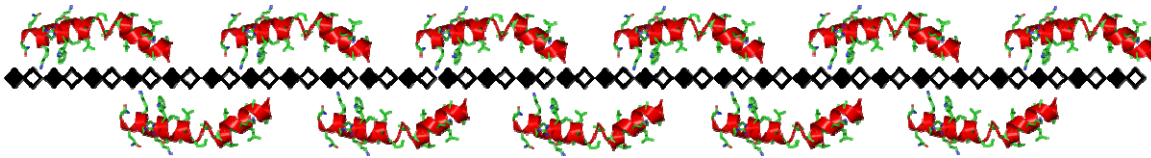
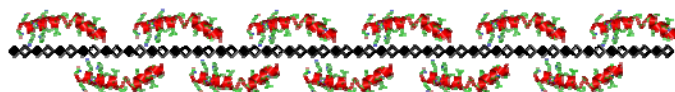


FIGURE 6

FOR TABLE OF CONTENTS USE ONLY

Title: Melittin Interaction with Sulfated Cell Surface Sugars

Authors: Gabriela Klocek and Joachim Seelig

APPENDIX – LIGHT SCATTERING MEASUREMENTS

Static light scattering studies. A turbid solution is observed when melittin is mixed with HS and the association reaction can conveniently be followed by light scattering. The measurements were performed in a Jasco FP 777 spectrofluorimeter (Japan-Spectroscopic, Tokyo, Japan). Typically, 2.8 mL solution of melittin (53 μM) was titrated with HS (200 μM) at 5 min intervals, under constant stirring at room temperature. The scattering intensity at 365 nm (with the excitation wavelength set to 350 nm) was measured and recorded as a function of time.

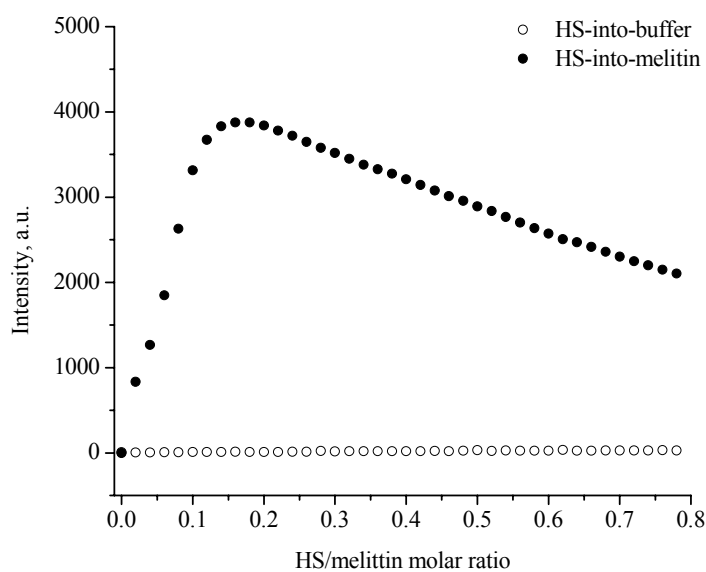


Figure 1. Right-angle static light scattering obtained by titration of HS into bee venom melittin. (●) Each data point corresponds to the injection of 15 μL of HS (200 μM) into a solution of melittin (53 μM). (○) Control titration, where HS is injected into pure buffer. Buffer: 10 mM Tris, 100mM NaCl, pH 7.4.

Figure 1 shows the scattering intensity when small aliquots of HS solution (200 μM) were titrated into melittin (53 μM) (●) or into pure buffer (○). The scattering intensity of melittin

solution increases upon addition of HS, reaching the maximum at a HS/melittin molar ratio of ~ 0.16 , which corresponds to a peptide/HS ratio of 6.3. Beyond this point a decrease in scattering intensity was observed, indicating that some of the larger aggregates/complexes were dissolved in the presence of excess HS.

Dynamic light-scattering studies. To determine the size of the complexes/aggregates which are formed upon titration of melittin with HS and to confirm results obtained in static light scattering studies, we have applied dynamic light scattering. Dynamic light scattering measurements were performed in Zetasizer Nano ZS (Malvern Instruments Ltd., Worcestershire, UK). Typically, 0.6 mL solution of melittin ($65.7 \mu\text{M}$) was titrated with small aliquots of HS ($200 \mu\text{M}$).

Figure 2A shows the correlation function for aggregates/complexes formed at HS-to-melittin molar ratio of 0.20. The rate of decay for the correlation function is related to a particle size and it is much slower for large particles than it is for small ones. After the correlation function was measured, the software of the instrument provides the decay rates and calculates the size distribution. A typical size distribution graph is shown in Figure 2B. It is the relative intensity of the scattered light as a function of size. In Figure 2B size distribution shows one single peak with average diameter of particles of 171.3 nm.

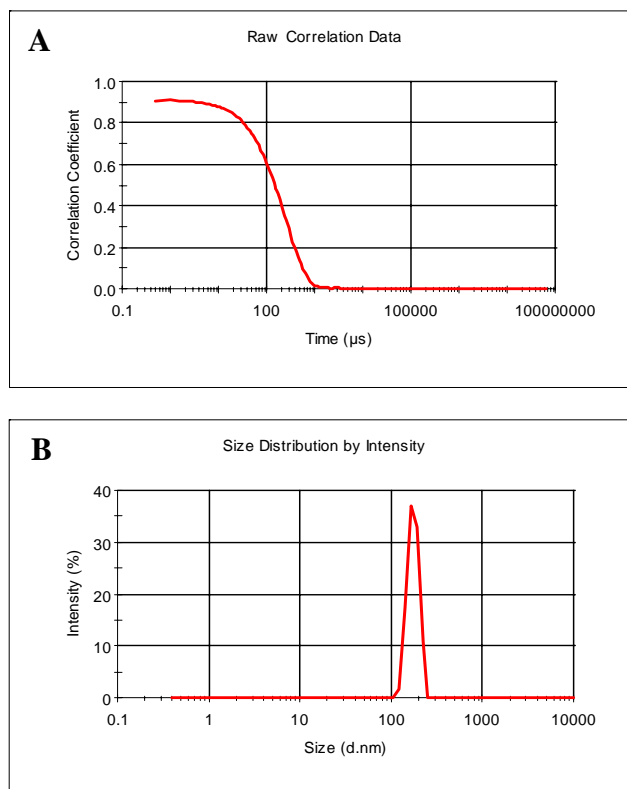


Figure 2. (A) Correlation function and (B) size distribution graph for aggregates/complexes at HS-to-melittin molar ratio of 0.20. Buffer: 10 mM Tris 100 mM NaCl at pH 7.4.

The intensity distribution was converted using Mie theory to volume distribution by software provided with the instrument. The volume distribution was then used in further analysis. Figure 3 shows the size distribution by volume of melittin upon titration with HS.

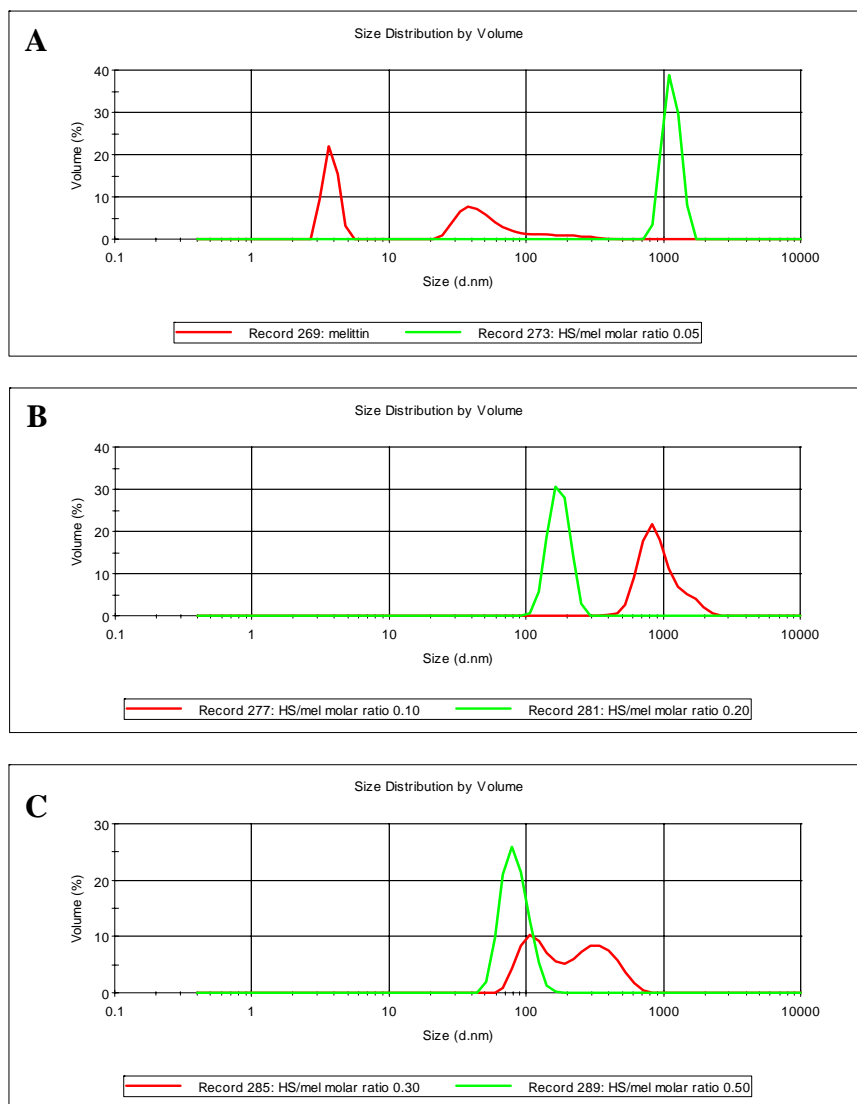


Figure 3. Size distribution by volume for titration of melittin solution ($65.7 \mu\text{M}$) with HS ($200 \mu\text{M}$) determined by dynamic light scattering. Buffer: 10mM Tris 100 mM NaCl at pH 7.4.

For melittin in the absence of HS two populations of different size particles are found (Figure 3A). One population of the particles has the size of 3.8 nm, corresponding approximately corresponds to the length of the peptide molecules. The size of the second population is determined as 66.6 nm, suggesting the presences of the peptide aggregates.

To compare results obtained for different HS-to-melittin molar ratios the z-average size (also known as the “cumulants mean”), a mean value for the size, is used. However when the polydispersity index (PDI) is larger than 0.5, it is not advised to rely on the z-average

size, but rather a distribution analysis should be used to determine the peak position. PDI of 0.723 was found at HS-to melittin molar ratio of 0.05. The plot of the size distribution shows a single peak with maximum at ~ 1148 nm at a HS-to-melittin molar ratio of 0.05 (Figure 3A). These results indicate presence of very big and heterogeneous aggregates/complexes. At higher molar ratios of HS-to-melittin the PDI decreases below 0.5. At a HS-to-melittin ratio of 0.10 (PDI of 0.236) the peak position at 959.4 nm (Figure 3B) and the z-average size of 921.1 nm are found. Further addition of HS moves the peak position towards smaller particles (Figure 3B and 3C) and a significant decrease in the z-average size is observed (Figure 4), indicating that big aggregates/complexes are dissolved again. The z-average size of 171.3 nm (PDI of 0.024), 180 nm (PDI of 0.197), and 87.35 nm (PDI of 0.047) are found at HS-to-melittin molar ratios of 0.20, 0.30, and 0.50 respectively.

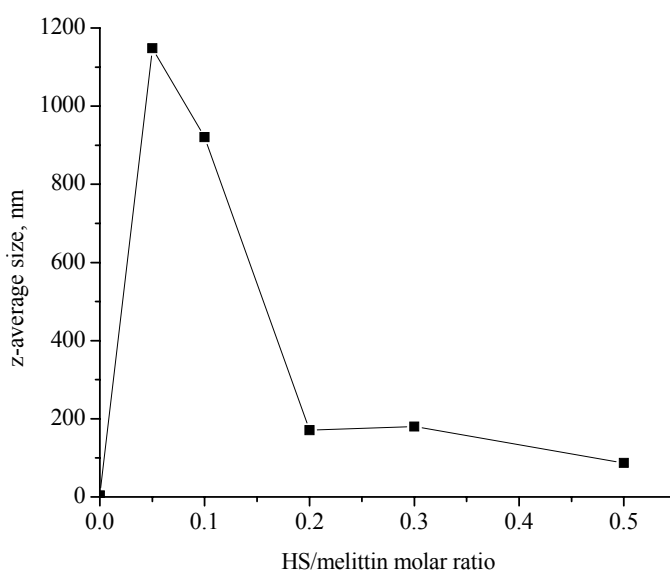


Figure 4. The z-average size of melittin-HS aggregates/complexes determined by Dynamic Light Scattering plotted as a function of HS/melittin molar ratio. For melittin in the absence of HS the particles size of 3.8 nm is taken. For HS/melittin molar ratio of 0.05 the distribution analysis of the peak position to determine the size of the particles was used, since PDIs was found to be 0.723.

The maximum sizes of the particles are found at HS to melittin molar ratios of 0.05 and 0.10, what correspond to peptide/HS molar ratio of 20 and 10, respectively. This result corresponds better to stoichiometry found by ITC than the result obtained by static light scattering method.

4. CYTOTOXICITY OF MELITTIN ON CELLS

INTRODUCTION

In addition to its powerful antimicrobial and lytic activity melittin exhibits a variety of other biological effects such as inhibition and aggregation of membrane proteins (1-4), inhibition ($H^+ + K^+$) ATPase (5) and ($Na^+ + K^+$) ATPase (6), increasing cell membranes permeability to ions and stimulating activity of phospholipase A_2 (7). Although extensive studies on the interaction between melittin and cell membranes or lipids have been performed, the molecular origin of the cytolytic activity of melittin is not fully established.

It was shown that melittin has a higher affinity to membranes composed of negatively charged lipids than for zwitterionic lipids, indicating that electrostatic interactions are involved in the binding of melittin to membranes (8, 9). The membrane of the eukaryotic cells contains only about 10% anionic lipids which are mainly localized in the inner leaflet of the healthy cell membrane. The outer membrane of eukaryotic cells contains predominantly neutral lipids such as phosphatidylcholine (10). However, almost all cell surfaces are decorated with sulfate carrying glycosaminoglycans (GAGs). It was shown that GAGs have been implicated in the internalization of several CPPs, including the full TAT protein and oligoarginine (11, 12). Also many pathogenic microorganisms use cell surface GAGs as receptors for attachment and invasion. Adherence and penetration of herpes simplex virus (HSV) depends on cell surface heparan sulfate (13, 14). In *Chlamydia trachomatis*, heparan sulfate acts as bridge, binding both host cell receptors and *Ch. trachomatis* (15, 16). In the present study we have shown that melittin has a high affinity to heparan sulfate (HS) with a microscopic binding constant of $\sim 10^5 M^{-1}$ at temperatures from 5 to 50 °C. Two other antimicrobial, but non-lytic peptides, magainin 2 and nisin Z do not bind to HS. These results suggest that GAGs could be involved in the mode of action of melittin on the eukaryotic cells. In order to study *in vivo* involvement of GAGs in the

binding of melittin to cell membranes, cell lines deficient in GAGs would be the most suitable. Mutants of Chinese hamster ovary cells (CHO) lacking GAGs have been reported (17). Some lines lack both heparan and chondroitin sulfate. Other strains produce heparan sulfate or chondroitin sulfate only. Some cell lines are defective in polymer modifications reactions, such as GlcNAc deacetylation/N sulfation or IdUA 2-O sulfation (17-20).

In this study we have used the pgsA-745 mutant cell line, which is deficient in xylosyltransferase, the enzyme responsible for the initiation of chondroitin sulfate and heparan sulfate biosynthesis *in vivo*. These mutant cells do not produce GAGs (17).

Cell viability can be defined based on the integrity of the cell membrane. One of the methods to estimate the number of non-viable cells is to measure the leakage of cytoplasmic components into the surrounding culture medium, when the membrane integrity is lost. A particularly useful cytoplasmic metabolite released upon cell death is lactate dehydrogenase (LDH). By estimating the amount of LDH in the culture medium, it is possible to estimate the number of non-viable cells and, in turn, the influence of external agents on the cell metabolism. To determine the cytotoxic effect of melittin on different cell lines, we have used the CytoTox-ONE™ Homogenous Membrane Integrity Assay (Promega Corporation, Madison, WI, USA). This assay reveals the release of LDH from cells with damaged membranes. Release of LDH from damaged cells is measured by supplying lactate, NAD^+ , resazurin as substrates in the presence of diaphorase. Generation of the fluorescent resorufin product is proportional to the amount of LDH. The scheme is shown in Figure 1.

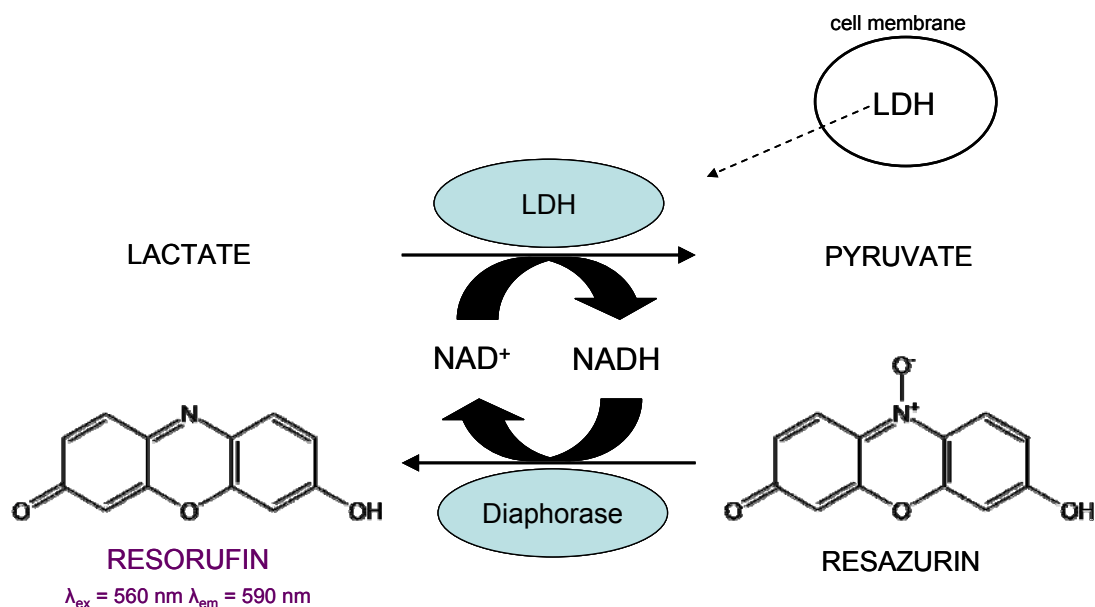


Figure 1. Release of LDH from damaged cells is measured by supplying lactate, NAD⁺, and resazurin as substrates in the presence of diaphorase. Generation of the fluorescent resorufin product is proportional to the amount of LDH (adapted from CytoTox-ONE™ Technical Bulletin, Promega Corporation, Madison, WI).

MATERIALS AND METHODS

Materials. Synthetic melittin was purchased from Bachem (Bubendorf BL, Switzerland) (purity >97% by reverse phase HPLC). The peptide was used without further purification. The concentration of melittin stock solution in HEPES buffer (20 mM HEPES, 118 mM NaCl, 5 mM KCl, 1.3 mM CaCl₂, 0.5 mM MgCl₂) was determined by UV spectroscopy at 280 nm using absorption coefficient of 5570 M⁻¹cm⁻¹. Serial dilution of melittin stock solution were prepared in Dulbecco's modified Eagle's medium (DMEM) with 2 mM L-Glutamine, 4500 mg/L D-Glucose, without sodium pyruvate, supplemented with 7% (v/v) fetal bovine serum. All cell culture media and supplements were from Gibco-BRL (Basel, Switzerland).

Cell Lines. Chinese hamster ovary cell line CHO K1 (ATCC, Manassas, VA, USA) and pgsA-745 cells (ATCC, Manassas, VA, USA), a mutant deficient in xylosyltransferase were kindly provided by Prof. Ballmer (Paul Scherrer Institut, Villingen, Switzerland). Both cell lines were grown in F12-K medium with 2 mM L-Glutamine, 100 U/mL penicillin, 100 µg/mL streptomycin and 10% (v/v) fetal bovine serum.

Both cell lines were grown at 37 °C in a humidified atmosphere with 5% CO₂.

Cytotoxicity assay. CHO K1, pgsA-745 cells (10,000 cells per well in 96-well plates) were seeded in growth medium for 24 h and cultured at 37 °C and 5% CO₂. Melittin stock solution in HEPES buffer was diluted in Dulbecco's modified Eagle's medium (DMEM) with 2 mM L-Glutamine, 4500 mg/L D-Glucose, 7% fetal bovine serum, without sodium pyruvate (GIBCO) and added to the cells. Then the cells were incubated for 30 min at 37 °C and 5% CO₂. After incubation time, the cell viability was determined with CytoTox-One™ Homogenous Membrane Integrity Assay (Promega Corporation, Madison, WI, USA) according to the manufacturer's instructions. Briefly, after the incubation with peptide the assay plate was removed from 37 °C incubator and equilibrated 5 min at room temperature. 100 µL of CytoTox-ONE™ Reagent was added to 100 µL of medium containing cells. Plate was shaken for 30 s and incubated at RT for 10 min. After incubation time 50 µL of Stop Solution was added to each well to rapidly stop the continued generation of fluorescent product. Plate was shaken for 10 s and fluorescence with $\lambda_{\text{ex}} = 560 \text{ nm}$ and $\lambda_{\text{em}} = 590 \text{ nm}$ was recorded.

In parallel, control measurements were performed. No-cell control was used to determine the background fluorescence. A control of untreated cells served as a vehicle control. A maximum LDH release control allowed to determine the maximum LDH release. To generate maximum LDH release, Lysis solution [9% (w/v) solution of Triton X-100] was used.

The average fluorescence values from experimental, maximum LDH release and culture medium background were used to calculate the percent of cytotoxicity for a given experimental treatment in the following way:

$$\text{percent of cytotoxicity} = \frac{(\text{Experimental} - \text{Culture Medium Background})}{(\text{Maximum LDH Release} - \text{Culture Medium Background})}$$

RESULTS

The cytotoxic effect of melittin on the integrity of the plasma membrane of CHO K1 and pgsA-745 is shown in Figure 2.

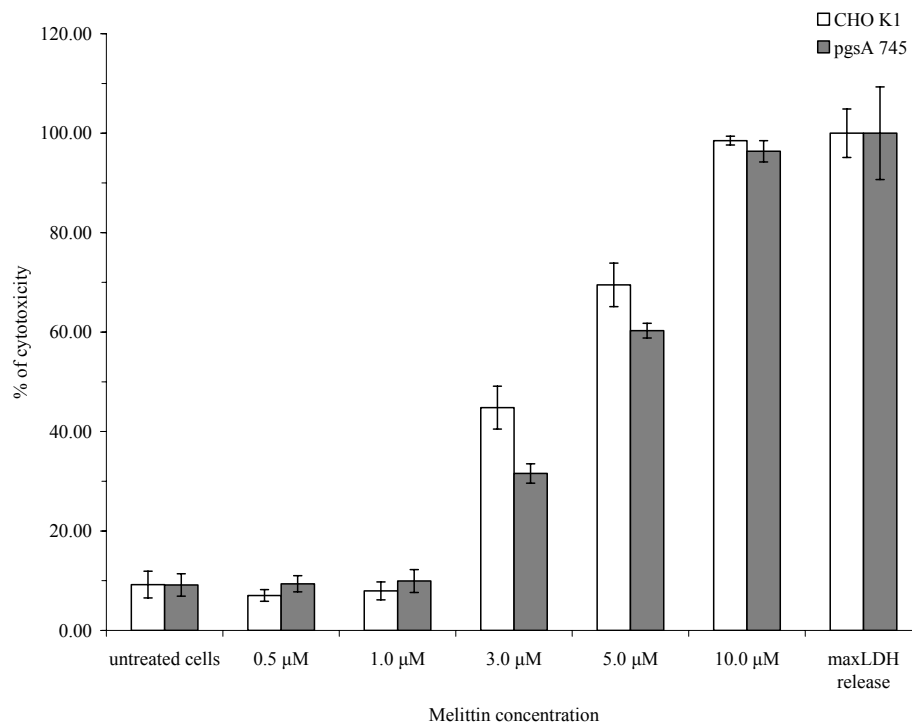


Figure 2. Cytotoxic effect of melittin on the CHO K1 and pgsA-745 cells was measured using LDH release assay after incubation with various concentration of melittin for 30 min at 37 °C and 5% CO₂. Data are expressed as the mean of three independent experiments \pm SE.

At low concentrations up to 1 μ M of melittin we did not observe any effect of the peptide on both cell lines, the percent of cytotoxicity is in the same range of about 8 to 9% as for untreated cell control. At high concentration of 10 μ M effect of melittin is almost the same as the maximum LDH release. The percent of cytotoxicity is $98.5 \pm 0.9\%$ for CHO K1 and $96.4 \pm 2.1\%$ for pgsA-745 cells. These results indicate that all cells are lysed. The differences in the cytotoxic effect of melittin for these two cells lines are observed in the

range of peptide concentration of 3 to 5 μM . The value of the percent of cytotoxicity is higher for CHO K1 cells than for pgsA-745 at the same concentration. At 3 μM of melittin the percent of cytotoxicity are $44.8 \pm 4.3\%$ for CHO K1 cells and $31.6 \pm 2.0\%$ for pgsA-745 cells. At higher concentration of the peptide of 5 μM , the percent of cytotoxicity is $69.5 \pm 4.4\%$ and $60.3 \pm 1.5\%$ for CHO K1 and pgsA-745, respectively. IC_{50} (the dose required to kill 50% of a tested population) values were then extrapolated from graphical plots of cytotoxicity curves. For CHO K1 cell line the IC_{50} was determined to be $3.4 \pm 0.3 \mu\text{M}$. For pgsA-745 cells deficient in GAGs the value of IC_{50} is higher and is $4.3 \pm 0.1 \mu\text{M}$.

DISCUSSION

Melittin belongs to the family of antimicrobial peptides and kills various bacteria already in micromolar range of concentrations. The inhibitory concentration, IC_{90} , for the antimicrobial activity for melittin towards *Escherichia Coli* and *Micrococcus Luteus* were 5.7 μM and 8.8 μM , respectively (21). In the other study minimal inhibitory concentration towards *E. Coli*, *Bacillus subtilis* and *Staphylococcus aureus* are found to be 3.9 μM , 2.0 μM and 3.6 μM , respectively (22). These values are comparable to the concentration required to induce lysis of the eukaryotic cells. Weston and Raison examined the cytolytic effect of melittin on a human lymphoblastoid cell line (HMy2) and found that the toxicity of melittin was linear over the concentration range 0.875-3.5 μM (23). Tosteson showed that already 0.6 μM of melittin induce lysis of 70% of erythrocytes. In another study lower hemolysis was showed. It was observed that 10 $\mu\text{g/mL}$ (3.5 μM) of melittin induce lysis of 60% of the red blood cells (24). In case of other antimicrobial peptides such as magainin 2 and nisin A, concentrations required to induce hemolysis are much higher. A lack of hemolysis for magainin 2 was demonstrated up to 150 $\mu\text{g/mL}$, what corresponds to 60.8

μM (25). In the recent study Maher and McClean showed minimal hemolysis of magainin 2 even up to $400 \mu\text{g/mL}$ ($162.14 \mu\text{M}$) (21). They also observed that 1000-fold greater concentration of nisin A than the antimicrobial IC_{90} value ($18.7 \mu\text{M}$ towards *E. Coli*) lysed only 12% of sheep erythrocytes. Cell viability can be determined, not only with the LDH release assay, but also with MTT assay and neutral red uptake assay. MTT assay is based on the reduction of the tetrazolium salt, methylthiazolyldiphenyl (MTT) into blue formazan product by oxidoreductases of viable cell. The resultant formazan formation is proportional to the number of viable cells. The neutral red uptake assay is based on the neutral red (toluylene red) dye, which is actively transported into lysosome of viable cells. The cellular uptake of the dye is proportional to the number of viable cells. The IC_{50} values for melittin determined with MTT assay for HT29 and Caco-2 cells are $1.2 \mu\text{M}$ and $1.8 \mu\text{M}$, respectively, whereas the IC_{50} determined in the same assay for magainin 2 were $81 \mu\text{M}$ for HT29 cells and $79.9 \mu\text{M}$ for Caco-2 cells. In the assay based on neutral red dye uptake, the IC_{50} values for melittin were $5.6 \mu\text{M}$ for HT29 cells and $4.7 \mu\text{M}$ for Caco-2 cells. In the case of magainin 2 for both cell lines concentrations of up to $100 \mu\text{M}$ were employed without reaching the IC_{50} value (21).

The IC_{50} value, determined with LDH release assay, for melittin-induced lysis in control cell line, CHO K1, is $3.4 \mu\text{M}$. The IC_{50} value for melittin-induced lysis in cell line which lacks GAGs is found to be $4.3 \mu\text{M}$. Surprisingly the IC_{50} for the mutant cell line is only 1.3 higher than this one obtained for the wild type cells.

Table 1. The p values determined by student's t-test for each concentration of melittin tested and IC₅₀ from three independent experiments.

| 0.5 μM | 1.0 μM | 3.0 μM | 5.0 μM | 10.0 μM | IC ₅₀ |
|--------|--------|--------|--------|---------|------------------|
| 0.152 | 0.268 | 0.024 | 0.059 | 0.201 | 0.032 |

Only at 3 μM concentration of melittin and IC₅₀, the p values are less than 0.05, but higher than 0.01, which is considered as a borderline statistically significant. The level of significance, $p \leq 0.05$, still involves high probability of error (5%).

If the GAGs are involved in the lytic mechanism of action of melittin, it was hoped that the differences in the toxic effect of the peptide on the two cell lines discussed above would be much more pronounced. However the surface of eukaryotic cells is not only decorated with sulfated GAGs, but also with other charged glycolipids and glycoproteins. For instance, gangliosides; contain negatively charged sialic acid residues, which contribute to the negative charge of the cell surface. More detailed studies on the interaction of melittin and other microbial peptides with glycolipids and glycoproteins are required to better understand the mechanism of melittin-induced toxicity.

It is also known that the lysis of eukaryotic cells is a fast process and that most cells die within 30 min (23). Observations under the light microscope showed that the red blood cells were lysed within two minutes after exposure to melittin (26). If there are any differences in the mode of action of melittin between wild type cells and mutant cells deficient in GAGs, these should only be observed in the very short time after addition of the peptide to the cells. Unfortunately, the assay used in our studies does not have a sufficiently short time resolution and it was not possible to follow the early stages of the melittin-cell membranes interaction. The fluorescence-activated cell sorting (FACS)

analysis seems to be appropriate for such an approach. This technique allows rapid analyses of large populations of cells using the appropriate fluorescence signal. Using this method it should be possible to record the cytotoxicity of melittin within minutes after addition of the peptide to the cells.

REFERENCES

1. Clague, M. J., and Cherry, R. J. (1988) Comparison of p25 presequence peptide and melittin. Red blood cell haemolysis and band 3 aggregation. *Biochem J* 252, 791-4.
2. Dufton, M. J., Hider, R. C., and Cherry, R. J. (1984) The influence of melittin on the rotation of band 3 protein in the human erythrocyte membrane. *Eur Biophys J* 11, 17-24.
3. Hu, K. S., Dufton, M. J., Morrison, I. E., and Cherry, R. J. (1985) Protein rotational diffusion measurements on the interaction of bee venom melittin with bacteriorhodopsin in lipid vesicles. *Biochim Biophys Acta* 816, 358-64.
4. Mahaney, J. E., and Thomas, D. D. (1991) Effects of melittin on molecular dynamics and Ca-ATPase activity in sarcoplasmic reticulum membranes: electron paramagnetic resonance. *Biochemistry* 30, 7171-80.
5. Cuppoletti, J., Blumenthal, K. M., and Malinowska, D. H. (1989) Melittin inhibition of the gastric (H⁺ + K⁺) ATPase and photoaffinity labeling with [125I]azidosalicylyl melittin. *Arch Biochem Biophys* 275, 263-70.
6. Cuppoletti, J., and Abbott, A. J. (1990) Interaction of melittin with the (Na⁺ + K⁺)ATPase: evidence for a melittin-induced conformational change. *Arch Biochem Biophys* 283, 249-57.

7. Mollay, C., and Kreil, G. (1974) Enhancement of bee venom phospholipase A2 activity by melittin, direct lytic factor from cobra venom and polymyxin B. *FEBS Lett* 46, 141-4.
8. Beschiaschvili, G., and Seelig, J. (1990) Melittin binding to mixed phosphatidylglycerol/phosphatidylcholine membranes. *Biochemistry* 29, 52-8.
9. Kuchinka, E., and Seelig, J. (1989) Interaction of melittin with phosphatidylcholine membranes. Binding isotherm and lipid head-group conformation. *Biochemistry* 28, 4216-21.
10. Ziegler, A. (2007) Thermodynamic studies and binding mechanism of cell-penetrating peptides with lipids and glycosaminoglycans. *Adv Drug Deliv Rev*.
11. Fuchs, S. M., and Raines, R. T. (2004) Pathway for polyarginine entry into mammalian cells. *Biochemistry* 43, 2438-44.
12. Tyagi, M., Rusnati, M., Presta, M., and Giacca, M. (2001) Internalization of HIV-1 tat requires cell surface heparan sulfate proteoglycans. *J Biol Chem* 276, 3254-61.
13. Shieh, M. T., and Spear, P. G. (1994) Herpesvirus-induced cell fusion that is dependent on cell surface heparan sulfate or soluble heparin. *J Virol* 68, 1224-8.
14. Shieh, M. T., WuDunn, D., Montgomery, R. I., Esko, J. D., and Spear, P. G. (1992) Cell surface receptors for herpes simplex virus are heparan sulfate proteoglycans. *J Cell Biol* 116, 1273-81.
15. Chen, J. C., Zhang, J. P., and Stephens, R. S. (1996) Structural requirements of heparin binding to *Chlamydia trachomatis*. *J Biol Chem* 271, 11134-40.
16. Zhang, J. P., and Stephens, R. S. (1992) Mechanism of *C. trachomatis* attachment to eukaryotic host cells. *Cell* 69, 861-9.
17. Esko, J. D., Stewart, T. E., and Taylor, W. H. (1985) Animal cell mutants defective in glycosaminoglycan biosynthesis. *Proc Natl Acad Sci U S A* 82, 3197-201.

18. Bame, K. J., and Esko, J. D. (1989) Undersulfated heparan sulfate in a Chinese hamster ovary cell mutant defective in heparan sulfate N-sulfotransferase. *J Biol Chem* 264, 8059-65.
19. Bame, K. J., Lidholt, K., Lindahl, U., and Esko, J. D. (1991) Biosynthesis of heparan sulfate. Coordination of polymer-modification reactions in a Chinese hamster ovary cell mutant defective in N-sulfotransferase. *J Biol Chem* 266, 10287-93.
20. Bame, K. J., Reddy, R. V., and Esko, J. D. (1991) Coupling of N-deacetylation and N-sulfation in a Chinese hamster ovary cell mutant defective in heparan sulfate N-sulfotransferase. *J Biol Chem* 266, 12461-8.
21. Maher, S., and McClean, S. (2006) Investigation of the cytotoxicity of eukaryotic and prokaryotic antimicrobial peptides in intestinal epithelial cells in vitro. *Biochem Pharmacol* 71, 1289-98.
22. Asthana, N., Yadav, S. P., and Ghosh, J. K. (2004) Dissection of antibacterial and toxic activity of melittin: a leucine zipper motif plays a crucial role in determining its hemolytic activity but not antibacterial activity. *J Biol Chem* 279, 55042-50.
23. Weston, K. M., and Raison, R. L. (1998) Interaction of melittin with a human lymphoblastoid cell line, HMy2. *J Cell Biochem* 68, 164-73.
24. Blondelle, S. E., and Houghten, R. A. (1991) Hemolytic and antimicrobial activities of the twenty-four individual omission analogues of melittin. *Biochemistry* 30, 4671-8.
25. Zasloff, M. (1987) Magainins, a class of antimicrobial peptides from *Xenopus* skin: isolation, characterization of two active forms, and partial cDNA sequence of a precursor. *Proc Natl Acad Sci U S A* 84, 5449-53.
26. Tosteson, M. T., Holmes, S. J., Razin, M., and Tosteson, D. C. (1985) Melittin lysis of red cells. *J Membr Biol* 87, 35-44.

5. BINDING OF RiDOM TO SULFATED CELL SURFACE SUGARS

INTRODUCTION

Melittin possesses membrane disturbing properties and the net positive charge and therefore it can be an interesting candidate for gene delivery. Melittin binds to DNA by charge interaction, but the melittin/DNA complex does not mediate transfection. Instead it induces toxicity, due to fast partitioning of the peptide into cell membrane (1-3). To overcome the problem of toxicity and in order to increase the stability of the DNA-melittin complex and transfection efficiency, additional effectors can be used. A hybrid molecule, obtained by covalent coupling of an amphiphatic, membrane disturbing peptide to lipid moiety, can create a stable and efficient gene transfer system. Dioleoylmelittin (DOM) is such a hybrid molecule resulting from the conjugation of dioleoylphosphatidylethanolamine-*N*-[3-(2-pyridyldithio)propionate] with [Cys¹]melittin, an analog of melittin in which the N-terminus glycine was replaced by cysteine. It was shown that DOM can form homogenous small particles with DNA and it mediates efficient transfection of various cell lines. Successful transfections have been reported for cells CV-1 (monkey kidney fibroblasts), CHO K1 (Chinese hamster ovary cells) and HEK 293 (human embryonic kidney cells) (4). But it was also shown that DOM is toxic and not stable. Retro-inverso dioleoylmelittin (riDOM), the structure of which is shown in Figure 1, is another hybrid molecule, in which the lipid is coupled to retro-inverso analog of [Cys¹]melittin, where all L-amino acids residues are replaced by the corresponding D-isomers and the amino acid sequence of the peptide is reversed. RiDOM shows no hemolytic activity, is much less toxic in transfection than DOM, and it is stable over months.

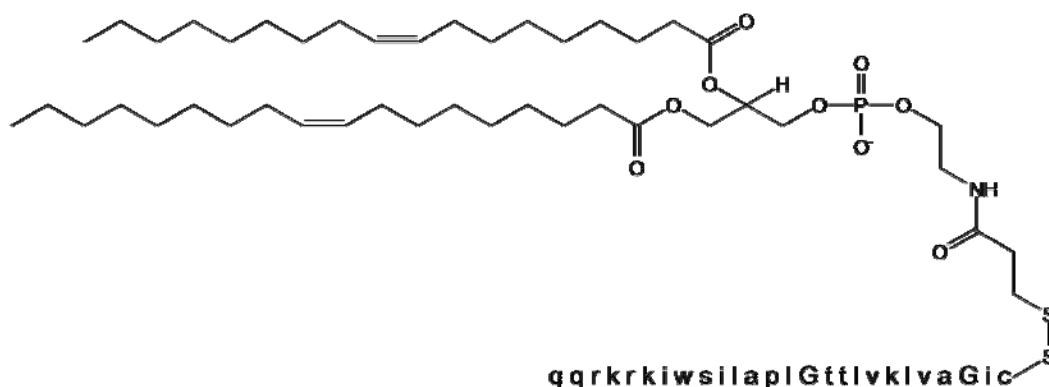


Figure 1. Structure of riDOM (retro-inverso dioleoylmelittin).

The net positive charge of melittin conjugates suggest that similarly to other cationic lipids and cell-penetrating peptides, the cellular uptake of these molecules is mediated by GAGs. We have also already shown that melittin interacts strongly with sulfated cell surface sugars; therefore we have decided to study thermodynamic equilibrium of the riDOM/HS interactions.

MATERIALS AND METHODS

Materials. RiDOM was kindly provided by Dr. Eric Kitas from F. Hoffman-La Roche Ltd (Basel, Switzerland). Heparan sulfate (HS) sodium salt (from porcine intestinal mucosa, average molecular weight, 13 655 Da, sulfur content 5.51%) and dermatan sulfate (DS) sodium salt (from porcine intestinal mucosa, average molecular weight, 41 400 Da, sulfur content 6.85%) were from Celsus Laboratories (Cincinnati, OH). Low molecular weight heparin sodium salt (from porcine intestinal mucosa, average molecular weight 3000) was from SIGMA (St. Louis, MO, USA).

All other chemicals were of analytical or reagent grade. Tris buffer (10 mM tris(hydroxymethyl)aminoethane, pH 7.4) was prepared from 18 M Ω water obtained from a

NANOpure A filtration system. NaCl concentrations were variable (50 to 250 mM) and are specified in the legends of each figure. The samples were degassed immediately before use.

Isothermal Titration Calorimetry. All measurements were made with a MicroCal VP-ITC calorimeter (MicroCal, Northampton, MA, USA). Titrations were performed by injecting 5-10 μL aliquots of the glycosaminoglycan solution into the calorimeter cell ($V_{\text{cell}} = 1.4037$ mL) containing riDOM at a concentration of typically 100-200 μM . The concentrations of the injected glycosaminoglycan solution were about 50 μM for HS, 21 μM for DS and 490 μM for heparin.

The heats of dilution were determined in control titrations by injecting a glycosaminoglycan or lipid solution into pure buffer. The heats of dilution were small (~ -1 to 1 μcal), and were included in the final analysis. Raw data were processed using Origin software provided with the instrument. The temperature was set as indicated in the legends of the figures. All measurements were performed in Tris buffer (10 mM, pH 7.4) with varying NaCl concentrations.

Binding model. For a complete thermodynamic characterization of the binding process, the calorimetric data were analyzed with a multisite binding model, which was also used to describe the binding equilibrium of other peptides to HS (5, 6). In this model a long polymer such as HS is described as a macromolecule with n independent and equivalent binding sites for a ligand like melittin. The binding model is represented by the following equation:

$$\frac{[\text{P}]_{\text{b}}}{[\text{HS}]_{\text{t}}} = \frac{nK[\text{P}]}{1 + K[\text{P}]} \quad (1)$$

$[P]$ and $[P]_b$ are the concentrations of free and bound melittin, respectively, $[HS]_t$ is the total concentration of HS, K is the intrinsic binding constant, n is the number of melittin. Because of mass conservation, the concentration of bound peptide can be described by:

$$[P]_b = \frac{1}{2} \left(\frac{1}{K} + [P]_t + n[HS]_t \right) - \frac{1}{2} \sqrt{\left(\frac{1}{K} + [P]_t + n[HS]_t \right)^2 - 4n[HS]_t[P]_t} \quad (2)$$

The index t denotes the total concentration of peptide and HS in the calorimeter cell after each injection step. The peptide concentration changes during the titration with HS because of dilution effects.

The concentration of bound peptide is linked to the calorimetric data by the following equation:

$$\delta Q_i = \Delta H_{riDOM}^0 \delta [P]_{b,i} V \quad (3)$$

where δQ_i is the heat absorbed or released in injection i^{th} , ΔH_{riDOM}^0 is the peptide binding enthalpy, $\delta [P]_{b,i}$ is the change (increase) in *bound* peptide concentration upon injection i , and V is the volume of the calorimeter cell (7).

Circular Dichroism Spectroscopy. CD measurements of riDOM in the absence and the presence of glycosaminoglycan (buffer 10 mM Tris, 100 mM NaF, pH 7.4) were made using a Chirascan CD spectrometer (Applied Photophysics Ltd. Leatherhead, UK). A quartz cuvette with a path length of 0.1 cm was used. All spectra were corrected by subtracting the buffer baseline. Results are reported as mean residue ellipticity in units of

$\text{deg cm}^2 \text{ dmol}^{-1}$. The percentage of peptide secondary structure was estimated from a computer simulation based on the reference spectra obtained by Reed and Reed (8)

Dynamic Light Scattering. Dynamic light scattering measurements were performed in Zetasizer Nano ZS (Malvern Instruments Ltd., Worcestershire, UK). Typically, 1.3 mL solution of riDOM (50 μM) was titrated with HS (150 μM). The results of the volume distribution are shown.

RESULTS

Binding of riDOM to HS. Figure 2 shows a calorimetric heat flow trace (Figure 2A) and the corresponding titration curve (Figure 2B) obtained at 5 °C by titration of riDOM (100 μM) with 5 μL aliquots of HS (50 μM). The integrated heats in Figure 2B represent the net heats of each injection after correcting for the heats of dilution of the HS obtained in separate HS-into-buffer titration.

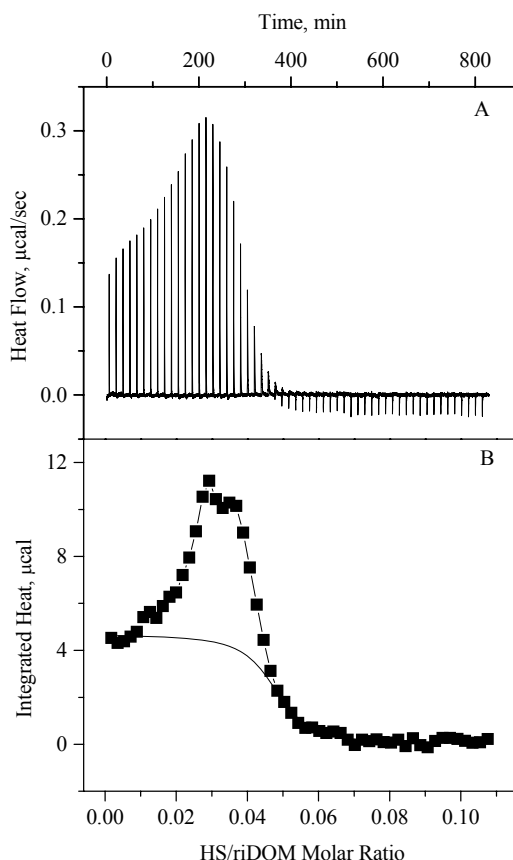


Figure 2. Titration of HS into riDOM. (A) Calorimetric trace obtained at 5 °C by titration of HS (50 μM) into a solution of riDOM (100 μM). Each peak corresponds to the injection of 5 μL into the calorimeter cell. (B) Heats of reaction (integrated from the calorimetric trace) plotted as a function of the HS/riDOM ratio. The solid line is the best fit to the experimental data (\blacksquare) using the binding model described by eqs 1-3 with the following parameters: $\Delta H_{\text{riDOM}}^0 = 0.85 \text{ kcal/mol}$, $K = 2.5 \times 10^5 \text{ M}^{-1}$, $n = 23$. Buffer: 10mM Tris, 10mM NaCl, pH 7.4.

Figure 2 demonstrates an *endothermic* reaction at 5 °C. The heats measured during the few injections are relatively constant with $h_i \approx 4.52 \mu\text{cal}$ per injection. The theoretical curve (solid line calculated using the binding model of eqs 1-3 with $n = 23$, $K = 2.5 \times 10^5 \text{ M}^{-1}$, and $\Delta H_{\text{riDOM}}^0 = 0.85 \text{ kcal/mol}$) indicates that after five injections $\sim 20\%$ of the total riDOM in the calorimeter cell is bound to HS. At this point, an additional *endothermic* reaction takes place, which extends between $\sim 20\%$ and $\sim 89\%$ of bound riDOM. The additional

heat, referenced to the total amount of riDOM, is $\Delta H \sim 0.46$ kcal/mol, which is $\sim 54\%$ of the total reaction heat. The molecular nature of this second reaction is unclear. A similar behavior has been observed for the titration of one of the analogs of melittin, [Cys]¹melittin, with HS (9). It was also reported for the titration of DNA with multivalent cations, and was interpreted in terms of DNA condensation and aggregation (10). The second additional reaction in the riDOM-HS interaction could correspond to a reorganization of the complex to more compact aggregate.

Calorimetric titrations were performed at different temperatures in the range of 5-50 °C. Table 1 summarizes the thermodynamic parameters obtained by using the binding model described by eqs 1-3.

Table 1. Titration of riDOM with HS. Thermodynamic parameters as a function of temperature in buffer (10 mM Tris, 10 mM NaCl at pH 7.4)

| T (°C) | n | K (M ⁻¹) | ΔH_{riDOM}^0 (kcal/mol) | ΔG_{riDOM}^0 (kcal/mol) | $T\Delta S_{riDOM}^0$ (kcal/mol) |
|-----------|------|-------------------------|------------------------------------|------------------------------------|-------------------------------------|
| 5 | 23.0 | 2.5×10^5 | 0.85 | -6.87 | 7.72 |
| | 24.0 | 2.6×10^5 | 0.77 | -6.91 | 7.68 |
| 15 | 23.0 | 3.1×10^5 | 0.65 | -7.24 | 7.89 |
| 25 | 18.0 | 3.5×10^5 | 0.65 | -7.56 | 8.21 |
| | 20.0 | 3.5×10^5 | 0.65 | -7.56 | 8.21 |
| 37 | 20.0 | 4.0×10^5 | 0.40 | -7.95 | 8.35 |
| 50 | 20.0 | 4.0×10^5 | 0.20 | -8.28 | 8.48 |

The binding stoichiometry of riDOM/HS varies between 18 and 24. $\Delta H_{\text{riDOM}}^0$ is positive at all temperatures tested, decreasing from ~ 0.85 kcal/mol to ~ 0.20 kcal/mol as the temperature is raised from 5 to 50 °C. From the slope of the straight line in Figure 3A, we obtained a very small negative molar heat capacity change of $\Delta C_{\text{p,riDOM}}^0 = -13$ cal mol⁻¹ K⁻¹. The solid line in Figure 3B describes the predicted temperature dependence of the binding constant K based on the van't Hoff law $\ln K/dT = \Delta H_{\text{riDOM}}^0 / RT^2$ taking into account the temperature dependence of the reaction enthalpy as $\Delta H(T) = \Delta H^0 + \Delta C_p^0(T - T_0)$.

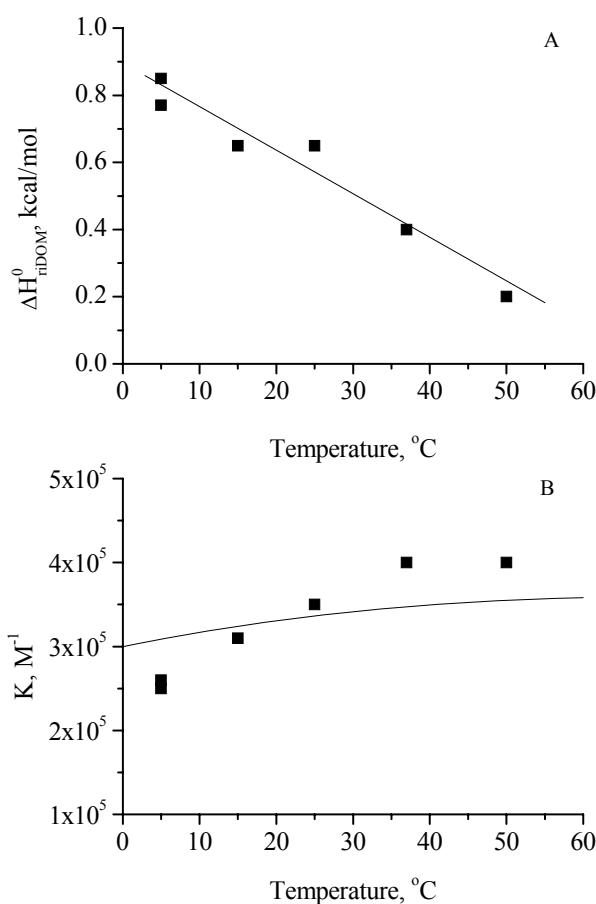


Figure 3. Temperature dependence of the thermodynamic parameters. (A) $\Delta H_{\text{riDOM}}^0$, for riDOM binding to HS. Linear regression analysis of the experimental data yields $\Delta H_{\text{riDOM}}^0 = 0.88 - 0.013T$ (°C) (solid line). (B) Binding constant K_0 . The solid line in (B) is predicted temperature dependence of K_0 based on the van't Hoff equation and using the above regression formula for $\Delta H_{\text{riDOM}}^0(T)$. Buffer: 10mM Tris, 10mM NaCl, pH 7.4.

We have also studied interaction of riDOM with heparin and DS. ITC titration curves exhibits the same pattern as those observed for HS at the identical temperatures (Figure 4).

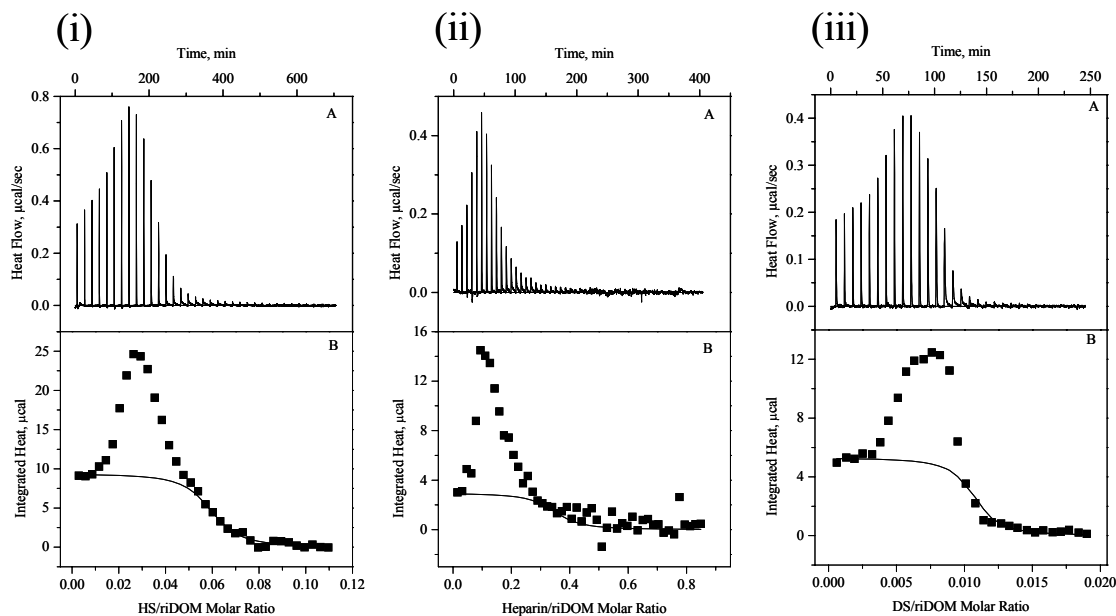


Figure 4. Titration of HS, heparin, DS into riDOM. (A) Calorimetric trace obtained at 25 °C by titration of HS (100 μ M), heparin (490 μ M), DS (21 μ M) into a solution of riDOM (112-200 μ M). Each peak corresponds to the injection of 8 μ L of HS and 5 μ L of heparin and DS into the calorimeter cell. (B) Heats of reaction (integrated from the calorimetric trace) plotted as a function of the HS/heparin/DS to melittin ratio. The solid line is the best fit to the experimental data (■) using the binding model described by eqs 1-3 with the following parameters: for (i) HS-into-riDOM: $\Delta H_{riDOM}^0 = 0.65$ kcal/mol, $K = 5.0 \times 10^5$ M $^{-1}$, $n = 18$; (ii) heparin-into-riDOM: $\Delta H_{riDOM}^0 = 0.4$ kcal/mol, $K = 5.0 \times 10^5$ M $^{-1}$, $n = 3$; (iii) DS-into-riDOM: $\Delta H_{riDOM}^0 = 0.53$ kcal/mol, $K = 1.0 \times 10^6$ M $^{-1}$, $n = 95$. Buffer: 10mM Tris, 10mM NaCl, pH 7.4.

For DS the binding constant, K , is larger than those obtained for HS and heparin at 25 °C. For DS the binding constant is of order 10^6 M $^{-1}$. The riDOM molar binding enthalpies, ΔH_{riDOM}^0 at 25 °C are 0.4 kcal/mol for heparin and 0.53 kcal/mol for DS. The main difference found between these glycosaminoglycans is the binding stoichiometry. The

number of binding sites for riDOM at 25 °C is 3 for heparin, 18 for HS, and 95 for DS. Since the three polysaccharides have a different molecular weight, a better comparison is the binding capacity per 1 kDa which is ~ 1 for heparin, ~ 1.3 for HS, and ~ 2.3 for DS.

Salt effect on binding of riDOM to HS. We have also performed titrations of riDOM with HS at different salt concentrations.

The ITC titrations patterns were identical to those observed for titrations done at low salt concentrations (10 mM NaCl), but the total heat released during the titrations was lower. At 25 °C the total enthalpy of the reaction determined from the total heat released in the titration (~ 109.6 µcal) and the amount of the riDOM in the calorimeter cell (280.7 nmol) is 0.39 kcal/mol, whereas for the same experiment performed at 10 mM NaCl in buffer, the enthalpy derived from the total heat released in the titrations (~ 280.3 µcal) and the amount of riDOM (~280.7 nmol) is 1.0 kcal/mol.

The calorimetric data were then analyzed with the binding model described by Eqs 1-3.

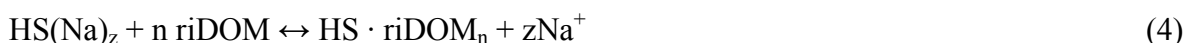
The thermodynamic parameters obtained at 25 °C are summarized in Table 2.

Table 2. The effect of NaCl on the thermodynamic parameters of HS binding to riDOM at 25 °C. Buffer: 10 mM Tris and variable concentrations of NaCl at pH 7.4. * Mean ± SD of three measurement.

| NaCl (mM) | n | K (M ⁻¹) | ΔH_{riDOM}^0 (kcal/mol) | ΔG_{riDOM}^0 (kcal/mol) | $T\Delta S_{riDOM}^0$ (kcal/mol) |
|-----------|----------------|-----------------------------|---------------------------------|---------------------------------|----------------------------------|
| 10 | 18 | 3.5×10^5 | 0.65 | -7.56 | 8.21 |
| | 20 | 3.5×10^5 | 0.65 | -7.56 | 8.21 |
| 50 | 18.0 | 3.0×10^5 | 0.30 | -7.47 | 7.77 |
| 100* | 25.3 ± 6.0 | $(2.6 \pm 0.7) \times 10^5$ | 0.20 ± 0.02 | -7.37 ± 0.17 | 7.57 ± 0.19 |
| 150 | 23.0 | 2.0×10^5 | 0.08 | -7.23 | 7.31 |

The binding affinity of HS to riDOM decreases with increasing salt concentration in the buffer. Therefore we can analyze the salt dependence of the binding constant with a model for protein-polyelectrolyte interactions (11).

HS is a highly charged poly-anion but a considerable fraction of its sulfate groups is probably neutralized by Na^+ due to counterion condensation (12). Upon binding of riDOM the counterions are released into the bulk solution as described by the following reaction scheme:



with the corresponding equilibrium

$$K_T = \frac{[\text{HS} \cdot \text{riDOM}_n][\text{Na}^+]^z}{[\text{HS}(\text{Na})_z][\text{riDOM}]^n} = K[\text{Na}^+]^z \quad (5)$$

K_T is the binding constant at 1 M Na^+ concentration and is usually described as K_{nonionic} , as ionic interactions are much reduced at this concentration. On the other hand, K is the actual binding constant derived directly from the ITC experiment which varies with Na^+ concentration (Table 2). Taking the logarithm on both sides of the equation (5) and rearranging gives

$$\log K = \log K_T - z \log[\text{Na}^+] \quad (6)$$

A plot of the experimental $\log K$ as a function of $\log [\text{Na}^+]$ shows linear dependency in the riDOM/HS system (Figure 5). Linear regression analysis yields $\log K = 5.1 - 0.3 \log [\text{NaCl}]$. The y-intercept is the nonionic binding constant at 1 M Na^+ of $1.26 \times 10^5 \text{ M}^{-1}$.

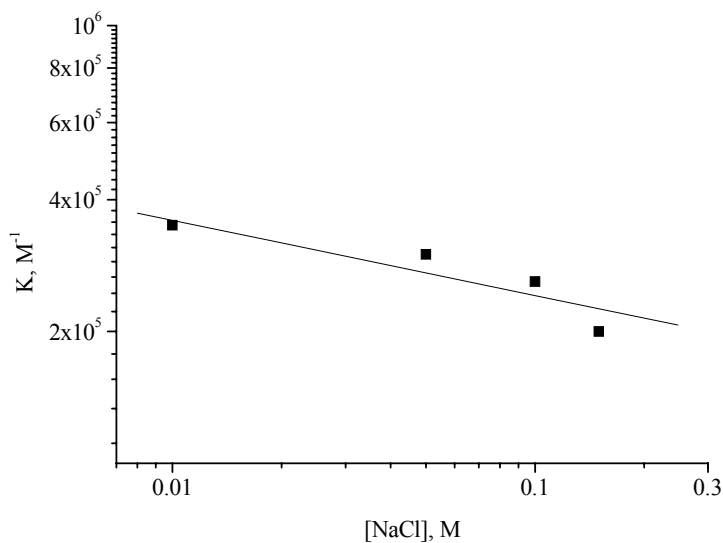


Figure 5. Salt dependence of the interaction between riDOM and HS. Binding constant (K_0) for HS binding to riDOM was determined as a function of NaCl concentration in Tris buffer (10 mM Tris, pH 7.4) from ITC measurements at 25 °C. K values are plotted as a function of the NaCl concentration on log/log scale. Linear regression analysis of the experimental data yields $\log K = 5.1 - 0.3 \log[\text{NaCl}]$ (solid line).

The variation of the thermodynamic parameters with changing salt concentration is displayed in Figure 6. The thermodynamic parameters of riDOM, $\Delta H_{\text{riDOM}}^0$, $\Delta G_{\text{riDOM}}^0$, and $\Delta S_{\text{riDOM}}^0$, are dependent on the NaCl concentration. Enthalpy and entropy of the binding reaction, $\Delta H_{\text{riDOM}}^0$ and $\Delta S_{\text{riDOM}}^0$ (Figure 6A, B), decrease with increasing ionic strength.

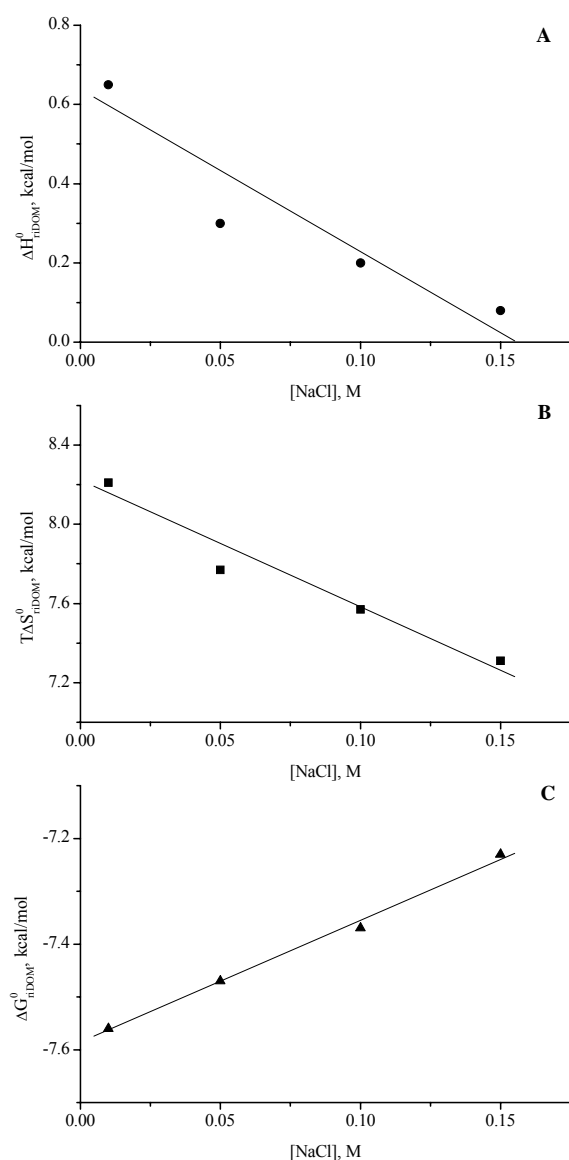


Figure 6. Dependence of (A) ΔH_{riDOM}° , (B) $T\Delta S_{riDOM}^{\circ}$, and (C) ΔG_{riDOM}° on the NaCl concentration in Tris buffer (10mM Tris, pH 7.4) at 25 °C for the interaction of riDOM with HS.

Structural properties of riDOM binding to HS. To check structural changes in riDOM induced by interaction with HS, we have analyzed the secondary structure of riDOM in the absence and presence of HS with CD spectroscopy. The CD spectra were obtained at 25 °C in 10 mM Tris, 10 mM NaF and pH 7.4. RiDOM at concentration of 50 μ M was titrated with 150 μ M solution of HS. The CD spectrum of riDOM is mirror-imaged at the x-axis

compared to the conventional α -helix spectrum because riDOM is composed of all D-amino acids (Figure 7).

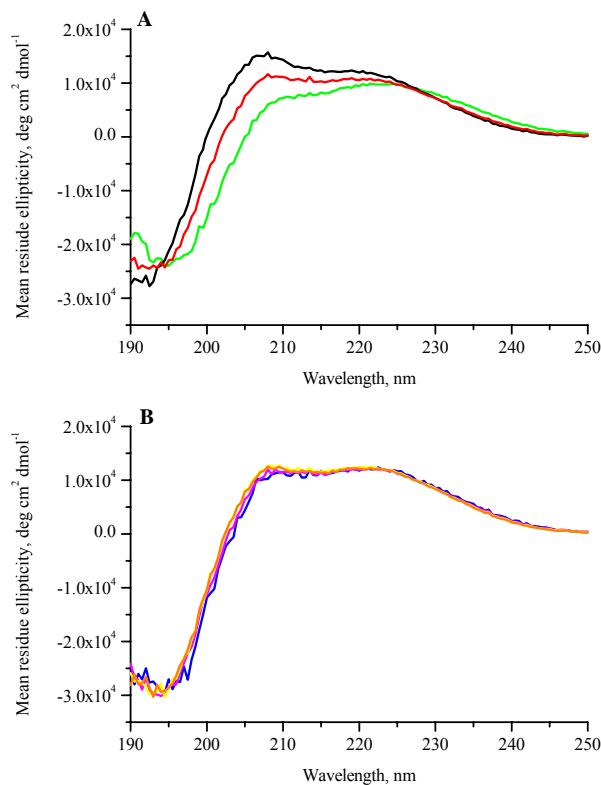


Figure 7. CD spectra monitoring conformational changes in riDOM upon addition of HS. Mean residue ellipticity values of riDOM (50 μ M) in the absence and upon titration with HS (150 μ M) are plotted as a function of wavelength. (A) black – riDOM; red – HS/riDOM 0.02; green – HS/riDOM 0.06; (B) blue – HS/riDOM 0.08; magenta – HS/riDOM 0.10; yellow – HS/riDOM 0.15; orange – HS/riDOM 0.20. Buffer: 10 mM Tris, 10mM NaF, pH 7.4.

Figure 8 shows calculated content of α -helix, β -structure and random coil (RC) of riDOM upon addition of HS. In the absence of HS α -helix and RC contribute almost equally to the secondary structure of riDOM. The content of α -helix and RC is $\sim 35.1\%$ and $\sim 34.6\%$, respectively. The β -structure content is not much lower and is $\sim 30.3\%$. Upon titration with HS the α -helix content decreases to 11.3% at 0.06 HS-to-riDOM molar ratio, and then

increases slowly again up to 31.1% with further addition of HS. The β -structure content increases to the highest value of $\sim 70\%$ at 0.06 HS-to-riDOM molar ratio. Further addition of HS causes slow decrease of β -structure. At HS/riDOM molar ratio of 0.2 the β -structure content is $\sim 42.2\%$. The RC content first decreases to 18.8% at HS-to-riDOM molar ratio of 0.06, and then increases to $\sim 26.4\%$ at HS-to-riDOM molar ratio of 0.2.

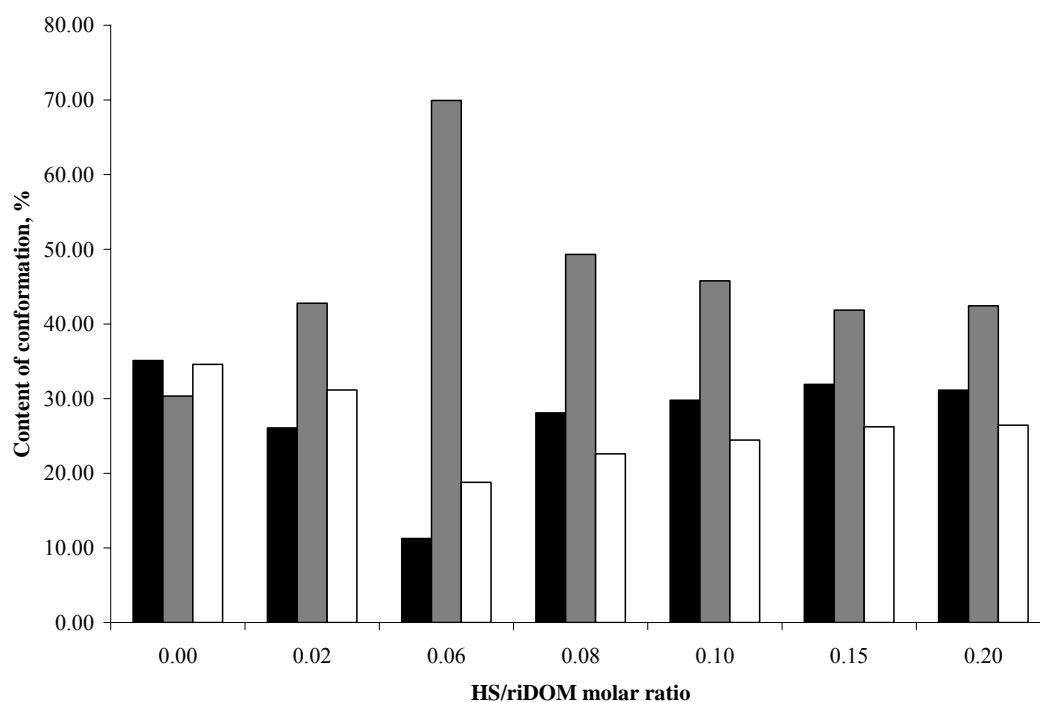


Figure 8. Calculated content of α -helix (black bars), β -structure (grey bars) and RC (white bars) of riDOM upon titration with HS. Buffer: 10 mM Tris, 10 mM NaF, pH 7.4.

Dynamic light scattering studies. A turbid solution is observed when riDOM is mixed with HS. Formation of complexes/aggregates and determination of their size can be followed with Dynamic Light Scattering. Figure 9 shows the size distribution by volume of when the HS solution (150 μM) is titrated into riDOM (50 μM).

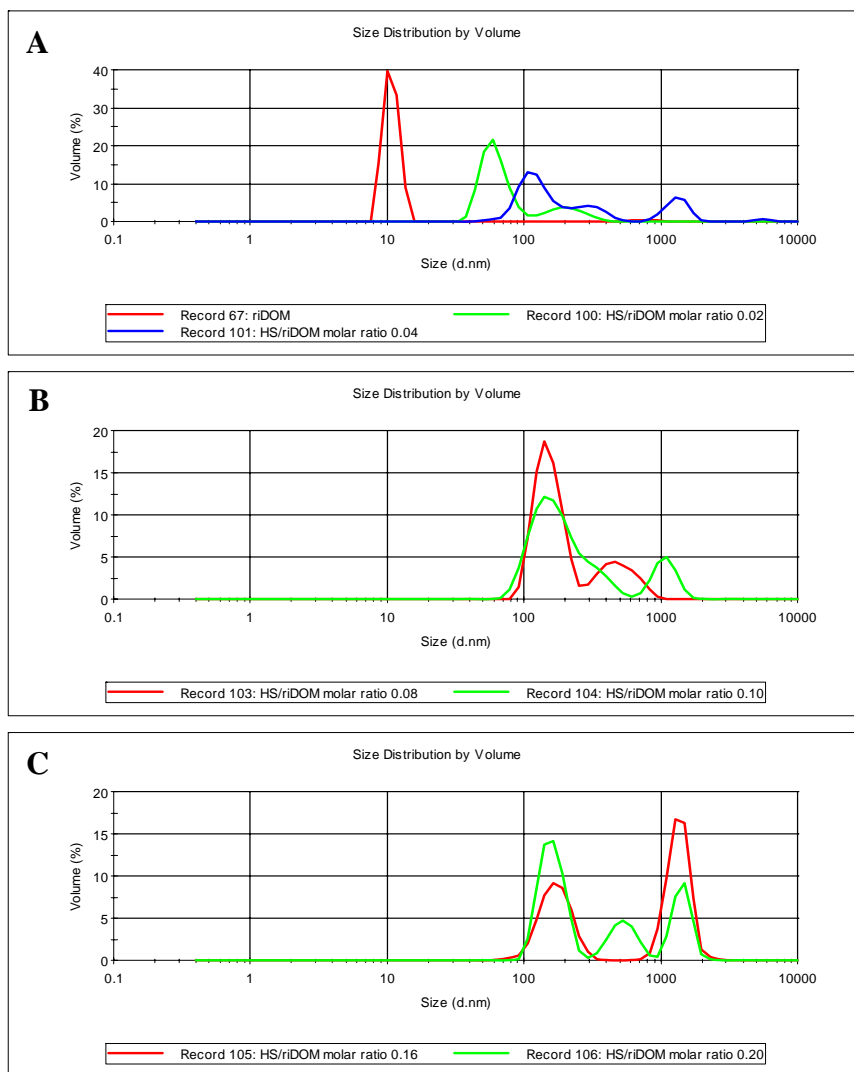


Figure 9. Size distribution by volume for titration of riDOM solution (50 μM) with HS (150 μM) determined by dynamic light scattering. Buffer: 10mM Tris 10 mM NaF at pH 7.4

For riDOM in the absence of HS the very high PDI of 0.842 is found. The particle size of 10.10 nm is determined from the peak position. Addition of HS causes an increase in size and increase in the number of populations of different size aggregates/complexes. Already at low HS-to-riDOM molar ratio of 0.02 two population of particles are observed. Their size determined from the peak position is about 63 nm and 212 nm and the volume they occupied is 80% and 20%, respectively. The PDI of 0.258 and the z-average size of 115 nm are found. At 0.04 HS-to-riDOM molar ratio three populations of particles with different

size are observed. The largest fraction (60%) are particles with size of 126 nm. Two additional fractions are about equal in size and contribute particles with 306 nm and 1311 nm. Further addition of HS does not dramatically change the situation in the system. We still observe presence of two populations of different size aggregates/complexes. The size of one group changes from about 150 nm at 0.08 HS-to-riDOM molar ratio to 174 nm at 0.16 HS-to-riDOM molar ratio. The size of the second population varies from about 490 nm at 0.04 HS-to-riDOM molar ratio to 1362 nm at 0.16 HS-to-riDOM molar ratio. At 0.20 HS-to-riDOM molar ratio part of the large aggregates is dissolved and a third population is observed with size of about 534 nm. The PDI for all presented molar ratios (except riDOM in the absence of HS) is below 0.5, so the results can be compared by the z-average size. Figure 9 shows z-average size as a function of HS-to-riDOM molar ratio. At the beginning of titration the z-average size increase steeply to value of about 182 nm at 0.04 HS-to-riDOM molar ratio. Further addition of HS causes at first a slow increase to maximum z-average size of 238 nm at 0.16 HS-to-riDOM and then a decrease to 222 nm at 0.20 HS-to-riDOM molar ratio.

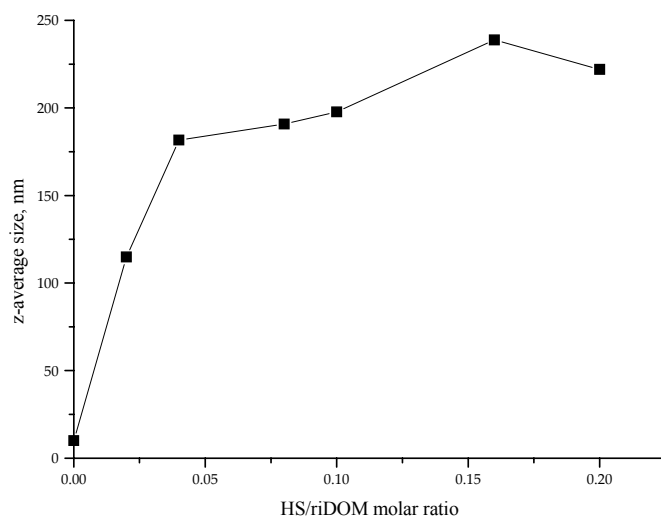


Figure 10. The z-average size of riDOM-HS aggregates/complexes determined by Dynamic Light Scattering plotted as function of HS/riDOM molar ratio. For riDOM in the absence of HS the distribution analysis of the peak position to determine size of particles was used, since PDI was found to be 0.842.

DISCUSSION

The calorimetric data show that riDOM has a high affinity to heparan sulfate (HS). The binding constant at 50 mM NaCl and 25 °C is $K = 3.5 \times 10^5 \text{ M}^{-1}$, corresponding to a dissociation constant of 2.9 μM . This result is similar to binding data obtained for melittin and melittin analogs: at 50 mM NaCl binding constants of $K = 1.0 \times 10^6 \text{ M}^{-1}$, $6.5 \times 10^5 \text{ M}^{-1}$ and $6.3 \times 10^5 \text{ M}^{-1}$ were found for melittin, ri-mel-SH and mel-SH, respectively (9).

RiDOM binds rapidly and tightly to two other glycosaminoglycans, heparin and dermatan sulphate. ITC titration curves and thermodynamic parameters are similar to those of HS indicating that the binding process occurs in the same way as for the interaction of riDOM with HS.

For riDOM the reaction enthalpies are positive and unfavourable for binding in the range of temperature tested (5-50 °C) and the binding of riDOM to HS is entropy driven. Again similar to mel-SH and ri-mel-SH.

The essential element of the binding process is the electrostatic interaction between the cationic riDOM and the anionic groups of HS. The binding constant decreases upon increasing the ionic strength of the buffer. The contribution of electrostatics in the binding process can be estimated from the extrapolated binding constant at 1M NaCl from Figure 5, which shows a linear relation between the observed binding constant of HS to riDOM and the NaCl concentration in double logarithmic plot. The slope of the regressed line in Figure 5 gives the number of Na^+ ions released in the association reaction, whereas the y-intercept at 1 M NaCl provides an estimate of the non-ionic binding constant with $1.3 \times 10^5 \text{ M}^{-1}$. When compared to the binding constant measured at 25 °C and 10 mM NaCl, this value suggests contribution of electrostatics to the free energy of binding ~10%. This is confirmed by the salt dependence of the binding equilibrium. The increase of NaCl content

results in decrease of the binding heats. The reaction enthalpy, $\Delta H_{\text{riDOM}}^0$, at 10 mM NaCl is 0.65 kcal/mol, whereas at 100 mM NaCl the reaction enthalpy is found to be 3 times lower. Enthalpies close to zero and large positive entropy values are typical of hydrophobic interactions (13). The temperature dependence of the reaction enthalpy reveals the negative value of the molar heat capacity change indicating hydrophobic component in the binding process of riDOM with HS. The negative values of heat capacity change were also observed for the interaction of melittin and melittin analogous with HS (9). The hydrophobic interactions are also observed for the binding of cationic lipids to DNA (14, 15). The hydrophobic contribution to the binding process could arise from the interaction between solvent and solvent exposed hydrophobic lipid part of the molecule, aggregation of the riDOM-HS complexes or self association of the riDOM molecules. The binding of riDOM to HS cause formation of bigger complexes/aggregates. Initially, addition of HS to riDOM results in dramatic increase in the mean size of the particles to about 180 nm at HS/riDOM molar ratio of 0.04. At this molar ratio the end of the aggregation process at the calorimetric trace is observed. Indeed, further additions of HS to riDOM cause only slight increase of the mean size of the particles to about 200-220 nm. Formation of homogenous particles with the diameter of about 200 nm was also observed for DOM-DNA complexes (4).

In summary, the overall interaction of riDOM with HS comprises both ionic and hydrophobic components. Ionic contributions result from the interaction of the cationic moiety of riDOM with the negatively charged sulfate groups of the HS chain. Hydrophobic interaction arises from the interaction between hydrocarbon groups of the lipid moiety, aggregation of the formed complexes and conformational changes upon binding of riDOM with HS.

REFERENCES

1. Boeckle, S., Fahrmeir, J., Roedl, W., Ogris, M., and Wagner, E. (2006) Melittin analogs with high lytic activity at endosomal pH enhance transfection with purified targeted PEI polyplexes. *J Control Release* 112, 240-8.
2. Boeckle, S., Wagner, E., and Ogris, M. (2005) C- versus N-terminally linked melittin-polyethylenimine conjugates: the site of linkage strongly influences activity of DNA polyplexes. *J Gene Med* 7, 1335-47.
3. Ogris, M., Carlisle, R. C., Bettinger, T., and Seymour, L. W. (2001) Melittin enables efficient vesicular escape and enhanced nuclear access of nonviral gene delivery vectors. *J Biol Chem* 276, 47550-5.
4. Legendre, J. Y., Trzeciak, A., Bohrmann, B., Deuschle, U., Kitas, E., and Supersaxo, A. (1997) Dioleoylmelittin as a novel serum-insensitive reagent for efficient transfection of mammalian cells. *Bioconjug Chem* 8, 57-63.
5. Goncalves, E., Kitas, E., and Seelig, J. (2005) Binding of oligoarginine to membrane lipids and heparan sulfate: structural and thermodynamic characterization of a cell-penetrating peptide. *Biochemistry* 44, 2692-702.
6. Ziegler, A., and Seelig, J. (2004) Interaction of the protein transduction domain of HIV-1 TAT with heparan sulfate: binding mechanism and thermodynamic parameters. *Biophys J* 86, 254-63.
7. Wiseman, T., Williston, S., Brandts, J. F., and Lin, L. N. (1989) Rapid measurement of binding constants and heats of binding using a new titration calorimeter. *Anal Biochem* 179, 131-7.
8. Reed, J., and Reed, T. A. (1997) A set of constructed type spectra for the practical estimation of peptide secondary structure from circular dichroism. *Anal Biochem* 254, 36-40.

9. Goncalves, E., Kitas, E., and Seelig, J. (2006) Structural and thermodynamic aspects of the interaction between heparan sulfate and analogues of melittin. *Biochemistry* 45, 3086-94.
10. Matulis, D., Rouzina, I., and Bloomfield, V. A. (2000) Thermodynamics of DNA binding and condensation: isothermal titration calorimetry and electrostatic mechanism. *J Mol Biol* 296, 1053-63.
11. Record, M. T., Jr., Anderson, C. F., and Lohman, T. M. (1978) Thermodynamic analysis of ion effects on the binding and conformational equilibria of proteins and nucleic acids: the roles of ion association or release, screening, and ion effects on water activity. *Q Rev Biophys* 11, 103-78.
12. Manning, G. S. (1978) The molecular theory of polyelectrolyte solutions with applications to the electrostatic properties of polynucleotides. *Q Rev Biophys* 11, 179-246.
13. Tanford, C. (1980) The Hydrophobic Effect. Formation of Micelles and Biological Membranes. *Wiley-Interscience: New York*, 60.
14. Lobo, B. A., Davis, A., Koe, G., Smith, J. G., and Middaugh, C. R. (2001) Isothermal titration calorimetric analysis of the interaction between cationic lipids and plasmid DNA. *Arch Biochem Biophys* 386, 95-105.
15. Spink, C. H., and Chaires, J. B. (1997) Thermodynamics of the binding of a cationic lipid to DNA. *J Am Chem Soc* 119, 10920-10928.

6. INTERACTION OF MELITTIN WITH LIPIDS

INTRODUCTION

Melittin, the main component of bee venom from *Apis mellifera*, is short cationic peptide composed mainly of hydrophobic amino acid residues at the amino terminus (positions 1-20) and hydrophilic amino acid residues at the carboxy terminus (positions 21-26) (1). This uneven distribution of hydrophilic and polar residues gives melittin amphiphilic properties. Melittin, unstructured in water, adopts an α -helical conformation upon binding to lipids membranes (2). Melittin-lipid membrane interactions have been studied extensively and it was shown that they depend on the lipid composition, the peptide concentration, the hydration level and the membrane potential (3-7). For instance the binding of melittin to membranes composed of negatively charged lipids is stronger compared to neutral membranes (4, 8). Different mechanisms have been proposed for the activity of melittin. In one model, melittin insert into the hydrophobic core of the membrane and forms either barrel-stave (9, 10) or toroidal (7, 11) pores. In the other model, ‘detergent-like’, melittin due to a cluster of cationic residues at carboxy terminus and a stretch of hydrophobic residues behaves much as a detergent (12). Positively charged melittin binds onto the surface of the membrane. At low concentrations of the peptide, molecules are oriented parallel to the surface of the bilayer. An increase of the peptide concentration causes further aggregation and reduction of bilayer thickness. When the threshold concentration is reached, the peptide changes its orientation and disrupts the bilayer curvature inducing destabilization and disintegration of the membrane (12-15).

There are many studies, which have used many different biophysical techniques, but so far no thermodynamic equilibrium using titration calorimetry was described. We used high-sensitivity isothermal titration calorimetry (ITC) to study the thermodynamic equilibrium

between melittin and electrically neutral large unilamellar vesicles composed of 1-palmitoyl-2-oleoyl-*sn*-glycero-3-phosphatidylcholine (POPC).

MATERIALS AND METHODS

Materials. Melittin was purchased from BACHEM AG (Bubendorf BL, Switzerland) (purity > 97% by reverse phase HPLC). The concentration of melittin in aqueous solution was determined by UV spectroscopy at 280 nm using an absorption coefficient of $5570 \text{ M}^{-1} \text{ cm}^{-1}$ (16). POPC was obtained from Avanti Polar Lipids Inc. (Alabaster, AL, USA).

All other chemicals were of analytical or reagent grade. Tris buffer (25 mM tris(hydroxymethyl)aminoethane, pH 7.4) was prepared from 18 M Ω water obtained from a NANOpure A filtration system. NaCl concentrations were variable (50 and 100 mM) and are specified in the legends of each figure. The samples were degassed immediately before use.

Preparation of lipid vesicles. A defined amount of POPC was dried from a stock solution in chloroform under a gentle stream of nitrogen followed by high vacuum overnight. The lipids were resuspended in buffer (25 mM Tris, 50 mM or 100 mM NaCl at pH 7.4) with gentle vortex mixing leading to multilamellar vesicles (MLVs) with a final lipid concentration of 20-25 mM. Large unilamellar vesicles (LUVs) were prepared by extrusion of MLV suspensions using extruder. After five consecutive freeze-thaw cycles, MLVs were extruded 12 times through polycarbonate membrane with pore diameter of 100 nm (Whatman, Clifton, NJ).

Isothermal Titration Calorimetry. All measurements were made with a MicroCal VP-ITC calorimeter (MicroCal, Northampton, MA, USA). Titrations were performed by injecting 10 μL aliquots of POPC (25 mM) at constant time interval (10 min) into the calorimeter cell ($V_{\text{cell}} = 1.4037 \text{ mL}$) containing peptide at a concentration of typically 8-16 μM .

The heats of dilution were determined in control titrations by injecting a lipid solution into pure buffer and were included in the final analysis. Raw data were processed using Origin software provided with the instrument. The temperature was set as indicated in the legends of the figures.

RESULTS

The interaction of melittin with uncharged lipid vesicles was studied with by ITC. Following the protocol for lipid-into-peptide titrations (17), a diluted solution of melittin (8-16 μM) in buffer was filled in the calorimeter cell ($V_{\text{cell}} = 1.4037 \text{ mL}$) and small aliquots (10 μL) of vesicle suspension (20-25 mM total lipid) were injected at defined time intervals into the peptide solution.

Figure 1A shows a representative calorimetric heat flow trace obtained at 60 $^{\circ}\text{C}$ by titration of melittin with POPC large unilamellar vesicles (LUVs). The corresponding titration curve is shown in Figure 1B, where the reaction heats are plotted as a function of the injection number. The reaction heats were obtained by integration of the titrations peaks shown in Figure 1A and were corrected for the heats of dilution obtained in a separate lipid-into-buffer titration.

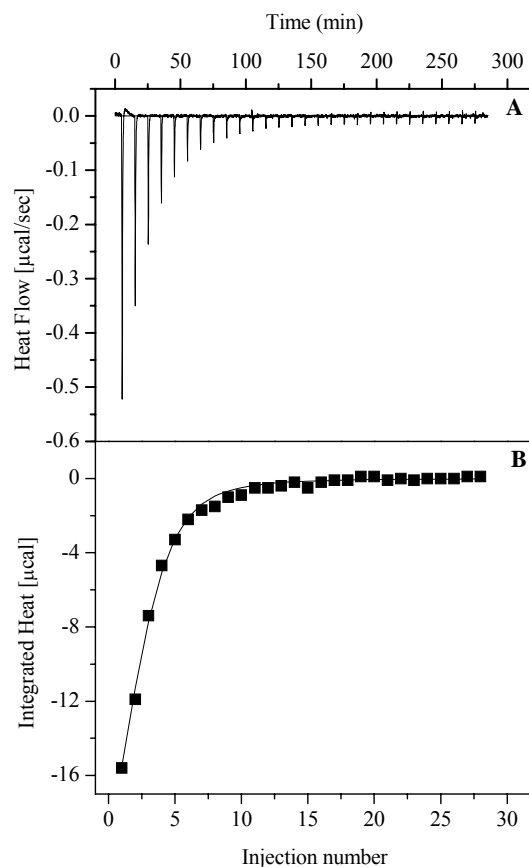


Figure 1. Titration of POPC into melittin. (A) Calorimetric trace obtained at 60 °C by titration of POPC LUV suspension (22 mM) into a solution of melittin (14.5 μM). Each peak corresponds to the injection of 10 μL of lipid suspension into the calorimeter cell. (B) Heats of reaction (integrated from the calorimetric trace) plotted as a function of injection number. The heat of dilution was measured in a separate control experiment and was included in the final analysis. The solid line is the best fit to the experimental data (\blacksquare) using the surface partition equilibrium model. Buffer: 25mM Tris and 50 mM NaCl at pH 7.4.

Figure 1 demonstrates an *exothermic* reaction at 60 °C. The heat of reaction decreases with increasing number of injections, since less and less peptide is available for binding. When all peptide is bound to POPC vesicles, the residual heats of the last injections are due to dilution of lipid vesicles into buffer. The molar binding enthalpy of melittin is then determined from the total heat released in the titration ($\sim 50.9 \mu\text{cal}$) and the amount of

peptide in the calorimeter cell (20.35 nmol). For the experiment shown in Figure 1 the heat of reaction is $\Delta H_{\text{melittin}}^0 \approx -2.5$ kcal/mol.

To obtain binding isotherm the experimental data should be treated with appropriate binding model. For the neutral membranes electrostatic effects must also be taken into account as long as the peptide is charged. Upon binding of charged peptide to an initially neutral membrane, the surface of the bilayer becomes gradually charged, leading to a membrane surface potential. The concentration of the peptide near the membrane surface is then different that in the bulk solution. To account for such effects, the binding isotherm was then calculated using a surface partition equilibrium model (17-21). In this model the extent of peptide adsorption is linearly related to the peptide surface concentration C_M (and not to the bulk concentration):

$$X_b = KC_M \quad (1)$$

where X_b denotes the molar amount of peptide bound per mole of lipid and K is the partition coefficient.

C_M can be calculated using the Boltzmann relation:

$$C_M = C_f \exp(-z_p F_o \varphi_o / RT) \quad (2)$$

where z_p is the effective charge of the peptide, F_o is the Faraday constant, φ_o is the membrane surface potential, RT is the thermal energy. The membrane surface potential is not known, but can be calculated from the degree of binindg, X_b using the Gouy-Chapman theory [for reviews, see ref (22, 23)].

The free energy of binding ΔG^0 can be calculated according to

$$\Delta G^0 = -RT \ln 55.5K \quad (3)$$

where the factor 55.5 is the molar concentration of water and corrects for the cratic contribution to the binding event (24).

Finally the entropy of binding ΔS^0 can be calculated using the relation

$$\Delta G^0 = \Delta H^0 - T\Delta S^0 \quad (4)$$

Calorimetric titrations were performed at various temperatures in the range of 10-60 °C at two different salt concentrations (50 mM NaCl and 100 mM NaCl). Table 1 summarizes the thermodynamic parameters obtained by using model described above.

Table 1. Temperature dependence of the thermodynamic parameters for the binding of melittin to POPC LUVs. Buffer: 25 mM Tris and variable concentrations of NaCl at pH 7.4.

| T (°C) | $\Delta H_{\text{melittin}}^0$ (kcal/mol) | K (M ⁻¹) | $\Delta G_{\text{melittin}}^0$ (kcal/mol) | T $\Delta S_{\text{melittin}}^0$ (kcal/mol) | $\Delta S_{\text{melittin}}^0$ (kcal/mol K) |
|--------------------|--|-------------------------|--|--|--|
| <u>50 mM NaCl</u> | | | | | |
| 10 | 8.1 | 4.0 x 10 ⁴ | -8.2 | 16.3 | 57.6 |
| 20 | 5.9 | 6.0 x 10 ⁴ | -8.7 | 14.6 | 49.8 |
| 30 | 2.5 | 7.0 x 10 ⁴ | -9.1 | 11.6 | 38.2 |
| 50 | -1.1 | 9.0 x 10 ⁴ | -9.9 | 8.8 | 27.4 |
| 60 | -2.5 | 8.0 x 10 ⁴ | -10.1 | 7.6 | 22.9 |
| <u>100 mM NaCl</u> | | | | | |
| 10 | 9.9 | 4.0 x 10 ⁴ | -8.2 | 18.2 | 64.2 |
| 20 | 4.8 | 4.5 x 10 ⁴ | -8.6 | 13.4 | 45.6 |
| 30 | 1.2 | 6.0 x 10 ⁴ | -9.0 | 10.2 | 33.7 |
| 50 | -0.7 | 6.2 x 10 ⁴ | -9.7 | 9.0 | 27.7 |
| 60 | -2.2 | 5.7 x 10 ⁴ | -9.9 | 7.7 | 23.0 |

The reaction enthalpy shows strong temperature dependence at both (50 mM and 100 mM NaCl) salt concentrations and changes from *endothermic* below 50 °C to *exothermic* above this temperature. $\Delta H_{\text{melittin}}^0$ varies almost linearly between 10 and 60 °C as demonstrated in Figure 2A. The slope of the straight lines yields a molar heat capacity change of $\Delta C_{p,\text{melittin}}^0 = -213 \text{ cal mol}^{-1} \text{ K}^{-1}$ at 50 mM NaCl content in the buffer and $\Delta C_{p,\text{melittin}}^0 = -221 \text{ cal mol}^{-1} \text{ K}^{-1}$ at 100 mM NaCl content in the buffer. The solid line in Figure 2B describes the

predicted temperature dependence of the binding constant K based on van't Hoff's law

$$d\ln K/dT = \Delta H_{\text{melittin}}^0 / RT^2.$$

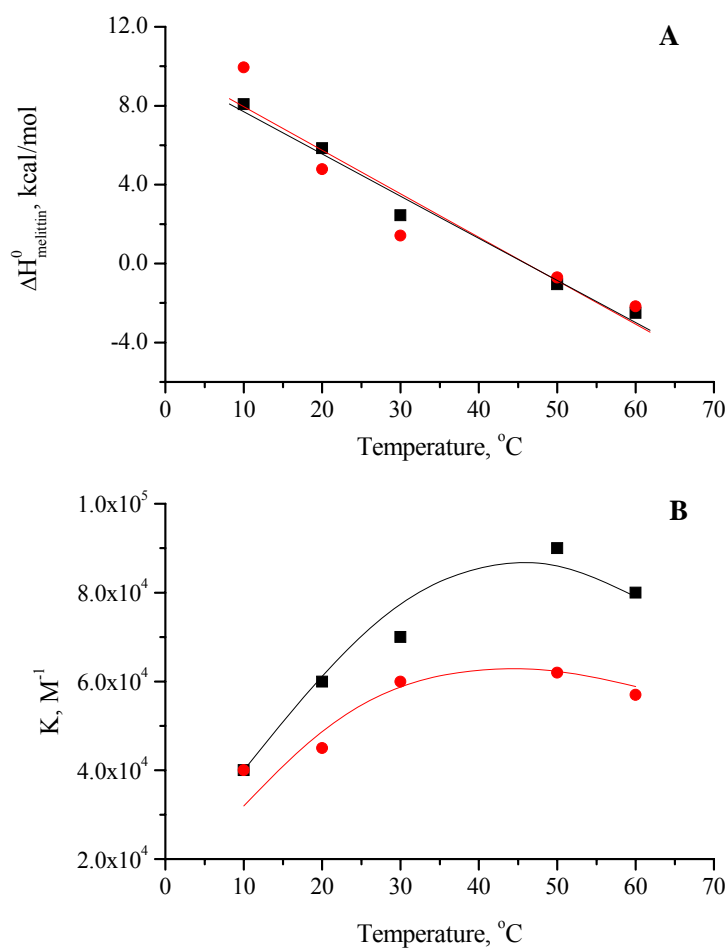


Figure 2. Temperature dependence of the thermodynamic parameters. (A) for melittin binding to POPC LUVs in (■) 25 mM Tris 50 mM NaCl and (●) 25 mM Tris 100 mM NaCl at pH 7.4. (B) Binding constant K in (■) 25 mM Tris 50 mM NaCl and (●) 25 mM Tris 100 mM NaCl at pH 7.4. The solid lines in B are the predicted temperature dependence of K based on the van't Hoff equation.

Table 1 demonstrates that the reaction is completely entropy driven below 50 °C as $\Delta H^0 > 0$. The free energy of binding is fairly constant. A plot of ΔH^0 vs. $T\Delta S^0$ yields a straight

line in the temperature range tested (Figure 3). The large heat capacity change provides an explanation for this enthalpy-entropy compensation phenomenon, that is, the linear correlation between ΔH^0 and $T\Delta S^0$. The temperature coefficient of ΔH^0 is ΔC_p^0 , that of $T\Delta S^0$ is close to $\Delta C_p^0 + \Delta S^0$. As $\Delta C_p^0 \gg \Delta S^0$ the two thermodynamic parameters ΔH^0 and $T\Delta S^0$ vary in parallel.

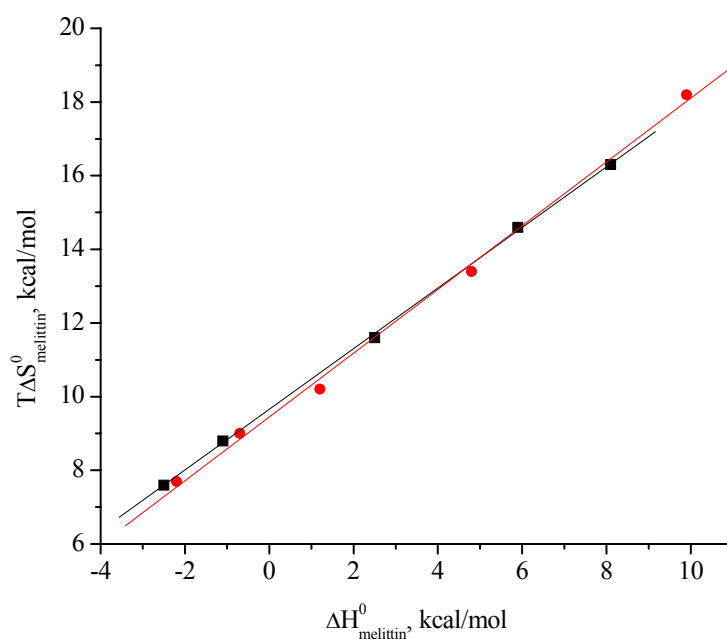


Figure 3. Enthalpy-entropy compensation plot for melittin binding to POPC LUVs. ITC measurement were performed in (■) 25mM Tris and 50 mM NaCl at pH 7.4; (●) 25 mM Tris 100 mM NaCl at pH 7.4.

DISCUSSION

Almost all chemical and physical processes are associated with absorption or release of heat, which can be measured by titration calorimetry. Isothermal Titration Calorimetry (ITC) is a very sensitive technique, which allows the simultaneously measurement of the

binding constant K_0 and the reaction enthalpy ΔH^0 . The corresponding free energy ΔG^0 and the reaction entropy ΔS^0 are then obtained via the standard thermodynamic relations (17). Melittin is one of the most studied antimicrobial peptides, but so far no direct thermodynamic characterization of melittin binding to lipid membranes using ITC was reported in the literature.

The binding of melittin to the neutral lipid membrane is mainly entropy driven as $\Delta H^0 > 0$. The binding constant is of order 10^4 M^{-1} in the temperature range of 10-60 °C at 50 mM NaCl as well as at 100 mM NaCl content in the buffer and shows weak temperature dependence. Corresponding free energies change modestly from $\sim -8 \text{ kcal/mol}$ at 10 °C to $\sim -10 \text{ kcal/mol}$ at 60 °C. Previous studies using NMR spectroscopy and fluorescence techniques showed that melittin binds to lipid membranes with a partition coefficient of order 10^3 - 10^5 M^{-1} (4, 6, 25) and the free energy of partitioning of melittin into the POPC vesicles has been estimated to be -7 to -8 kcal/mol (2, 6, 25). The binding is driven by hydrophobic interactions between non polar amino acid residues of melittin and the phospholipid hydrocarbon layer. In case of negatively charged lipids additional electrostatic interactions between the negatively charged membrane surface and the positively charged amino acid residues are involved.

There are few other processes associated with melittin binding to lipid membranes. The NMR studies showed that the binding of melittin to membranes composed of different lipids induces a conformational change of the lipid headgroups (4-6, 26). Other studies showed that binding of melittin to lipid membranes induces an α -helix formation and this process is tightly coupled to the partitioning of the peptide into lipid membranes (7, 13, 27-29). The free energy of partitioning of melittin into the membrane is reduced by 0.4 kcal/mol per residue, when the peptide folds into the α -helix structure (30). Upon binding and partitioning of melittin into the lipid membrane, the peptide can also adopt different

orientations. The orientation of melittin helices depends on the membrane composition, its hydration, the temperature, and the phase state of the lipid (28, 31). An additional complication concerning the orientation of the peptide in the membrane is depicted in the observation that melittin does not adopt a fully transmembrane orientation in membranes, only so called pseudo-transmembrane orientation (32, 33). One of the key parameters which determine orientation of melittin in the lipid bilayer is the peptide concentration. At low concentrations of the peptide, the melittin molecules are oriented parallel to the surface bilayer. When the peptide reaches a critical (threshold) concentration the molecules change their orientation into perpendicular to the lipid bilayer and start to produce pores in the membrane (34). Also the self association of melittin from monomer to tetramer and the opposite reaction of dissociation can contribute to the overall process of binding of melittin to the lipid membranes. The enthalpy of $\Delta H^0 = -4.8$ kcal/mol of monomer and entropy of $\Delta S^0 = 0.05$ kcal/(K. mol of monomer) of self-aggregation of melittin from monomer to tetramer were determined using fluorescent spectroscopy (16).

REFERENCES

1. Habermann, E. (1972) Bee and wasp venoms. *Science* 177, 314-22.
2. Vogel, H. (1981) Incorporation of melittin into phosphatidylcholine bilayers. Study of binding and conformational changes. *FEBS Lett* 134, 37-42.
3. Berneche, S., Nina, M., and Roux, B. (1998) Molecular dynamics simulation of melittin in a dimyristoylphosphatidylcholine bilayer membrane. *Biophys J* 75, 1603-18.
4. Beschiasvili, G., and Seelig, J. (1990) Melittin binding to mixed phosphatidylglycerol/phosphatidylcholine membranes. *Biochemistry* 29, 52-8.

5. Dempsey, C., Bitbol, M., and Watts, A. (1989) Interaction of melittin with mixed phospholipid membranes composed of dimyristoylphosphatidylcholine and dimyristoylphosphatidylserine studied by deuterium NMR. *Biochemistry* 28, 6590 - 6596.
6. Kuchinka, E., and Seelig, J. (1989) Interaction of melittin with phosphatidylcholine membranes. Binding isotherm and lipid head-group conformation. *Biochemistry* 28, 4216-21.
7. Yang, L., Harroun, T. A., Weiss, T. M., Ding, L., and Huang, H. W. (2001) Barrel-stave model or toroidal model? A case study on melittin pores. *Biophys J* 81, 1475-85.
8. Batenburg, A. M., van Esch, J. H., and de Kruijff, B. (1988) Melittin-induced changes of the macroscopic structure of phosphatidylethanolamines. *Biochemistry* 27, 2324-31.
9. Ladokhin, A. S., Selsted, M. E., and White, S. H. (1997) Sizing membrane pores in lipid vesicles by leakage of co-encapsulated markers: pore formation by melittin. *Biophys J* 72, 1762-6.
10. Rex, S., and Schwarz, G. (1998) Quantitative studies on the melittin-induced leakage mechanism of lipid vesicles. *Biochemistry* 37, 2336-45.
11. Allende, D., Simon, S. A., and McIntosh, T. J. (2005) Melittin-induced bilayer leakage depends on lipid material properties: evidence for toroidal pores. *Biophys J* 88, 1828-37.
12. Bechinger, B., and Lohner, K. (2006) Detergent-like actions of linear amphipathic cationic antimicrobial peptides. *Biochim Biophys Acta* 1758, 1529-39.
13. Ladokhin, A. S., and White, S. H. (2001) 'Detergent-like' permeabilization of anionic lipid vesicles by melittin. *Biochim Biophys Acta*. 1514, 253-60.

14. Monette, M., and Lafleur, M. (1995) Modulation of melittin-induced lysis by surface charge density of membranes. *Biophys J* 68, 187-95.
15. Shai, Y. (2002) Mode of action of membrane active antimicrobial peptides. *Biopolymers* 66, 236-48.
16. Quay, S. C., and Condie, C. C. (1983) Conformational studies of aqueous melittin: thermodynamic parameters of the monomer-tetramer self-association reaction. *Biochemistry* 22, 695-700.
17. Seelig, J. (1997) Titration calorimetry of lipid-peptide interactions. *Biochim Biophys Acta* 1331, 103-16.
18. Seelig, J., Nebel, S., Ganz, P., and Bruns, C. (1993) Electrostatic and nonpolar peptide-membrane interactions. Lipid binding and functional properties of somatostatin analogues of charge $z = +1$ to $z = +3$. *Biochemistry* 32, 9714-21.
19. Terzi, E., Holzemann, G., and Seelig, J. (1994) Alzheimer beta-amyloid peptide 25-35: electrostatic interactions with phospholipid membranes. *Biochemistry* 33, 7434-41.
20. Wenk, M. R., and Seelig, J. (1998) Magainin 2 amide interaction with lipid membranes: calorimetric detection of peptide binding and pore formation. *Biochemistry* 37, 3909-16.
21. Wieprecht, T., Beyermann, M., and Seelig, J. (1999) Binding of antibacterial magainin peptides to electrically neutral membranes: thermodynamics and structure. *Biochemistry* 38, 10377-87.
22. Hiemenz, P. C., and Rajagopalan, R. (1997) Principles of Colloid and Surface Chemistry. 3rd ed., Marcel Dekker, Inc., New York.
23. McLaughlin, S. (1989) The electrostatic properties of membranes. *Annu Rev Biophys Chem* 18, 113-36.

24. Cantor, C. R., and Schimmel, P. R. (1980) The Behavior of Biological Macromolecules *pp 849-885*, *W. H. Freeman and Company, San Francisco, CA*.
25. Schwarz, G., and Beschiaschvili, G. (1989) Thermodynamic and kinetic studies on the association of melittin with a phospholipid bilayer. *Biochim Biophys Acta* 979, 82-90.
26. Dempsey, C. E., and Watts, A. (1987) A deuterium and phosphorus-31 nuclear magnetic resonance study of the interaction of melittin with dimyristoylphosphatidylcholine bilayers and the effects of contaminating phospholipase A2. *Biochemistry* 26, 5803-11.
27. Dempsey, C. E., and Butler, G. S. (1992) Helical structure and orientation of melittin in dispersed phospholipid membranes from amide exchange analysis in situ. *Biochemistry* 31, 11973-7.
28. Vogel, H. (1987) Comparison of the conformation and orientation of alamethicin and melittin in lipid membranes. *Biochemistry* 26, 4562-72.
29. Vogel, H., and Jahnig, F. (1986) The structure of melittin in membranes. *Biophys J* 50, 573-82.
30. Ladokhin, A. S., and White, S. H. (1999) Folding of amphipathic alpha-helices on membranes: energetics of helix formation by melittin. *J Mol Biol* 285, 1363-9.
31. Frey, S., and Tamm, L. K. (1991) Orientation of melittin in phospholipid bilayers. A polarized attenuated total reflection infrared study. *Biophys J* 60, 922-30.
32. Bachar, M., and Becker, O. M. (2000) Protein-induced membrane disorder: a molecular dynamics study of melittin in a dipalmitoylphosphatidylcholine bilayer. *Biophys J* 78, 1359-75.
33. Toraya, S., Nishimura, K., and Naito, A. (2004) Dynamic structure of vesicle-bound melittin in a variety of lipid chain lengths by solid-state NMR. *Biophys J* 87, 3323-35.

-
34. Huang, H. W. (2000) Action of antimicrobial peptides: two-state model. *Biochemistry* 39, 8347-52.

7. SUMMARY

The presented work focused on an alternative mechanism of action of melittin on the cell membranes. The study using ITC reveals that melittin has a high affinity for several glycosaminoglycans (GAGs), i.e. heparan sulfate (HS), dermatan sulfate and heparin. The interaction between peptide and GAGs comprised both electrostatic and non-ionic components. Circular dichroism (CD) spectroscopy demonstrates that the binding of melittin to HS and other GAGs induces a conformational change to a predominantly α -helical structure. A model of the melittin-HS complex is presented. Furthermore the melittin binding was compared with that of magainin 2 and nisin Z to HS. Magainin 2 and nisin Z are two amphiphatic and antimicrobial peptides with similar lipid binding properties as melittin, but in opposite to melittin they do not cause lysis of the eukaryotic cells. ITC demonstrates that magainin 2 and nisin Z do not bind to HS. This result could indicate that the interaction with GAGs is unique property of melittin.

In order to study *in vivo* involvement of GAGs in the binding of melittin to cell membranes, the cytotoxic effect of the peptide on the cells deficient in GAGs and the corresponding wild type cell line was investigated. The lactate dehydrogenase (LDH) release assay was employed. The differences in the toxic effect of the peptide on both cell lines were hoped to be much more pronounced, what would indicate that indeed GAGs are involved in the action mechanism of melittin on the cell membranes. The significant difference in the cytotoxic effect of melittin was observed only at one peptide concentration. However the surface of the eukaryotic cells is not only decorated with sulfated GAGs, but also with other negatively charged molecules and it cannot be excluded that they are also a potential target for melitin.

Furthermore the interactions of retro-inverso dioleoylmelittin (riDOM) with HS were studied. RiDOM is a hybrid molecule, obtained by covalently coupling of retro-inverso

analog of melittin to a lipid moiety, to form a stable and efficient gene transfer system, which shows no haemolytic activity. ITC demonstrates that riDOM has a high affinity to HS, and two other GAGs, namely dermatan sulfate and heparin. CD spectroscopy reveals no conformational changes of riDOM upon binding to HS. Dynamic light-scattering measurements showed formation of bigger aggregates/complexes when riDOM is titrated with HS. Both ionic and hydrophobic interactions contribute to the binding of riDOM to HS.

Last part of the thesis described melittin-lipid membrane interaction using ITC. The binding equilibrium between melittin and electrically neutral large unilamellar vesicles composed of 1-palmitoyl-2-oleoyl-*sn*-glycero-3-phosphatidylcholine (POPC) was studied. ITC demonstrates that melittin has a high affinity to neutral lipid membranes.

8. ACKNOWLEDGMENTS

This work was carried out from the February 2005 until January 2008 in the laboratory of Prof. Dr. Joachim Seelig in the Department of Biophysical Chemistry at the Biozentrum of the University of Basel.

First of all I would like to express my sincere gratitude to my supervisor Professor Joachim Seelig who gave me the opportunity to be part of his research group and who introduced me to this very interesting field of science. I am grateful for his constant support and the valuable advices which helped me a lot during course of this work. I have learned a lot from him.

I want to thank to Professor Anna Seelig, who introduced me in the field of cell biology. Her advices and knowledge concerning this topic were very helpful to me, especially during the experiments with cells.

I also appreciate the work of Professor Dagmar Klostermeier as a referee of this thesis.

I want to thank to Dr. Matthias Meier and Dr. André Ziegler for their help and time for discussion, and to Dr. Elisabete Gonçalves for her advices and introductory help at the beginning of my studies. I owe my thanks to Dr. Päivi Äänisma for teaching me how to handle with the cells, Peter Ganz for teaching me how to work with the ITC instrument and Xiaochun Li Blatter for introducing me in the CD spectroscopy technique.

Many thanks to the present and former members of my lab and the floor mates for the friendly working environment: Susanna Notz, Andreas Beck, Andreas Bruns, Sarah Güthe, Gregori Gerebtzoff, Michael Hayley, Heiko Herklotz, Götz Kohler, Caroline Loew, Koji Mochizuki, Christian Müller, Samantha Perspicace, Renete Reiter, Reto Sauder, Therese

Shulthess, Alekos Tsamaloukas, Andreas Zumbühl, Christophe Bodenreider, Beat Fierz, Stefan Langheld, Andreas Reiner. A lot of thanks belong to the people from our technical workshop: Hans Vogt, Leo Faletti and Simon Saner. I want to also thank to my friends in Poland and Switzerland, especially to Milena Lis, Martyna Szyszkowska, Ela Świerczek and Kasia Szarzec for cheering me on the all stages of my studies.

I owe my greatest thanks to my family: my mother, my father and my brother and to Maxime for their support, help, patience and love. Without you it would have not been possible. Dziękuję.

9. CURRICULUM VITAE

PERSONAL DETAILS

Name and address: Gabriela Klocek
Biozentrum, University of Basel
Department of Biophysical Chemistry
Klingelbergstrasse 50-70
CH-4056 Basel
Tel.: +41 612672192
gabriela.klocek@unibas.ch

Date and place of Birth: February 17th 1978
Cieszyn, Poland

Nationality: polish

EDUCATION

02/2005 – 02/2008 Biozentrum, University of Basel, Switzerland
Graduate (PhD) studies in Biophysics
Thesis supervisor: Prof. Dr. Joachim Seelig
Thesis title: Melittin Interaction with Sulfated Sugars and Cell Membranes.

1997-2002 Silesian Technical University in Gliwice, Poland
M. Sc studies in Chemical Technology
Specialization: Technology of Polymers and Plastics
Thesis supervisor: Prof. Dr Hab. Jolanta Maślinska-Solich
Thesis title: Polycondensation of diacetals of salicylaldehyde with dihalides.

1993-1997 M. Kopernik Secondary School in Cieszyn
Profile of Biology and Chemistry

10. DECLARATION

I declare that I wrote this thesis “Melittin Interaction with Sulfated Sugars and Cell Membranes” with help indicated and only handed it in to the Faculty of the Science of the University of Basel and to no other faculty or other university.

Basel, 9th of January, 2008